

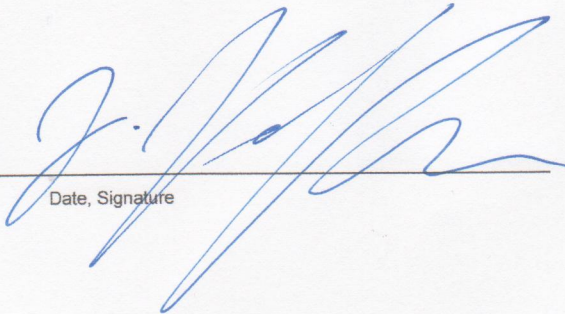


AFFIDAVIT

I declare that I have authored this thesis independently, that I have not used other than the declared sources/resources, and that I have explicitly indicated all material which has been quoted either literally or by content from the sources used. The text document uploaded to TUGRAZonline is identical to the present master's thesis.

29.08.2020,

Date, Signature

A handwritten signature in blue ink, consisting of several large, sweeping loops and strokes, positioned to the right of the date and above a horizontal line.

Abstract

Reformulation of lattice field theories in terms of dual variables is a powerful tool, that has been studied intensively in recent years. A dual formulation may overcome complex action problems and provides a different, very geometrical view on lattice field theories. For the abelian case the dualisation is relatively easy and straightforward, whereas in non-abelian theories this procedure turns out to be more difficult due to the non-commutative character of the group elements. Nevertheless dual formulations for non-abelian theories were suggested and are still subject of current intensive research.

In this work we present different approaches for solving the "artificial" sign problem of the dual representation of $SU(2)$ pure lattice gauge theory. Sign problems are very common in lattice field theory, the reason why we call this sign problem "artificial" is, that the conventional $SU(2)$ lattice gauge theory does not have a sign problem while it appears in the theory during the dualisation procedure.

The three different approaches discussed in this thesis are: *i)* analysing contributions from the center group of $SU(2)$ in search for new constraints for the theory, *ii)* resumming the different contributions to obtain positive overall weights and *iii)* truncation of the theory. The most promising approach turns out to be the truncation approach, where we naively reformulate our dual theory to resemble a qubit representation. This idea originated from the paper: *Qubit regularization of the $O(3)$ sigma model* [1] and the fact, that $SU(2)$ can be related to $O(3)$ by an isomorphism.

Finally we carry out simulations of the theory using the undualised and the truncated representation of the theory. We then compare the data obtained by the simulations for different lattice sizes and discuss the implications of our results.

Kurzfassung

Reformulierung von Gitterfeldtheorien mittels dualer Variablen ist eine sehr mächtige Methode, an welcher in den letzten Jahren verstärkt geforscht wurde. Eine duale Formulierung kann dabei helfen komplexe Wirkungsprobleme zu lösen und eine solche Darstellung bietet eine sehr geometrische Sichtweise von Gitterfeldtheorien. Im abelschen Fall ist die Dualisierung relativ leicht zu bewerkstelligen, wohingegen sich dieses Prozedere in nicht-abelschen Theorien wegen dem nicht-kommutativen Charakter der Guppenelemente deutlich schwieriger gestaltet. Trotzdem sind duale Formulierungen solcher nicht-abelschen Theorien vorgestellt worden und sind weiterhin Gebiet intensiver Forschung.

In dieser Masterarbeit präsentieren wir verschiedene Ansätze zum Lösen des "artificialen" Vorzeichenproblems der dualen Representation von der reinen $SU(2)$ Gittereichtheorie. Vorzeichenprobleme sind sehr häufig in Gitterfeldtheorien, der Grund warum wir dieses hier als "artifizial" betiteln ist der, dass die konventionelle $SU(2)$ Gittereichtheorie gar kein Vorzeichenproblem aufweist, sondern dieses erst durch den Dualisationsprozess hinzugefügt wird.

Die drei erwähnten Ansätze, die wir in dieser Masterarbeit besprechen sind folgende: *i)* Suche nach neuen Einschränkungen der Theorie durch Analyse der Zentrumsgruppenbeiträge von $SU(2)$, *ii)* Resummation verschiedener Beiträge in der Hoffnung positive Gewichte zu erhalten und *iii)* Trunkierung der Theorie. Der Trunkierungsansatz, bei dem wir die Variablen unserer dualen Theorie so umformulierten, dass diese einer Qubit Diskretisierung ähneln, kristallisiert sich als der am vielversprechendste heraus. Die Idee mit der Qubit Diskretisierung ist angelehnt an die Thematik von folgendem Artikel: *Qubit regularization of the $O(3)$ sigma model* [1] und dem Fakt, dass $SU(2)$ isomorph zu $O(3)$ ist.

Schließlich simulieren wir die Theorie einmal mit der nicht-dualisierten und einmal mit der trunkierten Formulierung der Theorie. Anschließend vergleichen wir die Datensätze der verschiedenen Simulationen auf verschiedenen Gittergrößen und Diskutieren die Implikationen dieser Resultate.

Contents

1	Introduction	1
2	Overview of Lattice Field Theories	3
2.1	Path integrals in quantum field theories	3
2.1.1	From continuum to lattice	4
2.1.1.1	The path integral formulation in quantum mechanics	4
2.1.1.2	Path integral and lattice regularisation of quantum field theory	6
2.2	Gauge theories on the lattice	9
2.2.1	Continuum formulation	9
2.2.1.1	U(1) gauge theory	9
2.2.1.2	SU(N) gauge theory	11
2.2.1.3	Lattice regularisation of SU(N) gauge theory	11
2.3	Monte Carlo simulation in lattice field theory	14
2.4	Dual approach to lattice theories	16
2.4.1	Dualisation of $U(1)$ gauge theory	16
2.5	Observables in the dual representation	19
3	Dual representation of pure $SU(2)$ lattice gauge theory	21
3.1	Dualisation of $SU(2)$ lattice gauge theory	22
3.2	Observables of $SU(2)$ lattice gauge theory	30
4	Possible approaches for a simulation	33
4.1	Factoring out the center group of $SU(2)$	33
4.2	Dualisation with index parametrisation	36
4.3	Truncation and connection to qubit regularisation	43
5	Numerical Simulation	48
5.1	Simulation of conventional $SU(2)$ lattice gauge theory	48
5.1.1	Description of the algorithm	48
5.1.2	Results	53
5.2	Simulation using cycle occupation numbers (ACC's)	56
5.3	Simulation using the truncated theory	60
5.3.1	The algorithm	60
5.3.2	Results	65
5.4	Error calculation	68

6 Summary	71
A Reordering of the $U(1)$ gauge links	73
B Reordering for the gauge links of $SU(2)$ lattice gauge theory	75
C Differential forms on the lattice	78
D Dualisation of \mathbb{Z}_2 gauge theory	81
Acknowledgements	84
Bibliography	85

Dedicated to my loved ones...

Chapter 1

Introduction

The appearance of sign problems is a very common feature in lattice field theory and has been the subject of major research activities more or less since the lattice formulation of quantum field theory was first introduced. There are various ways how these sign problems come about, most notably complex action problems introduced by finite densities, topological terms or a non-zero chemical potential. Over the years, various methods have been developed and proposed to try and overcome these problems. One approach, that especially in recent years succeeded in solving different types of sign problems is the method of using a dual representation of lattice field theory. In the past this method has successfully been applied to solve the complex action problem of various abelian theories. More recent research is focused on developing this formalism for non-abelian theories.

”Dual representation” refers to a method of exactly rewriting the partition sum of the theory in terms of new, dual variables. These new degrees of freedom are world-lines of conserved flux for the matter fields and world-sheets for gauge fields. This rewriting of the theory can help uncover new symmetry aspects of the theory. However, we need to stress, that the dual representations are not unique. This is to say, that using different dualisation schemes may highlight different symmetry aspects of the theory. There is however one caveat: just because a dual representation of the theory exists does not automatically guarantee that the sign problem is solved. This is because the weights in the dual formulation can be negative or even complex. A good overview of the dual formulation of lattice field theories is given in [2].

This thesis explores the dual representation of non-abelian lattice field theories. But in contrast to the examples of the complex action sign problems mentioned above, the sign problem only gets introduced by the dualisation scheme. Conventional $SU(2)$ lattice gauge theory does not have a sign problem. However, during the dualisation, because we

need to choose a specific representation of the $SU(2)$ matrices, we introduce a relative sign. This thesis is devoted to developing methods to overcome this sign problem. Thus, the work done in this thesis is mostly of algebraic nature. To check the validity of our approach, we also perform simulations of the theory and compare these results to the results obtained by the conventional simulation.

This thesis is structured as follows: **Chapter 2** serves as an introduction for the topic of lattice field theories. Here we explain in great detail why lattice field theories are useful, how to obtain the lattice formulation of a theory, e.g., $U(1)$ gauge theory. Furthermore in this chapter we explain the basics of the Monte Carlo simulation technique, which was used to obtain the numerical results given in Chapter 5.

In **Chapter 3** we give the dualisation of $SU(2)$ lattice gauge theory and elaborate on how the sign problem emerges. We also discuss the dual representation of the theory originally developed in [3] using the Abelian Colour Cycles. Last but not least we discuss the observables of interest, namely the plaquette expectation value $\langle U_p \rangle$ and the susceptibility χ .

Chapter 4 explains the approaches we developed to try and overcome the sign problem. These methods are: Factoring out the center group of $SU(2)$, dualisation with index parametrization and finally truncation of the theory. In this chapter we give the full mathematical reformulations for each of the approaches and discuss the individual advantages and disadvantages.

Finally in **Chapter 5** we explain how to simulate the theory using two different simulation schemes, i.e., the conventional matrix valued simulation and the simulation using the dual variables from the truncated approach. We then compare and discuss the results for the observables obtained by the two simulation methods.

Chapter 6 ends this master thesis with a summary of the results we achieved in the previous chapters.

Chapter 2

Overview of Lattice Field Theories

Lattice discretisation or lattice regularisation is one of the most powerful tools to further our understanding of non-perturbative phenomena in quantum field theories. The full formulation of this method as well as introductions to quantum field theories in general can be found in great detail in many textbooks (e.g. [4], [5], [6]), however for self consistency and to set our notation we provide a short introduction to the topic and the methods used in this thesis.

Thus we will first give an outline of the main concepts of the lattice regularisation method, after which we will provide an overview of the formulation of pure lattice gauge theory, as this is the main focus of this thesis. For completeness we also include a short remark on fermions in lattice field theory. To conclude this section we will introduce the concept of Monte Carlo simulation of a lattice field theory and afterwards discuss the dual variable approach as well as interesting observables to compute.

Sections 2.1, 2.2 and 2.3 follow closely an introductory book to quantum chromodynamics on the lattice [7].

2.1 Path integrals in quantum field theories

Quantum field theories are may be described and quantised using the path integral method, first introduced by Feynman [8], which has become a very popular method and is a useful tool for elementary particle physics. Hence this method is also used when quantising lattice field theories, with the slight difference, that here we are dealing with Euclidean rather than Minkowski space-time. The main principle of the path integral description of quantum mechanics is to sum over all trajectories of a particle from a point \vec{x} to a point \vec{y} and to use a Boltzmann factor with the classical action as a weight

factor for these paths. Because of this form there exists an analogy between quantum field theories and statistical mechanics, which in turn allows one to perform Monte Carlo simulations. In this first section we will give a short overview of the path integral formulation in the continuum and how to discretise it on a lattice.

2.1.1 From continuum to lattice

2.1.1.1 The path integral formulation in quantum mechanics

To introduce the Feynman path integral method, we will first discuss it in a quantum mechanical setting and only afterwards expand it to quantum field theory. To describe a propagation from a state $|x\rangle$ to a state $\langle y|$ in quantum mechanics one has to evaluate the matrix element with the time evolution operator, which is computed from the Hamiltonian. This matrix element can also be computed with the path integral method and one arrives at the following relation:

$$\langle y|e^{i\hat{H}t}|x\rangle = \int D[\vec{r}] e^{iS[\vec{r}]}, \quad (2.1)$$

where S denotes the classical action associated with a specific trajectory \vec{r} , \hat{H} is the Hamilton operator of the quantum mechanical system and $\int D[\vec{r}]$ is the functional integral over all classical paths \vec{r} from \vec{x} to \vec{y} . As one can see from this formula, instead of operators we are now dealing with functions and infinite-dimensional integrals. Having infinite dimensional integrals is almost never a good sign, and indeed a rigorous definition of $\int D[\vec{r}]$ is possible in the continuum, but only for very few cases. However, when we discretise the theory on a lattice, a rigorous definition of the path integral is possible.

One more problem arises, because the term e^{iS} is complex and strongly oscillating, therefore preventing the use of Monte Carlo methods. Luckily there is a way to bypass this problem by performing a Wick rotation of the time coordinate $t \rightarrow -ix_4$, with x_4 being the Euclidean time coordinate. After performing the Wick rotation, the Euclidean space-time version of (2.3) reads

$$\langle y|e^{-\hat{H}x_4}|x\rangle = \int D[\vec{r}] e^{-S_E[\vec{r}]}, \quad (2.2)$$

with $-S_E = iS$ being the Euclidean action.

To show the analogy of quantum field theory to statistical mechanics let us consider the known partition function from statistical mechanics

$$Z_\beta = \text{Tr}[e^{-\beta\hat{H}}], \quad (2.3)$$

with the quantum mechanical Hamiltonian $\hat{H} = \frac{\hat{p}^2}{2m} + \hat{V}$. We here discuss the partition sum for finite inverse temperature $\beta = \frac{1}{k_B T}$. Later we will be interested in the limit $T \rightarrow 0$, i.e., $\beta \rightarrow \infty$. The trace from Equation (2.3) can be written in terms of the position eigenstates $|x\rangle$,

$$\mathrm{Tr}[e^{-\beta\hat{H}}] = \int dx \underbrace{\langle x|e^{-\beta\hat{H}}|x\rangle}_{\text{Matrix elements}} . \quad (2.4)$$

The evaluation of the exponential $e^{-\beta\hat{H}}$ is not straightforward since the kinetic and the potential part in \hat{H} do not commute due to the relation $[\hat{x}, \hat{p}] = i$ from quantum mechanics (here \hbar is set to 1). Because of $[\hat{p}^2, \hat{V}] \neq 0$ we have to use the Trotter decomposition for evaluating $e^{-\beta\hat{H}}$. For this we write $\beta = N \cdot \epsilon$ where ϵ is an infinitely small quantity and perform the decomposition in the following way:

$$e^{-\beta\hat{H}} = \lim_{N \rightarrow \infty} (e^{-\epsilon\hat{H}})^N , \quad \text{with } e^{-\epsilon\hat{H}} = e^{-\frac{\epsilon}{2}\hat{V}} e^{-\epsilon\frac{\hat{p}^2}{2m}} e^{-\frac{\epsilon}{2}\hat{V}} [1 + O(\epsilon)] . \quad (2.5)$$

We then consider the operator $\hat{W}_\epsilon := e^{-\frac{\epsilon}{2}\hat{V}(\hat{x})} e^{-\epsilon\frac{\hat{p}^2}{2m}} e^{-\frac{\epsilon}{2}\hat{V}(\hat{x})}$, and calculate the matrix elements $\langle x|\hat{W}_\epsilon|y\rangle$. The calculation of these matrix elements is straightforward using the following relations:

- $\hat{V}(\hat{x})|x\rangle = V(x)|x\rangle$,
- $\langle x|p\rangle = \frac{1}{\sqrt{2\pi}} e^{ipx}$,
- $\mathbb{I}_x = \int dx |x\rangle\langle x|$,
- $\mathbb{I}_p = \int dp |p\rangle\langle p|$,
- $\int dp e^{-\epsilon\frac{p^2}{2m}} \frac{1}{2\pi} e^{ip(x-y)} = \sqrt{\frac{m}{2\pi\epsilon}} e^{-\frac{(x-y)^2 m}{2\epsilon}}$,

with the last equation being just an ordinary Gaussian integral. After a bit of algebra, we arrive at the expression

$$\langle x|\hat{W}_\epsilon|y\rangle = \sqrt{\frac{m}{2\pi\epsilon}} e^{-\frac{\epsilon}{2}V(x)} e^{-\frac{(x-y)^2 m}{2\epsilon}} e^{-\frac{\epsilon}{2}V(y)} . \quad (2.6)$$

What remains to be done to compute $e^{-\beta\hat{H}}$ is to take the limit: $\lim_{N \rightarrow \infty} (\hat{W}_\epsilon)^N = e^{-\beta\hat{H}}$, with $\epsilon = \frac{\beta}{N}$. The final steps of the construction are

$$Z_\beta = \mathrm{Tr}[e^{-\beta\hat{H}}] = \int dx_0 \langle x_0|e^{-\beta\hat{H}}|x_0\rangle = \lim_{N \rightarrow \infty} \int dx_0 \langle x_0| \underbrace{\hat{W}_\epsilon \cdots \hat{W}_\epsilon}_{N \text{ times}} |x_0\rangle .$$

and inserting $\mathbb{I}_x = \int dx |x\rangle\langle x|$ in between every \hat{W}_ϵ yields

$$Z_\beta = \lim_{N \rightarrow \infty} \int dx_0 dx_1 \cdots dx_{N-1} \langle x_0 | \hat{W}_\epsilon | x_1 \rangle \langle x_1 | \hat{W}_\epsilon | x_2 \rangle \cdots \langle x_{N-1} | \hat{W}_\epsilon | x_0 \rangle .$$

Evaluating all the matrix elements as described above, we can finally complete the construction of the path integral description. We therefore have obtained the full path integral formulation of our quantum mechanical system with Euclidean time:

$$\mathcal{Z}_\beta = \lim_{N \rightarrow \infty} (C_\epsilon)^N \int D[x] e^{-\epsilon \sum_{j=0}^{N-1} \left[\frac{m}{2} \left(\frac{x_{j+1} - x_j}{\epsilon} \right)^2 + V(x_j) \right]} \approx \int D[x] e^{-S_E[x]} [1 + O(\epsilon)] , \quad (2.7)$$

where the overall constants C_ϵ have been dropped in the last step. The integral $\int D[x]$ over all paths is now rigorously defined as

$$D[x] = \prod_{j=0}^{N-1} \int_{-\infty}^{\infty} dx_j , \quad (2.8)$$

and we use periodic boundary conditions $x_N = x_0$. The Euclidean action $S_E[x]$ is given by

$$S_E[x] = -\epsilon \sum_{j=0}^{N-1} \left[\frac{m}{2} \left(\frac{x_{j+1} - x_j}{\epsilon} \right)^2 + V(x_j) \right] . \quad (2.9)$$

2.1.1.2 Path integral and lattice regularisation of quantum field theory

Considering quantum field theories, all the steps described in the previous section work in principle analogously. But as the name suggests, we are now dealing with fields instead of a single degree of freedom. To briefly demonstrate the path integral formulation in a quantum field theoretical setting, let us consider a simple example theory, namely the Klein-Gordon equation with a potential. The Lagrangian of the theory is given by:

$$\mathcal{L} = \frac{1}{2} (\partial_\mu \phi) (\partial^\mu \phi) - \frac{1}{2} m^2 \phi^2 - V(\phi(x)) . \quad (2.10)$$

It needs to be stressed, that the fields $\phi(t, \vec{x})$ are not quantised yet and we still consider classical fields. From Eq. (2.8) we can easily obtain the Hamiltonian by using the canonical momentum field $\pi(t, \vec{x}) = \frac{\partial \mathcal{L}}{\partial \dot{\phi}(t, \vec{x})} = \dot{\phi}$ and a Legendre transformation,

$$H = \int d^3x \pi(t, \vec{x}) \dot{\phi}(t, \vec{x}) - L = \int d^3x \left[\frac{1}{2} \pi(t, \vec{x})^2 + \frac{1}{2} (\nabla \phi(t, \vec{x}))^2 + \frac{m^2}{2} \phi(t, \vec{x})^2 + V(\phi) \right] . \quad (2.11)$$

Now follows the quantisation procedure, where we promote the fields to operators in the Schödinger picture: $\phi(t, \vec{x}) \rightarrow \hat{\phi}(\vec{x})$ and $\pi(t, \vec{x}) \rightarrow \hat{\pi}(\vec{x})$, and require the following commutation relations to hold: $[\hat{\phi}(\vec{x}), \hat{\phi}(\vec{y})] = [\hat{\pi}(\vec{x}), \hat{\pi}(\vec{y})] = 0$ and $[\hat{\phi}(\vec{x}), \hat{\pi}(\vec{y})] = i\delta^{(3)}(\vec{x} - \vec{y})$,

$\forall \vec{x}, \vec{y}$. The Hamilton operator then becomes:

$$\hat{H} = \int d^3x \left[\frac{1}{2} \hat{\pi}(\vec{x})^2 + \hat{U}(\vec{x}) \right], \quad (2.12)$$

with $\hat{U}(\vec{x}) = \frac{1}{2} (\nabla \hat{\phi}(\vec{x}))^2 + \frac{m^2}{2} \hat{\phi}(\vec{x})^2 + V(\hat{\phi})$ denoting the potential term.

Using the Hamiltonian given in Equation (2.10) we are now able to obtain the path integral formulation of the quantum field theory, as stated before, in complete analogy to the steps described in Section 2.1. As this thesis is devoted to lattice field theory we now need to introduce the lattice regularisation of a quantum field theory.

To discretise the theory on a lattice, we first introduce a finite dimensional spatial lattice with a finite number of lattice sites and therefore a finite volume. To achieve the discretisation we replace the position vectors $\vec{x} \in \mathbb{R}^3$ in the Hamiltonian (2.10) with a 3-d, spatial lattice, we will refer to as Λ . Therefore the vector \vec{x} gets replaced by a site on that lattice Λ . To put these replacements into a mathematical description we write

$$\mathbb{R}^3 \rightarrow \Lambda a^3$$

$$\vec{x} \mapsto a\vec{n} \quad \text{with } \vec{n} = \begin{bmatrix} n_1 \\ n_2 \\ n_3 \end{bmatrix}, \quad n_i : 0, 1, 2, \dots, L-1$$

Thus we consider a 3-dimensional lattice of size L^3 and lattice spacing a .

There are some more substitutions needed to go from the continuum formulation to the lattice regularised theory, which will be shown and explained in the following. As just described, the position argument \vec{x} of the continuum fields gets replaced by the lattice vector \vec{n} . Also when considering discretised quantum field theories, we are dealing with sums over all lattice sites, rather than an integral over space, and last but not least we need to replace the derivative operators with suitable differences. Here a symmetric discretisation of the derivatives is used, such that the discretisation error is $\mathcal{O}(a^2)$ rather than $\mathcal{O}(a)$. We shortly summarize the steps of the discretisation as follows:

- $\hat{\phi}(\vec{x}) \longrightarrow \hat{\phi}(\vec{n})$,
- $\hat{\pi}(\vec{x}) \longrightarrow \hat{\pi}(\vec{n}), \vec{n} \in \Lambda$,
- $\int d^3x \longrightarrow a^3 \sum_{\vec{n} \in \Lambda}$,
- $\partial_j \hat{\phi}(\vec{x}) \longrightarrow \frac{\hat{\phi}(\vec{n}+\hat{j}) - \hat{\phi}(\vec{n}-\hat{j})}{2a} + \mathcal{O}(a^2)$,

Here \hat{j} denotes the unit vector in direction j . Using all these substitutions we arrive at the discretised Hamiltonian

$$\hat{H} = a^3 \sum_{\vec{n} \in \Lambda} \left[\frac{1}{2} \hat{\pi}(\vec{n})^2 + \frac{1}{2} \sum_{j=1}^3 \left(\frac{\hat{\phi}(\vec{n} + \hat{j}) - \hat{\phi}(\vec{n} - \hat{j})}{2a} \right)^2 + V(\hat{\phi}(\vec{n})) + \frac{m^2}{2} \hat{\phi}(\vec{n})^2 \right], \quad (2.13)$$

with the conjugate momentum given by $\hat{\pi}(\vec{n}) = -ia^{-3} \frac{\partial}{\partial \hat{\phi}(\vec{n})}$. Thus we have the following commutation relations:

- $[\hat{\phi}(\vec{n}), \hat{\phi}(\vec{m})] = [\hat{\pi}(\vec{n}), \hat{\pi}(\vec{m})] = 0$.
- $[\hat{\phi}(\vec{n}), \hat{\pi}(\vec{m})] = i\delta_{\vec{n}, \vec{m}}^{(3)} a^{-3}$, the factor a^{-3} is there to get the dimensions right.

If we now repeat all the steps from Section 2.1 in the quantum field theoretical setting, i.e., inserting $\mathbb{I} = \prod_{\vec{n} \in \Lambda} \int_{-\infty}^{\infty} d\phi(\vec{n}) |\phi\rangle \langle \phi|$ and using the "wave function of fields" $\langle \phi | \pi \rangle = \frac{1}{(2\pi)^{|\Lambda|/2}} e^{i \sum_{\vec{n} \in \Lambda} \pi(\vec{n}) \phi(\vec{n})}$ for the Gaussian integrals, we finally arrive at an analogous expression to Equation (2.7):

$$Z_\beta = \lim_{N \rightarrow \infty} (C)^N \prod_{j=0}^{N-1} \prod_{\vec{n} \in \Lambda} \int_{-\infty}^{\infty} d\phi(\vec{n}) e^{-\epsilon a^3 \sum_{j=0}^{N-1} \sum_{\vec{n} \in \Lambda} \left(\frac{\phi_{j+1}(\vec{n}) - \phi_j(\vec{n})}{\epsilon} \right)^2 - \epsilon \sum_{j=0}^{N-1} U[\phi_j]}. \quad (2.14)$$

Inserting the potential term and the abbreviation of the integral measure

$$\int D[\phi] = \prod_{j=0}^{N-1} \prod_{\vec{n} \in \Lambda} \int_{-\infty}^{\infty} d\phi(\vec{n}), \quad (2.15)$$

into Equation (2.12) gives

$$Z_\beta = \int D[\phi] e^{-\epsilon a^3 \left[\sum_{j=0}^N \sum_{\vec{n} \in \Lambda} \left(\frac{\phi_{j+1}(\vec{n}) - \phi_j(\vec{n})}{\epsilon} \right)^2 + \sum_{\mu=1}^3 \left(\frac{\phi_j(\vec{n} + \hat{\mu}) - \phi_j(\vec{n} - \hat{\mu})}{2a} \right)^2 + \frac{m^2}{2} \phi_j(\vec{n})^2 + V[\phi_j(\vec{n})] \right]}. \quad (2.16)$$

It needs to be stressed that the fields obey periodic boundary conditions in the Euclidean time direction $\phi_N(\vec{n}) = \phi_0(\vec{n})$. Now using this fact and promoting the subindex of the fields j to a new argument, we can now identify the whole argument as a 4-vector n on a 4-dimensional lattice of size $L^3 \times N$ which we denote by

$$\Lambda_4 = \{n = (\vec{n}, n_4) | n_i = 0, 1, \dots, L-1; i = 1, 2, 3; n_4 = 0, 1, \dots, N-1\}. \quad (2.17)$$

We relabel the fields in the following way: $\phi_j(\vec{x})|_{\vec{x}=a\vec{n}} \rightarrow \phi(\vec{n}, j) = \phi(n)$. Setting $\epsilon = a$ the term $\epsilon \sum_{j=0}^{N-1} a^3 \sum_{\vec{n} \in \Lambda}$ becomes $a^4 \sum_{n \in \Lambda_4}$, the integral measure term becomes $D[\phi] = \prod_{n \in \Lambda_4} \phi(n)$ and last but not least we change the one sided derivative term $\frac{\phi_{j+1}(\vec{n}) - \phi_j(\vec{n})}{\epsilon}$ to the symmetric form $\frac{\phi(\vec{n} + \hat{4}) - \phi(\vec{n} - \hat{4})}{2a}$. Using all this, we finally arrive at the following

term for the full 4-dimensional, discretised partition sum:

$$Z_\beta = \prod_{n \in \Lambda_4} \int d\phi(n) e^{-S_E[\phi]} , \quad (2.18)$$

with the Euclidean action now given by:

$$S_E[\phi] = a^4 \sum_{n \in \Lambda_4} \left[\left(\frac{\phi(n + \hat{\mu}) - \phi(n - \hat{\mu})}{2a} \right)^2 + \frac{m^2}{2} \phi(n)^2 + V[\phi] \right] . \quad (2.19)$$

Note that we have identified the inverse temperature β with $\beta = a \cdot N$. Thus for the zero temperature limit we need to consider $N \rightarrow \infty$.

2.2 Gauge theories on the lattice

Gauge theories have played an important role in physics since the discovery of Maxwells theory of classical electrodynamics. The gauge principle has led to the development of many interesting quantum field theories, among them the standard model of particle physics which is a gauge theory with the underlying gauge group being $SU(3) \times SU(2) \times U(1)$. Even general relativity and more so the quantum approach to general relativity may be considered as gauge theories. Although gauge theories are a key ingredient of all particle physics theories, there are still some unsolved problems.

The key idea of a gauge theory is to find certain local transformations of the fundamental fields such that the Lagrangian stays unchanged under these gauge transformations. In the following we will introduce the concept of gauge invariance and gauge transformations first in the continuum formulation and then construct the corresponding lattice formulation.

2.2.1 Continuum formulation

2.2.1.1 U(1) gauge theory

For our introduction to gauge theories, we will consider a simple example theory namely $U(1)$ gauge theory with fermions, which will help to illustrate many important facts of gauge theories. In the next section we will then generalise the introduced concepts to non-abelian Lie groups. Some reasons for choosing the $U(1)$ group as our showcase theory are:

- it is the simplest unitary Lie group
- it's the gauge group of electrodynamics
- it's abelian and thus simpler for a first discussion

As we have now specified the group in which our gauge fields live, let's introduce the fermion fields denoted by ψ and their adjoint fields $\bar{\psi} = \psi^\dagger \gamma^0$, which are the Dirac spinors

$$\psi(x) = \begin{bmatrix} \psi_1(x) \\ \psi_2(x) \\ \psi_3(x) \\ \psi_4(x) \end{bmatrix} \quad \bar{\psi}(x) = [\bar{\psi}_1(x), \bar{\psi}_2(x), \bar{\psi}_3(x), \bar{\psi}_4(x)] \quad .$$

The second type of fields we need are the gauge fields $A_\mu(x) \in \mathbb{R}$ and the corresponding field strength tensor

$$F_{\mu\nu}(x) = \partial_\mu A_\nu(x) - \partial_\nu A_\mu(x) \quad . \quad (2.20)$$

Here we use euclidean spacetime indices $\mu, \nu = 1, 2, 3, 4$. From a course in electrodynamics or various textbooks we know that for given electric and magnetic fields, the vector potential $A_\mu(x)$ is not unique and we have a certain freedom to change it with a gauge transformation. This also implies a gauge transformation for the fermion fields in the form of a local phase shift. We may summarize the $U(1)$ gauge transformation as follows:

$$A'_\mu(x) = A_\mu(x) - \partial_\mu \Lambda(x) \quad , \quad \Lambda(x) \in \mathbb{R} \text{ arbitrary} \quad , \quad (2.21)$$

$$\psi'(x) = e^{ie\Lambda(x)} \psi(x) \quad , \quad \bar{\psi}'(x) = \bar{\psi}(x) e^{-ie\Lambda(x)} \quad , \quad (2.22)$$

where e denotes the coupling constant which for $U(1)$ is the electric charge. The transformation of the fields leaves the field strength tensor invariant:

$$\begin{aligned} F'_{\mu\nu}(x) &= \partial_\mu A'_\nu(x) - \partial_\nu A'_\mu(x) = \partial_\mu(A_\nu(x) - \partial_\nu \Lambda(x)) - \partial_\nu(A_\mu(x) - \partial_\mu \Lambda(x)) \\ &= \partial_\mu A_\nu(x) - \partial_\nu A_\mu(x) - \partial_\mu \partial_\nu \Lambda(x) + \partial_\nu \partial_\mu \Lambda(x) = \partial_\mu A_\nu(x) - \partial_\nu A_\mu(x) = F_{\mu\nu}(x) \quad . \end{aligned}$$

The next step is to separate the Euclidean action into a gauge part and a fermionic part $S[\bar{\psi}, \psi, A] = S_G[A] + S_F[\bar{\psi}, \psi, A]$ and consider these parts individually with respect to their gauge invariance. The gauge part of the action reads

$$S_G[A] = \frac{1}{4} \int d^4x \quad F_{\mu\nu}(x) F^{\mu\nu}(x) \quad , \quad (2.23)$$

which we have just proven to be gauge invariant.

The fermionic part of the action is given by

$$S_F[\bar{\psi}, \psi, A] = \int d^4x \quad \bar{\psi}(x) [\gamma_\mu (\partial_\mu + ieA_\mu(x)) + m] \psi(x) \quad , \quad (2.24)$$

where the γ_μ are the Euclidean Dirac matrices. In the mass term the phases that

$\bar{\psi}(x)$ and $\psi(x)$ pick up in the gauge transformation (2.18) cancel, such that this term is trivially gauge invariant. To show that the other terms are gauge invariant, we introduce a quantity called covariant derivative $D_\mu = \partial_\mu + ieA_\mu(x)$ which can easily be seen to obey a transformation relation of the following form: $D'_\mu(x) = e^{ie\Lambda(x)}D_\mu(x)e^{-ie\Lambda(x)}$. With this, the theory is invariant under the gauge transformations (2.17),(2.18).

2.2.1.2 SU(N) gauge theory

As mentioned earlier, we can now easily generalise the procedure described in the previous section to gauge theories with arbitrary non-abelian Lie groups, such as $SU(N)$. These theories are generally also known as Yang-Mills theories. The key difference is now, that the gauge transformation is no longer just a phase shift, like in the $U(1)$ case, but rather a more general transformations with the generators of the $SU(N)$ group.

We consider a $SU(N)$ invariant theory, with arbitrary N . The action is now given by

$$S[\bar{\psi}, \psi, A] = \underbrace{\frac{1}{2g^2} \int d^4x \operatorname{Tr}[F_{\mu\nu}(x)F_{\mu\nu}(x)]}_{S_G[A]} + \underbrace{\sum_{f=1}^{N_f} \int d^4x \bar{\psi}^{(f)}(x)[m^{(f)} + \not{D}(x)]\psi^{(f)}(x)}_{S_F[\bar{\psi}, \psi, A]}, \quad (2.25)$$

with $F_{\mu\nu}(x) = \partial_\mu A_\nu(x) - \partial_\nu A_\mu(x) + i[A_\mu(x), A_\nu(x)]$ again denoting the field strength tensor, which in the $SU(N)$ case picks up a new term, due to the non-abelian character of the group. The gauge transformation of the fermion fields is simply given by $\psi(x)' = \Lambda(x)\psi(x)$, and for the adjoint fields $\bar{\psi}(x)' = \bar{\psi}(x)\Lambda(x)^\dagger$ where $\Lambda(x)$ denotes the gauge transformation matrix which is an element of the group $SU(N)$. Also here the kinetic term ∂_μ is the one that breaks the gauge symmetry. Thus we again need to introduce the covariant derivative $D_\mu = \partial_\mu + igA_\mu(x)$. As we are now dealing with a general theory, we denote the coupling constant with g , as stated before. For the covariant derivative we demand the following transformation rule

$$D'_\mu(x) = \Lambda(x)D_\mu(x)\Lambda(x)^\dagger, \quad (2.26)$$

which in turn implies the following transformation rule for the gauge field

$$A'_\mu(x) = \Lambda(x)A_\mu(x)\Lambda(x)^\dagger - \frac{i}{g}\Lambda(x)(\partial_\mu\Lambda(x)^\dagger), \quad (2.27)$$

such that the Lagrangian is now completely invariant.

2.2.1.3 Lattice regularisation of SU(N) gauge theory

If we now discretise the action given in Equation (2.22), we need to repeat the substitutions we performed to regularise the theory as described in Section 2.1.1.2. So we

replace the continuous spacetime by a hypercubic spacetime lattice, therefore the derivative $\partial_\mu \psi(x)$ becomes $\frac{\psi(n+\hat{\mu})-\psi(n-\hat{\mu})}{2a}$, x gets mapped to $n \in \Lambda_4$ and of course the integral over all configurations gets replaced by a sum over all lattice sites. When requiring invariance of the Lagrangian under the gauge transformation $\psi(n)' = \Lambda(n)\psi(n)$ with $\Lambda(n) \in SU(N)$ and $\Lambda(n)^\dagger \Lambda(n) = \mathbb{I}$, we see that in the fermionic part the mass term is invariant while the nearest neighbour terms of the derivative transform into

$$\bar{\psi}'(n)\gamma_\mu\psi'(n+\hat{\mu}) = \bar{\psi}(n)\underbrace{\Lambda(n)^\dagger\Lambda(n+\hat{\mu})}_{\neq\mathbb{I}}\gamma_\mu\psi(n+\hat{\mu}) \quad ,$$

which is definitely not invariant. Unlike in the continuum formulation we do not introduce a covariant derivative here to render this term invariant, but rather introduce quantities $U_\mu(n)$ which are commonly referred to as gauge links or link variables and are added in the nearest neighbour terms

$$\bar{\psi}(n)\gamma_\mu\psi(n+\hat{\mu}) \rightarrow \bar{\psi}(n)\gamma_\mu U_\mu\psi(n+\hat{\mu}) \quad . \quad (2.28)$$

These gauge links obey the transformation rule

$$U'_\mu(x) = \Lambda(n)U_\mu(n)\Lambda(n+\hat{\mu}) \quad ,$$

such that the nearest neighbour terms (2.25) are invariant. These gauge links sit on the



FIGURE 2.1: Graphical representation of the gauge link variables.

link between two lattice sites and may be illustrated as shown in Figure 2.1. The link variables play the role of the gauge fields on the lattice, which is justified as they have the information of the gauge fields encoded within them: we may write the group valued link variables $U_\mu(n)$ with the algebra valued fields $A_\mu(n)$: $U_\mu(n) = e^{iaA_\mu(n)}$ and using expansion in a one may show that the terms (2.25) give rise to the covariant derivative.

All that is left to do now is construct a gauge invariant term for the gauge part of the action. To achieve this we need to find a suitable expression for the field strength tensor in terms of the gauge links. For this we use the following notation of the field strength tensor $F_{\mu\nu}(x) = \frac{1}{ig}[D_\mu(x), D_\nu(x)]$ and then try to build a gauge invariant quantity using the gauge links. To achieve this we want to build a gauge invariant quantity formed by the gauge links $U_\mu(x)$. One quickly finds that a simple gauge invariant quantity one can construct out of the gauge links is the trace of a product of gauge links arranged along

the squares of the lattice. We denote the plaquettes as $p_{\mu\nu}$ and define them as

$$p_{\mu\nu}(n) = U_\mu(n) U_\nu(n + \hat{\mu}) U_\mu(n + \hat{\nu})^\dagger U_\nu(n)^\dagger . \quad (2.29)$$

These so-called plaquettes may be represented graphically as shown in Fig. 2.2.

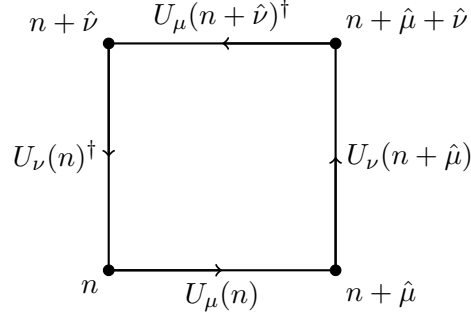


FIGURE 2.2: Graphical illustration of a plaquette on the lattice.

We now show that the trace of a plaquette is gauge invariant:

$$\begin{aligned} \text{Tr}[p_{\mu\nu}(n)] &= \text{Tr}[U_\mu(n) U_\nu(n + \hat{\mu}) U_\mu(n + \hat{\nu})^\dagger U_\nu(n)^\dagger] \\ &= \text{Tr}[\Lambda(n) U_\mu(n) \underbrace{\Lambda(n + \hat{\mu})^\dagger \Lambda(n + \hat{\mu})}_{\mathbb{I}} U_\nu(n + \hat{\mu}) \underbrace{\Lambda(n + \hat{\mu} + \hat{\nu})^\dagger \Lambda(n + \hat{\mu} + \hat{\nu})}_{\mathbb{I}} \\ &\quad U_\mu(n + \hat{\nu})^\dagger \underbrace{\Lambda(n + \hat{\nu})^\dagger \Lambda(n + \hat{\nu})}_{\mathbb{I}} U_\nu(n)^\dagger \Lambda(n)^\dagger] \\ &= \text{Tr}[\Lambda(n) U_\mu(n) U_\nu(n + \hat{\mu}) U_\mu(n + \hat{\nu})^\dagger U_\nu(n)^\dagger \Lambda(n)^\dagger] = \text{Tr}[p_{\mu\nu}(n)] . \end{aligned}$$

In the last step we used the cyclic permutation property of the trace. This then concludes our proof. Using the plaquette we can now identify the gauge part of the action for a $SU(N)$ theory to be

$$S_G[U] = \frac{2}{g^2} \sum_{n \in \Lambda_4} \sum_{\mu < \nu} \mathcal{R}e(\text{Tr}[\mathbb{I} - p_{\mu\nu}(n)]) , \quad (2.30)$$

commonly often referred to as Wilson gauge action. The factor $\frac{2}{g^2}$ is included to match the continuum action which again we may obtain by writing $U_\mu(n) = e^{iaA_\mu(n)}$ and expanding in a .

As promised in the beginning we will now give a short and rudimentary overview of the aspects of dealing with fermions in a lattice theory. The first thing to stress is that due to the Pauli exclusion principle, fermion field operators obey anti-commutation relations. In the path integral formulation we describe fermions with Grassmann numbers, which are anti-commuting and nilpotent. With these numbers and their properties one can easily derive derivation and integration rules for the fermion fields (see e.g. [9]). The

partition sum for the full theory can be written as follows:

$$Z = \int D[U] e^{-S_G[U]} \int \prod_{f=1}^{N_f} D[\bar{\psi}^{(f)}, \psi^{(f)}] \prod_{f=1}^{N_f} e^{-S_F[\bar{\psi}^{(f)}, \psi^{(f)}, U]} , \quad (2.31)$$

with N_f denoting the number of flavours. As in the continuum the fermion action is a bilinear form, where the kernel is lattice discretisation of the Dirac operator $m + \not{D}$. Thus we can write the lattice fermion action as

$$S_F = \sum_{x,y} \bar{\psi}(x) D(x,y) \psi(y) ,$$

where $D(x,y)$ is the lattice Dirac operator. We do not discuss further details of the lattice Dirac operator, but remark that it is necessary to add the so-called Wilson term which removes additional mass poles of the theory and has the properties of being irrelevant for $a \rightarrow 0$ and decoupling from the theory in this limit. With this we conclude our brief remarks on lattice fermions.

2.3 Monte Carlo simulation in lattice field theory

Monte Carlo simulations, originally developed in statistical physics, can be applied to numerous fields including stock market analysis, simulation of board games and many others. In the area of theoretical physics Monte Carlo methods play an important role in the simulation of lattice field theories. To be more precise in our work we actually use a specific Monte Carlo method called Metropolis algorithm. In lattice field theory as well as in statistical physics, Monte Carlo simulations based on the Metropolis algorithm are the method to use for simulating the dynamics of a theory and calculating observables.

For introducing the method, we again use a simple scalar theory with partition function defined by

$$Z = \int D[\phi] e^{-S[\phi]} , \quad (2.32)$$

and the action is given by

$$S[\phi] = a^4 \sum_{n \in \Lambda} \frac{1}{2} \left[m^2 + \frac{8}{a^2} \right] \phi(n)^2 + \lambda \phi(n)^4 - \sum_{\mu=1}^4 \phi(n) \phi(n + \hat{\mu}) ,$$

with $\Lambda = N_{\text{spatial}}^3 \cdot N_{\text{temporal}}$ being the spacetime lattice. Possible simple observables are, e.g., the mean value of ϕ^2 or the correlation function of the fields. We then can obtain the vacuum expectation value of an observable in the following way:

$$\langle \mathcal{O} \rangle = \frac{1}{Z} \int D[\phi] e^{-S[\phi]} \mathcal{O}[\phi] . \quad (2.33)$$

The reason to use Monte Carlo methods here is, that this integral cannot be solved exactly. Monte Carlo simulations approximate the integral by the average of the observables evaluated on N sample field configurations which are generated randomly according to a probability distribution. If we then would send N to infinity, we would obtain the exact value of the integral of interest. For the integral (2.29) we can identify the probability distribution as $P[\phi] = \frac{1}{Z} e^{-\frac{S}{\hbar}}$.

In this setting the Metropolis algorithm works like the following:

- 1) Generate a new proposal field configuration $\tilde{\phi}$ near the current one, typically by changing the field at a single site.
- 2) Calculate a quantity called Metropolis ratio $\rho = \frac{P[\tilde{\phi}]}{P[\phi]}$, which is given by the ratio of the weight factors of the proposal and the old field configuration.
- 3) Generate a random number r , uniformly distributed in the interval $[0, 1]$.
- 4) Check the relation $r < \rho$, if true, accept the new field configuration and overwrite the old one or else keep the old one as the current one.

The above described steps of the Metropolis algorithm are repeated in a loop over all lattice sites and updating all fields with the steps 1)-4) is called a sweep.

The general structure of the Monte Carlo simulation for our example theory is given in the following steps:

- i) Choose the values of the parameters m, λ and set $\phi(n) = 0, \forall n$.
- ii) Perform equilibrating sweeps of the order $O(10^4)$ - $O(10^6)$.
- iii) Loop over the number of measurements N one wants to perform, usually of the order $O(10^6)$. Inside this loop:
 - Perform sweeps of the order $O(10)$ - $O(10^2)$ to decorrelate the theory.
 - Calculate the observables.
 - Write them into an array.
- iv) calculate the mean value $\langle \mathcal{O} \rangle_N = \frac{1}{N} \sum_{i=1}^N \mathcal{O}[\phi^i]$ and the numerical statistical error, which scales $\sim \frac{1}{\sqrt{N}}$

All our simulation results have been obtained using the steps i)-iv).

2.4 Dual approach to lattice theories

It is well known that when dealing with lattice theories at finite chemical potential or with a topological term, one usually stumbles over a sign problem which causes problems for a Monte Carlo simulation. These sign problems arise from the fact, that the action S is complex and thus the Boltzmann factor e^{-S} cannot be used as a stochastic weight for the simulation process. The main idea for the dual approach is to exactly rewrite the partition sum of the theory in terms of new variables which are called *dual variables*. Using the concept of dual variables has a long history and one of its earliest applications was to compute the critical point of the 2-dimensional Ising model [10]. A key aspect of the dualisation method is that using different representations reveal different aspects of a theory. In more recent years it has been understood that the dualisation method may overcome and solve sign problems in many abelian theories. It gets a little more tricky when dealing with non-abelian theories due to the non-commutative factor of the group elements, but dual representations are known and are still subject of intensive research.

The general outline of the dualisation process is as follows. First one factorises the Boltzmann factor into local exponents and then expands them in a Taylor series. The next step is to perform the integration over the original fields, after which the expansion indices can be identified as our dual variables and replace the conventional fields as the new degrees of freedom for the theory.

In this introduction we will show how the dualisation method works using $U(1)$ lattice gauge theory. $U(1)$ lattice gauge theory has no sign problem, but it needs to be mentioned that we did encounter a sign problem in the $SU(2)$ theory this thesis is devoted to. But the appearance of that sign problem had a different reason than that of a normal complex action sign problem.

2.4.1 Dualisation of $U(1)$ gauge theory

Before we begin with the dualisation, we first need to introduce the theory. The degrees of freedom are the gauge link fields $U_{x,\nu} \in U(1)$ sitting on the links of the lattice. We use a 4-dimensional lattice with periodic boundary conditions. As we are dealing with a pure gauge theory, the action is simply the $U(1)$ Wilson gauge action, given by

$$S_G[U] = -\frac{\beta}{2} \sum_x \sum_{\nu < \rho} [U_{x,\nu\rho} + U_{x,\nu\rho}^*] \quad . \quad (2.34)$$

The variable β denotes the inverse gauge coupling and the arguments of the gauge action are the plaquette variables $U_{x,\nu\rho}$ which are formed by the oriented product of the link

variables

$$U_{x,\nu\rho} = U_{x,\nu} U_{x+\hat{\nu},\rho} U_{x+\hat{\rho},\nu}^* U_{x,\rho}^* .$$

We to stress, that the star denotes complex conjugation, which is justified because we are only dealing with elements of $U(1)$ here and hermitean conjugation reduces to complex conjugation. We now label the lattice sites with x rather than n , different from the notation used in the previous section, but that is just a convention.

The partition sum for the theory is given by

$$Z = \int D[U] e^{-S_G} , \quad (2.35)$$

with the integral measure being a product over all lattice sites x and all directions ν . We will later use the following parametrisation for the integration of our gauge variables: $U_{x,\nu} = e^{i\varphi_{x,\nu}} \in U(1)$, which then are integrated over the unit cycle. The integral measure then reads

$$\int D[U] = \prod_{x,\nu} \int_{-\pi}^{\pi} \frac{d\varphi_{x,\nu}}{2\pi} ,$$

where $\frac{1}{2\pi}$ is the normalisation factor of the integral.

The first step now is to insert the gauge action and write Equation (2.31) in the form

$$Z = \int D[U] e^{\frac{\beta}{2} \sum_x \sum_{\nu<\rho} [U_{x,\nu\rho} + U_{x,\nu\rho}^*]} . \quad (2.36)$$

We can now pull the sums in the exponents down as products and factorise the exponentials, as described in the introduction to this section, after which we Taylor-expand the individual components and arrive at the following expression

$$Z = \int D[U] \prod_x \prod_{\nu<\rho} \sum_{m_{x,\nu\rho}=0}^{\infty} \sum_{\bar{m}_{x,\nu\rho}=0}^{\infty} \frac{\left(\frac{\beta}{2}\right)^{m_{x,\nu\rho}}}{m_{x,\nu\rho}!} \frac{\left(\frac{\beta}{2}\right)^{\bar{m}_{x,\nu\rho}}}{\bar{m}_{x,\nu\rho}!} (U_{x,\nu\rho})^{m_{x,\nu\rho}} (U_{x,\nu\rho}^*)^{\bar{m}_{x,\nu\rho}} , \quad (2.37)$$

where we have introduced $(m_{x,\nu\rho}, \bar{m}_{x,\nu\rho}) \in [0, \infty)$ as expansion indices that are attached to the plaquettes. We can now introduce the sum over all configurations of our expansion indices as $\sum_{\{m,\bar{m}\}} = \prod_x \prod_{\nu<\rho} \sum_{m_{x,\nu\rho}=0}^{\infty} \sum_{\bar{m}_{x,\nu\rho}=0}^{\infty}$ and write the partition function as follows

$$Z = \int D[U] \sum_{\{m,\bar{m}\}} \prod_x \prod_{\nu<\rho} \left(\frac{\left(\frac{\beta}{2}\right)^{m_{x,\nu\rho} + \bar{m}_{x,\nu\rho}}}{m_{x,\nu\rho}! \bar{m}_{x,\nu\rho}!} \right) (U_{x,\nu\rho})^{m_{x,\nu\rho}} (U_{x,\nu\rho}^*)^{\bar{m}_{x,\nu\rho}} .$$

We can identify the factor that contains β and the factorials as a weight factor and introduce the abbreviation

$$W[\beta] = \prod_x \prod_{\nu < \rho} \left(\frac{\left(\frac{\beta}{2}\right)^{m_{x,\nu\rho} + \bar{m}_{x,\nu\rho}}}{m_{x,\nu\rho}! \bar{m}_{x,\nu\rho}!} \right), \quad (2.38)$$

for convenience. The next step is to write out the plaquette variables in terms of the link variables, factorise them and reorganise the terms, by shifting the indices, into powers of the gauge links $U_{x,\nu}$. The whole calculation can be found in Appendix A. The partition function now becomes

$$Z = \int D[U] \sum_{\{m, \bar{m}\}} W[\beta] \prod_x \prod_{\nu} (U_{x,\nu})^{\sum_{\rho: \nu < \rho} [m_{x,\nu\rho} + \bar{m}_{x-\hat{\rho},\nu\rho}] + \sum_{\rho: \rho < \nu} [m_{x-\hat{\rho},\rho\nu} + \bar{m}_{x,\rho\nu}]} \times \\ \prod_x \prod_{\nu} (U_{x,\nu}^*)^{\sum_{\rho: \nu < \rho} [\bar{m}_{x,\nu\rho} + m_{x-\hat{\rho},\nu\rho}] + \sum_{\rho: \rho < \nu} [\bar{m}_{x-\hat{\rho},\rho\nu} + m_{x,\rho\nu}]} .$$

As our gauge link variables are elements of $U(1)$, we can use the property $U_{x,\nu}^m = ((e^{i\varphi_{x,\nu}})^*)^m = (e^{-i\varphi_{x,\nu}})^m = (e^{i\varphi})^{-m} = (U_{x,\nu})^{-m}$ to rewrite the expression in the following way

$$Z = \int D[U] \sum_{\{m, \bar{m}\}} W[\beta] \times \\ \prod_x \prod_{\nu} (U_{x,\nu})^{\sum_{\rho: \nu < \rho} [m_{x,\nu\rho} - \bar{m}_{x,\nu\rho} + \bar{m}_{x-\hat{\rho},\nu\rho} - m_{x+\hat{\rho},\nu\rho}] + \sum_{\rho: \rho < \nu} [m_{x-\hat{\rho},\rho\nu} - \bar{m}_{x-\hat{\rho},\rho\nu} + \bar{m}_{x,\rho\nu} - m_{x,\rho\nu}]} .$$

We introduce a new variable $p_{x,\nu\rho} = m_{x,\nu\rho} - \bar{m}_{x,\nu\rho}$ which we promote to a new dynamical variable of our theory $p_{x,\nu\rho} \in \mathbb{Z}$. This together with another set of variables we call $q_{x,\nu} \in \mathbb{N}_0$. This is the final set of dual variables we use to describe our gauge fields. They are related to $m_{x,\nu\rho}$ and $\bar{m}_{x,\nu\rho}$ via the relations $m_{x,\nu\rho} - \bar{m}_{x,\nu\rho} = p_{x,\nu\rho}$ and $m_{x,\nu\rho} + \bar{m}_{x,\nu\rho} = |p_{x,\nu\rho}| + 2q_{x,\nu\rho}$. Inserting this in the equation from above gives

$$Z = \int D[U] \sum_{\{p, q\}} W[\beta] \prod_x \prod_{\nu} (U_{x,\nu})^{\sum_{\rho: \nu < \rho} [p_{x,\nu\rho} - p_{x-\hat{\rho},\nu\rho}] + \sum_{\rho: \rho < \nu} [p_{x-\hat{\rho},\rho\nu} - p_{x,\rho\nu}]} , \quad (2.39)$$

with $W[\beta]$ now given by

$$W[\beta] = \prod_x \prod_{\nu < \rho} \left(\frac{\left(\frac{\beta}{2}\right)^{|p_{x,\nu\rho}| + 2q_{x,\nu\rho}}}{(|p_{x,\nu\rho}| + q_{x,\nu\rho})! (q_{x,\nu\rho})!} \right) .$$

The variables p will be referred to as plaquette occupation numbers or plaquette variables and will in the end be identified as our new dual variables. The plaquette variables consist of an oriented flux running along the links, counterclockwise if positive and clockwise if negative. Note that also the plaquettes $U_{x,\nu\rho}$ had this kind of orientation.

After this rewriting and factorisation we can finally evaluate the integral. For this we plug in the $U(1)$ Haar measure given in Equation (2.32) and the definition for $U_{x,\nu}$ into Equation (2.34) and arrive at

$$Z = \sum_{\{p,q\}} W[\beta] \prod_{x,\nu} \frac{1}{2\pi} \int_{-\pi}^{\pi} d\varphi_{x,\nu} (e^{i\varphi_{x,\nu}})^{\sum_{\rho:\nu<\rho} [p_{x,\nu\rho} - p_{x-\hat{\rho},\nu\rho}] + \sum_{\rho:\rho<\nu} [p_{x-\hat{\rho},\rho\nu} - p_{x,\rho\nu}]} .$$

The terms in the integral are just integrations over a phase and give rise to Kronecker deltas. These in turn implement constraints for the flux running along links shared by two adjacent plaquette variables. For notational convenience the Kronecker deltas will be denoted as $\delta_{n,o} = \delta(n)$. Furthermore, since the $q_{x,\nu\rho}$ do not have any constraints, the summation over the variables $q_{x,\nu\rho}$ can in this case be done in closed form, using the series representation of the modified Bessel function $\sum_{q=0}^{\infty} \frac{(\frac{\beta}{2})^{|p|+2q}}{(|p|+q)! (q)!} = I_{|p|}(\beta) = I_p(\beta)$. With all this taken into account the partition function reads

$$Z = \sum_{\{p\}} \left(\prod_{x,\nu<\rho} I_{p_{x,\nu\rho}}(\beta) \right) \left(\prod_{x,\nu} \delta \left(\sum_{\rho:\nu<\rho} [p_{x,\nu\rho} - p_{x-\hat{\rho},\nu\rho}] + \sum_{\rho:\rho<\nu} [p_{x-\hat{\rho},\rho\nu} - p_{x,\rho\nu}] \right) \right) , \quad (2.40)$$

where we have finally obtained the dualised version of the theory, which only depends on the dual variable $p_{x,\nu\rho}$.

To shortly summarise what has been done in this chapter, we have mapped our original theory to a dual representation by integrating out the conventional $U(1)$ gauge fields and replacing them with plaquette variables $p_{x,\nu\rho} \in \mathbb{Z}$, which are our new degrees of freedom. The plaquette variables have to obey certain constraints concerning the flux that runs along the links of the lattice. Thus the configurations cannot be chosen arbitrarily.

As we will see in Chapter 3, the general steps of the dualisation work the same for any of the $SU(N)$ Lie groups, e.g. in our case $SU(2)$. However, these groups are no longer abelian which brings in new challenges for the dualisation.

2.5 Observables in the dual representation

As discussed in the beginning of this chapter, we will now briefly discuss some observables of interest. These observables are also the ones we calculated and analysed in our model. The first observable one can extract from equation (2.35) is the plaquette expectation value

$$\langle p_{x,\nu\rho} \rangle = -\frac{1}{6V} \frac{\partial \ln(Z)}{\partial (\frac{\beta}{2})} , \quad (2.41)$$

which is obtained in the same way as the energy of a canonical system in statistical physics, as a derivative with respect to the inverse gauge coupling. More specifically it

is the action density of the $U(1)$ lattice gauge theory we consider. The term $\frac{1}{6V}$ is the normalisation constant in 4-dimensions. The second observable we are interested in is the plaquette susceptibility χ of the system. The susceptibility is obtained by taking another derivative of equation (2.36) with respect to the inverse gauge coupling β , or otherwise written as

$$\chi = \frac{\partial}{\partial(\frac{\beta}{2})} \langle p_{x,\nu\rho} \rangle = -\frac{1}{6V} \frac{\partial^2 \ln(Z)}{\partial(\frac{\beta}{2})^2} . \quad (2.42)$$

Of course there are many other interesting observables, e.g. correlators, but as for this thesis we did not consider them and hence there is no use in dwelling on this topic any longer.

Chapter 3

Dual representation of pure $SU(2)$ lattice gauge theory

As mentioned in the introduction to Section 2.4., the dualisation method has been successfully applied to many abelian theories in the past. In recent years there have been efforts to extend the use of this technique to non-abelian theories. A few such representations are known by now, but they present some challenges for the dualisation procedure as well as for numerical simulations. One of the problems arises because of the non-commutative character of the group elements, while another problem concerns finding a suitable parametrisation of the group elements. The basis for our work is taken from the paper [3] in which a new technique was developed to dualise $SU(2)$ lattice gauge theory. The new technique featured in this paper is named Abelian Colour Cycles (ACC) and comes about when we decompose the gauge action into abelian parts, which after dualisation gives rise to new degrees of freedom that can be interpreted as loops around a plaquette in colour space, the ACCs. We remark that the paper also deals with the dualisation of fermions which will not be covered in this thesis.

One good reason to consider the $SU(2)$ model is that it is the easiest non-abelian Lie group which comes in handy for a first discussion and furthermore gives us a simplified model theory for QCD. The technique described in the paper above has also been extended to $SU(3)$ already [11]. However, the $SU(3)$ version however will not be featured here, as we use the $SU(2)$ "toy model" as a tool to search for different strategies to overcome the above mentioned problems and develop new dual representations for simulations.

In the following sections we will outline the dualisation steps of the theory, highlight the features and problems that arise during the procedure, and finally present a graphical representation of the new found approach. The discussion of the following sections follows closely the steps of [3].

3.1 Dualisation of $SU(2)$ lattice gauge theory

The model used in [3] is $SU(2)$ lattice gauge theory with the Wilson gauge action given by

$$S_G[U] = -\frac{\beta}{2} \sum_{x,\mu < \nu} \text{Tr}[U_{x,\mu} U_{x+\hat{\mu},\nu} U_{x+\hat{\nu},\mu}^\dagger U_{x,\nu}^\dagger] , \quad (3.1)$$

where the gauge link variables $U_{x,\mu} \in SU(2)$ denote the dynamical degrees of freedom which sit on the links of a 4-dimensional lattice with periodic boundary conditions. The trace operation here is understood as a trace in colour space. The partition function of the theory is given by

$$Z = \int D[U] e^{-S_G[U]} . \quad (3.2)$$

The key aspect of the new ACC technique is, as stated in the paper, to write the trace over the colour indices and the matrix multiplications as an explicit sum. With this Equation (3.1) takes the following form

$$S_G[U] = -\frac{\beta}{2} \sum_{x,\mu < \nu} \sum_{a,b,c,d=0}^1 U_{x,\mu}^{ab} U_{x+\hat{\mu},\nu}^{bc} U_{x+\hat{\nu},\mu}^{dc*} U_{x,\nu}^{ad*} . \quad (3.3)$$

If we compare the $U(1)$ theory given in Section 2.4 with the $SU(2)$ theory, we find that each lattice site picks up an additional degree of freedom, i.e., the colour dimension. Instead of a hermitean conjugation a complex conjugation is used in Equation (3.2) as we now consider the matrix elements $U_{x,\mu}^{ab}$, which are complex numbers. The products of these matrix components $U_{x,\mu}^{ab} U_{x+\hat{\mu},\nu}^{bc} U_{x+\hat{\nu},\mu}^{dc*} U_{x,\nu}^{ad*}$ are referred to as Abelian Colour Cycles. The ACCs are complex numbers and feature 4 colour indices (a, b, c, d) , one at each corner of the plaquette. Since we consider $SU(2)$ here we find that the colour indices can only take 2 different values, namely 0 or 1. These values were chosen differently in the paper (as 1,2), but our choice is more convenient when simulating the theory.

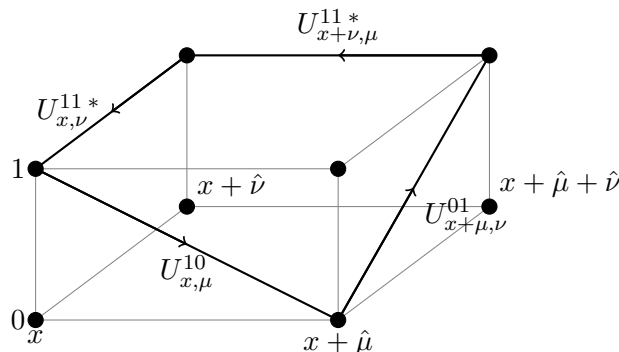


FIGURE 3.1: Graphical representation of the example 1011 ACC. This Figure adapted from [3]

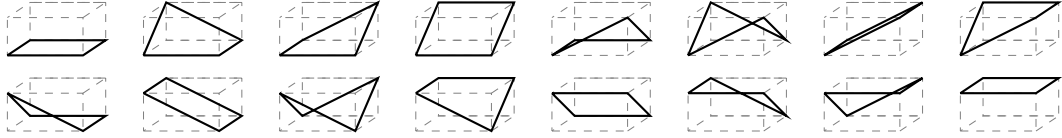


FIGURE 3.2: All 16 possible ACC configurations. (Figure taken from [3])

To get a better understanding of this and what is meant by the loops winding in colour space, it is useful to find a geometrical representation of the ACCs. In Fig. 3.1 we depict as an example the 1011 ACC in the $\mu-\nu$ -plane, which is given by $U_{x,\mu}^{10} U_{x+\hat{\mu},\nu}^{01} U_{x+\hat{\nu},\mu}^{11*} U_{x,\nu}^{11*}$ in terms of the elements of the link variables. Here we use two layers labeled 0 and 1 to illustrate the two different colours. As shown in the figure, each of the ACC elements is a directed flux running from one lattice site to a neighbour site, with the direction indicated by the arrow. The first element of the ACC is depicted by the front link in Figure 3.1 and connects the site x which has the associated colour value $a = 1$ with the site $x + \hat{\mu}$ with corresponding colour $b = 0$, with the flux running in positive μ direction. The element $U_{x+\hat{\mu},\nu}^{10}$ points in positive ν direction and connects site $x + \hat{\mu}$ and colour 0 with site $x + \hat{\mu} + \hat{\nu}$ and colour 1. The other two link representatives, i.e., $U_{x+\hat{\nu},\mu}^{11*}$, $U_{x,\nu}^{11*}$, in the ACC are complex conjugated, which we illustrate in Figure 3.1 by the arrow in negative direction, and thereby close the ACC. We stress that for $SU(2)$ the trace of the plaquette is already real. Because of this one does not need to explicitly project out the real part of the action. Thus all plaquettes are oriented in a mathematically positive sense.

As stated before, there are 16 possibilities a loop can wind around a plaquette all of which we depict in Figure 3.2.

If we insert the gauge action of Equation (3.3) into the partition function (3.2) we get

$$Z = \int D[U] e^{\frac{\beta}{2} \sum_{x,\mu<\nu} \sum_{a,b,c,d} U_{x,\mu}^{ab} U_{x+\hat{\mu},\nu}^{bc} U_{x+\hat{\nu},\mu}^{dc*} U_{x,\nu}^{ad*}} . \quad (3.4)$$

In complete analogy to the steps in Section 2.4 we can now pull the sums from the exponent down as products and expand the Boltzmann factors in a power series, such that the partition function becomes

$$Z = \int D[U] \prod_{x,\mu<\nu} \prod_{a,b,c,d} \sum_{p_{x,\mu\nu}^{abcd}=0}^{\infty} \frac{\left(\frac{\beta}{2}\right)^{p_{x,\mu\nu}^{abcd}}}{p_{x,\mu\nu}^{abcd}!} (U_{x,\mu}^{ab} U_{x+\hat{\mu},\nu}^{bc} U_{x+\hat{\nu},\mu}^{dc*} U_{x,\nu}^{ad*})^{p_{x,\mu\nu}^{abcd}} . \quad (3.5)$$

The expansion index $p_{x,\mu\nu}^{abcd} \in \mathbb{N}_0$ will be regarded as *cycle occupation number* which counts how many loops wind around the plaquette $(x, \mu\nu)$ with a specific configuration a, b, c, d of colours on the 4 corners. These cycle occupation numbers will later be identified as our dual variables.

One immediately notices that the term that contains β and the factorial does not depend on the link variables $U_{x,\mu}^{ab}$ and can therefore be pulled out of the integral as a weight factor. We introduce the sum over all configurations of the cycle occupation numbers as $\sum_{\{p\}} = \prod_{x,\mu < \nu} \prod_{a,b,c,d=0}^1 \sum_{p_{x,\mu\nu}^{abcd}=0}^{\infty}$ and write the integral measure as

$$\int D[U] = \prod_{x,\mu} \int dU_{x,\mu} \quad , \quad (3.6)$$

where $dU_{x,\mu}$ is the Haar measure for the link $U_{x,\mu}$. We arrive at the following expression for Equation (3.5)

$$Z = \sum_{\{p\}} \left[\prod_{x,\mu < \nu} \prod_{a,b,c,d} \frac{\left(\frac{\beta}{2}\right)^{p_{x,\mu\nu}^{abcd}}}{p_{x,\mu\nu}^{abcd}!} \right] \prod_{x,\mu} \int dU_{x,\mu} \prod_{x,\mu < \nu} \prod_{a,b,c,d=0}^1 (U_{x,\mu}^{ab} U_{x+\hat{\mu},\nu}^{bc} U_{x+\hat{\nu},\mu}^{dc} U_{x,\nu}^{ad})^{p_{x,\mu\nu}^{abcd}} \quad . \quad (3.7)$$

Note that the arguments in the integral, i.e., the ACC, are only complex numbers thus we can commute and rewrite them such that the integral takes a more convenient form. This is done in a similar way as for the $U(1)$ theory by reorganising the terms. The corresponding calculation can be found in Appendix B.

After the steps given in Appendix B, we arrive at the following expression:

$$Z = \sum_{\{p\}} W_{\beta}[p] \prod_{x,\mu} \int dU_{x,\mu} \prod_{a,b=0}^1 (U_{x,\mu}^{ab})^{N_{x,\mu}^{ab}} (U_{x,\mu}^{ab})^{\bar{N}_{x,\mu}^{ab}} \quad . \quad (3.8)$$

We have introduced abbreviations for the exponents

$$N_{x,\mu}^{ab} = \sum_{\nu:\mu < \nu} p_{x,\mu\nu}^{abss} + \sum_{\rho:\rho < \mu} p_{x-\hat{\rho},\rho\mu}^{sabs} \quad , \quad \bar{N}_{x,\mu}^{ab} = \sum_{\nu:\mu < \nu} p_{x-\hat{\nu},\mu\nu}^{ssba} + \sum_{\rho:\rho < \mu} p_{x,\rho\mu}^{assb} \quad , \quad (3.9)$$

and for notational convenience we introduced a shorthand notation for the weight factor in front of the integral in Eq. (3.7):

$$W_{\beta}[p] = \left[\prod_{x,\mu < \nu} \prod_{a,b,c,d} \frac{\left(\frac{\beta}{2}\right)^{p_{x,\mu\nu}^{abcd}}}{p_{x,\mu\nu}^{abcd}!} \right] \quad . \quad (3.10)$$

In Equation (3.9) we have introduced a summation index s to indicate that these colour indices are summed over, e.g., $p_{x,\mu\nu}^{abss} = \sum_{c,d} p_{x,\mu\nu}^{abcd}$.

The next step towards obtaining the final form of the dualised partition function is to perform the integration. For this we need to choose a representation of our gauge link variables and the corresponding $SU(2)$ Haar measure. The representation chosen in the

paper is

$$U_{x,\mu} = \begin{bmatrix} \cos(\theta_{x,\mu})e^{i\alpha_{x,\mu}} & \sin(\theta_{x,\mu})e^{i\beta_{x,\mu}} \\ -\sin(\theta_{x,\mu})e^{-i\beta_{x,\mu}} & \cos(\theta_{x,\mu})e^{-i\alpha_{x,\mu}} \end{bmatrix}, \quad (3.11)$$

with the angles $\theta_{x,\mu} \in [0, \frac{\pi}{2}]$ and $\alpha_{x,\mu}, \beta_{x,\mu} \in [0, 2\pi]$. Using this one can easily identify the normalised Haar measure to be

$$dU_{x,\mu} = 2 d\theta_{x,\mu} \cos(\theta_{x,\mu}) \sin(\theta_{x,\mu}) \frac{d\alpha_{x,\mu}}{2\pi} \frac{d\beta_{x,\mu}}{2\pi}. \quad (3.12)$$

Inserting the parametrisation (3.11) and the Haar measure (3.12) into (3.8) we get

$$\begin{aligned} Z &= \sum_{\{p\}} W_\beta[p] \prod_{x,\mu} (-1)^{\mathcal{J}_{x,\mu}^{01}} 2 \int_0^{\frac{\pi}{2}} d\theta_{x,\mu} (\cos(\theta_{x,\mu}))^{1+\mathcal{S}_{x,\mu}^{00}+\mathcal{S}_{x,\mu}^{11}} (\sin(\theta_{x,\mu}))^{1+\mathcal{S}_{x,\mu}^{01}+\mathcal{S}_{x,\mu}^{10}} \\ &\times \int_0^{2\pi} \frac{d\alpha_{x,\mu}}{2\pi} e^{i\alpha_{x,\mu}[\mathcal{J}_{x,\mu}^{00}-\mathcal{J}_{x,\mu}^{11}]} \int_0^{2\pi} \frac{d\beta_{x,\mu}}{2\pi} e^{i\beta_{x,\mu}[\mathcal{J}_{x,\mu}^{01}-\mathcal{J}_{x,\mu}^{10}]} , \end{aligned} \quad (3.13)$$

where we have introduced integer valued fluxes $\mathcal{J}_{x,\mu}^{ab}$ and $\mathcal{S}_{x,\mu}^{ab}$, given by

$$\mathcal{J}_{x,\mu}^{ab} = \sum_{\nu:\mu<\nu} [p_{x,\mu\nu}^{abss} - p_{x-\hat{\nu},\mu\nu}^{ssba}] - \sum_{\rho:\rho<\mu} [p_{x,\rho\mu}^{assb} - p_{x-\hat{\rho},\rho\mu}^{sabs}] , \quad (3.14)$$

$$\mathcal{S}_{x,\mu}^{ab} = \sum_{\nu:\mu<\nu} [p_{x,\mu\nu}^{abss} + p_{x-\hat{\nu},\mu\nu}^{ssba}] + \sum_{\rho:\rho<\mu} [p_{x,\rho\mu}^{assb} + p_{x-\hat{\rho},\rho\mu}^{sabs}] . \quad (3.15)$$

Note that the link (x, μ, a, b) is contained in 6 different plaquettes which all contribute to the final value of the \mathcal{J} -flux and \mathcal{S} -flux for a specific configuration.

We first consider the last two integrals in Equation (3.13). This type of integral can be solved in closed form and gives rise to Kronecker deltas, which we again denote in the form $\delta(n)$ (cf. Section 2.4). The Kronecker deltas in turn imply constraints on the fluxes \mathcal{J} in the following form

$$\mathcal{J}_{x,\mu}^{00} - \mathcal{J}_{x,\mu}^{11} = 0, \quad \mathcal{J}_{x,\mu}^{01} - \mathcal{J}_{x,\mu}^{10} = 0, \quad \forall x, \mu . \quad (3.16)$$

When we consider the integral over $\theta_{x,\mu}$, we recognise that it can be identified as a representation of the Beta function B , which is defined as follows

$$2 \int_0^{\frac{\pi}{2}} d\phi (\cos(\phi))^{1+m} (\sin(\phi))^{1+n} = B\left(\frac{m}{2} + 1 \middle| \frac{n}{2} + 1\right) . \quad (3.17)$$

In order to further simplify the Beta function we show the following properties of the fluxes \mathcal{S} :

$$\mathcal{S}_{x,\mu}^{00} + \mathcal{S}_{x,\mu}^{11} = \text{even}, \quad \mathcal{S}_{x,\mu}^{01} + \mathcal{S}_{x,\mu}^{10} = \text{even}, \quad \forall x, \mu . \quad (3.18)$$

To check these we write out the first equation in (3.16) in terms of the dual variables $p_{x,\mu\nu}^{abcd}$:

$$\begin{aligned} \sum_{\nu:\mu<\nu} [p_{x,\mu\nu}^{00ss} - p_{x-\hat{\nu},\mu\nu}^{ss00}] - \sum_{\rho:\rho<\mu} [p_{x,\rho\mu}^{0ss0} - p_{x-\hat{\rho},\rho\mu}^{s00s}] - \\ - \sum_{\nu:\mu<\nu} [p_{x,\mu\nu}^{11ss} - p_{x-\hat{\nu},\mu\nu}^{ss11}] + \sum_{\rho:\rho<\mu} [p_{x,\rho\mu}^{1ss1} - p_{x-\hat{\rho},\rho\mu}^{s11s}] = 0 \quad . \end{aligned}$$

We convert the minus signs into plus signs by adding 2-times the negative terms on both sides, which yields

$$\begin{aligned} \sum_{\nu:\mu<\nu} [p_{x,\mu\nu}^{00ss} + p_{x-\hat{\nu},\mu\nu}^{ss00}] + \sum_{\rho:\rho<\mu} [p_{x,\rho\mu}^{0ss0} + p_{x-\hat{\rho},\rho\mu}^{s00s}] + \sum_{\nu:\mu<\nu} [p_{x,\mu\nu}^{11ss} + p_{x-\hat{\nu},\mu\nu}^{ss11}] + \\ + \sum_{\rho:\rho<\mu} [p_{x,\rho\mu}^{1ss1} + p_{x-\hat{\rho},\rho\mu}^{s11s}] = 2 \left(\sum_{\nu:\mu<\nu} [p_{x-\hat{\nu},\mu\nu}^{ss00} + p_{x,\mu\nu}^{11ss}] + \sum_{\rho:\rho<\mu} [p_{x,\rho\mu}^{0ss0} + p_{x-\hat{\rho},\rho\mu}^{s11s}] \right) \quad . \end{aligned}$$

The left hand side can now trivially be identified as $\mathcal{S}_{x,\mu}^{00} + \mathcal{S}_{x,\mu}^{11}$, and we write

$$\mathcal{S}_{x,\mu}^{00} + \mathcal{S}_{x,\mu}^{11} = 2 \left(\sum_{\nu:\mu<\nu} [p_{x-\hat{\nu},\mu\nu}^{ss00} + p_{x,\mu\nu}^{11ss}] + \sum_{\rho:\rho<\mu} [p_{x,\rho\mu}^{0ss0} + p_{x-\hat{\rho},\rho\mu}^{s11s}] \right) \quad .$$

The terms on the right hand side of the equation above are now multiples of 2 and therefore always even, which concludes our proof.

For even m and n we can use

$$B \left(\frac{m}{2} + 1 \middle| \frac{n}{2} + 1 \right) = \frac{\Gamma(\frac{m}{2} + 1) \Gamma(\frac{n}{2} + 1)}{\Gamma(\frac{m+n+2}{2} + 1)} = \frac{(\frac{m}{2})! (\frac{n}{2})!}{(\frac{m+n+2}{2})!} \quad , \quad (3.19)$$

where we used: $\Gamma(n+1) = n!$. Inserting all this in the partition function (3.13) we arrive at the final dualised form

$$Z = \sum_{\{p\}} W_{\beta}[p] W_H[p] (-1)^{\sum_{x,\mu} \mathcal{J}_{x,\mu}^{01}} \prod_{x,\mu} \delta(\mathcal{J}_{x,\mu}^{00} - \mathcal{J}_{x,\mu}^{11}) \delta(\mathcal{J}_{x,\mu}^{01} - \mathcal{J}_{x,\mu}^{10}) \quad , \quad (3.20)$$

where we have introduced another weight factor $W_H[p]$ for the terms that originate from the Haar measure integration. This weight factor depends on the \mathcal{S} fluxes and has the following form

$$W_H[p] = \prod_{x,\mu} \frac{(\frac{\mathcal{S}_{x,\mu}^{00} + \mathcal{S}_{x,\mu}^{11}}{2})! (\frac{\mathcal{S}_{x,\mu}^{01} + \mathcal{S}_{x,\mu}^{10}}{2})!}{(\frac{\mathcal{S}_{x,\mu}^{00} + \mathcal{S}_{x,\mu}^{11} + \mathcal{S}_{x,\mu}^{01} + \mathcal{S}_{x,\mu}^{10}}{2} + 1)!} \quad . \quad (3.21)$$

We may shortly summarise our steps so far. The partition function in (3.19) now is a sum over the configurations of the cycle occupation numbers $p_{x,\mu\nu}^{abcd} \in \mathbb{N}_0$ attached to the plaquettes. We have introduced two different fluxes \mathcal{J} and \mathcal{S} that live on the links of the

$$\sum \boxed{\overrightarrow{\quad}}_{\mathcal{J}_{x,\mu}^{00}} = \sum \boxed{\overleftarrow{\quad}}_{\mathcal{J}_{x,\mu}^{11}} \quad \text{and} \quad \sum \boxed{\searrow}_{\mathcal{J}_{x,\mu}^{01}} = \sum \boxed{\nearrow}_{\mathcal{J}_{x,\mu}^{10}}$$

FIGURE 3.3: Graphical illustration of the constraints of the $\mathcal{J}_{x,\mu}^{ab}$ -fluxes. Figure adapted from [3].

lattice for notational and illustrative convenience. Also we have identified two weight factors, one containing the inverse gauge coupling β and explicitly the cycle occupation number $p_{x,\mu\nu}^{abcd}$ and the other one consisting of weights for the \mathcal{S} -fluxes. The Kronecker deltas give rise to constraints for the \mathcal{J} -flux running along the individual links, which can graphically be illustrated as shown in Fig. 3.3.

The constraints shown in Figure 3.3 imply that for the whole lattice, the total amount of \mathcal{J} -flux running in the 0 colour layer of the lattice must match the amount of flux running in the 1 layer. Also the number of flux crossings from 0 to 1 must be equal to the number of fluxes that cross from 1 to 0. All valid configurations one can construct have to obey these conditions.

Furthermore we recognise that Equation (3.19) has an explicit sign factor $(-1)^{\sum_{x,\mu} \mathcal{J}_{x,\mu}^{01}}$ which arises from the $(0,1)$ -matrix element of the parametrisation of the link variables in (3.11). This sign factor implies that certain configurations of the cycle occupation numbers to contribute negatively to the partition sum. Having negative contributions is a challenge for a numerical study due to the sign problem they introduce. The exponent of the sign contribution is the sum over all the fluxes $\mathcal{J}_{x,\mu}^{01}$ pointing from site x to site $x + \hat{\mu}$, with $\mu = 1, 2, 3, 4$ and from colour layer 0 to 1. Thus the sign of each contribution is depending on the number of flux crossings that occur on the whole lattice. Thus we may write

$$(-1)^{\sum_{x,\mu} \mathcal{J}_{x,\mu}^{01}} = (-1)^{\# \text{ flux crossings}} \quad . \quad (3.22)$$

As stated before and as can be seen from the definition of the \mathcal{J} -fluxes, there are 6 different plaquettes contributing to each link flux $\mathcal{J}_{x,\mu}^{01}$. The structure of the contribution is illustrated in Figure 3.4.

Having introduced and understood the geometrical representation along with the constraints to the fluxes, we can now go on to discuss examples of admissible configurations of our dual fields. It is straightforward to construct configurations which obey all the constraints, with the simplest being closed surfaces of oriented plaquettes where certain cycle occupation numbers are occupied. To give an example one may start with $p_{x,\mu\nu}^{abcd}$ set to 0 for all values of x, μ, ν, a, b, c, d . One may then set $p_{x,\mu\nu}^{0000} = 1$ for all plaquettes in the $\mu - \nu$ -plane. This trivially keeps all the constraints intact, as the fluxes all run in the same layer and compensate each other, because of the fact that all the plaquettes are mathematically positively oriented. To briefly elaborate this in more detail, the

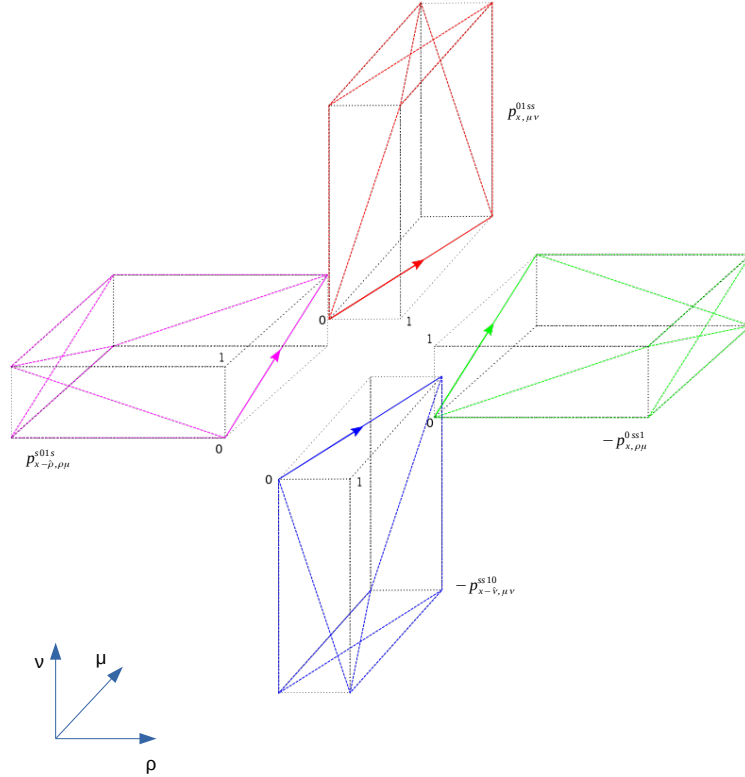


FIGURE 3.4: Schematic illustration of the ACCs contributing to the \mathcal{J} -flux. Here the example flux of $\mathcal{J}_{x,\mu\nu}^{01ss}$ is taken since it is the one contributing to the negative sign. The dashed lines are the summed up cycles indicated by the index s . This figure is adapted from [3].

flux of the link $(x, \mu, 0, 0)$ is pointing in positive μ -direction from plaquette $p_{x,\mu\nu}^{0000}$ and in negative μ -direction from plaquette $p_{x-\hat{\nu},\mu\nu}^{0000}$, thus the contributions cancel out. We stress that this configuration does not have any flux crossing and thus has a positive sign contribution. The next step one might perform is to change the configuration by inverting all the colour indices for one plaquette $p_{x_0,\mu\nu}^{0000} \rightarrow p_{x_0,\mu\nu}^{1111}$, where x_0 denotes a specific site. Subsequently certain colour indices of the adjacent plaquettes need to be adjusted according to the constraints, namely the colour indices that are situated at the links shared with the modified plaquette. This now generates flux crossings, but always in multiples of 2, which does not create a negative contribution.

Another modification for obtaining a different admissible configuration is to simply switch the colour indices of certain sites and afterwards adjusting the indices of the 4

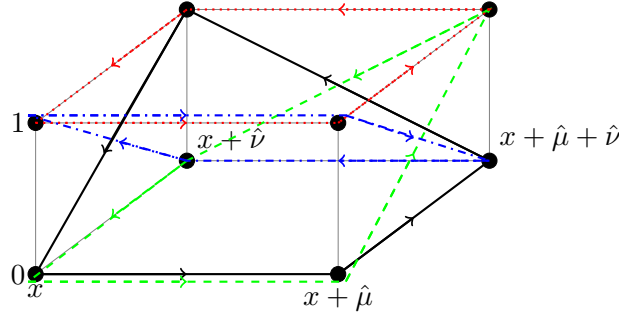


FIGURE 3.5: Graphical illustration of the example configuration given in Equation (3.23), which gives rise to a negative contribution. Drawn in black with the full line is $p_{x,\mu\nu}^{0001}$, in green with the dashed lines is $p_{x,\mu\nu}^{0010}$, the dotted red line is the ACC of $p_{x,\mu\nu}^{1111}$ and finally the blue, dash-dotted line is the $p_{x,\mu\nu}^{1100}$ ACC. This figure is adapted from [3].

plaquettes that contain this site accordingly. Again this will not give negative contributions to the partition function, since changing 2 colour indices also gives flux crossings in multiples of 2. One can repeat these two updates for all the sites in the plane $\mu - \nu$, thereby generating closed flux surfaces which contain all the 16 possible ACCs. This strategy is straightforwardly generalised to higher occupation numbers, surfaces winding around the periodic boundaries (which we will later refer to as "sheets") and non orientable surfaces.

As said before, having negative contributions in the theory is problematic for numerical simulations, but it can be shown that all configurations that can be constructed up to the order β^3 , i.e., 3 non-zero occupation numbers are positive. Only if we consider, e.g., 4 non-zero occupation numbers or higher there appear configurations that contribute with a negative sign. One example of such a configuration is given by:

$$p_{x,\mu\nu}^{0001} = 1, \quad p_{x,\mu\nu}^{0010} = 1, \quad p_{x,\mu\nu}^{1111} = 1, \quad p_{x,\mu\nu}^{1100} = 1. \quad (3.23)$$

To analyse it better, we illustrate this configuration graphically in Figure 3.5. We see clearly, that all the constraints of the theory are intact, but this configuration has an odd number of flux crossings and gives rise to a negative sign in Equation (3.19).

Before we discuss the observables of interest that can be computed from the dualised $SU(2)$ gauge theory, we would like to dwell a little longer on the negative contributions. The main motivation for our work is to find out whether this sign problem is fundamental, i.e., that it cannot be eliminated or somehow worked around, or if there exist some other representation of the theory that can be used during the dualisation such that it may resolve the problem. To check this we have developed 3 different methods to try and overcome the sign problem. The detailed discussion of these methods will be subject of the following chapters, but we nevertheless already want to mention them here:

- factorising out the center of the group $SU(2)$,

- introducing colour flux indices ,
- truncating the theory .

All these approaches have their positive and negative aspects all of which we will work out in detail in the chapters to come.

3.2 Observables of $SU(2)$ lattice gauge theory

The observables of interest are essentially the same as for the $U(1)$ case (cf. Section 2.4). These are the expectation value of the plaquette $\langle U_p \rangle$ which is defined as

$$\langle U_p \rangle \equiv \frac{1}{6V} \frac{\partial \ln(Z)}{\partial (\frac{\beta}{2})} = \frac{1}{6V} \frac{1}{Z} \frac{\partial Z}{\partial (\frac{\beta}{2})} , \quad (3.24)$$

and the plaquette susceptibility χ_p which can be computed in the following way

$$\chi_p = \frac{\partial \langle U_p \rangle}{\partial (\frac{\beta}{2})} = \frac{1}{6V} \frac{\partial^2 \ln(Z)}{\partial (\frac{\beta}{2})^2} . \quad (3.25)$$

The term $\frac{1}{6V}$ is the normalisation factor, with V being the total number of lattice sites and the factor 6 in the denominator denotes the number of different planes that come together at each site in 4-dimensions.

However, instead of immediately showing the results for the observables of the dual theory, we would like to take a short detour and first display the observables of the original matrix form of the theory. Having written this down will be useful once we discuss the simulation of the theory. The plaquette expectation value of the original $SU(2)$ theory with matrix valued link variables can be calculated as follows

$$\langle U \rangle = \frac{1}{6V} \left\langle \sum_{x,\mu < \nu} \text{Tr} [U_{x,\mu} U_{x+\hat{\mu},\nu} U_{x+\hat{\nu},\mu}^\dagger U_{x,\nu}^\dagger] \right\rangle . \quad (3.26)$$

Using Equation (3.24) we arrive at the following expression for the susceptibility

$$\chi = \frac{1}{6V} \left(\left\langle \left[\sum_{x,\mu < \nu} \text{Tr} [U_{x,\mu} U_{x+\hat{\mu},\nu} U_{x+\hat{\nu},\mu}^\dagger U_{x,\nu}^\dagger] \right]^2 \right\rangle - \left\langle \sum_{x,\mu < \nu} \text{Tr} [U_{x,\mu} U_{x+\hat{\mu},\nu} U_{x+\hat{\nu},\mu}^\dagger U_{x,\nu}^\dagger] \right\rangle^2 \right) . \quad (3.27)$$

Equation (3.25) and (3.26) can be obtained trivially, hence we do not show the calculation.

To conclude this section we will now also compute the observables in the dual representation. For this we need to evaluate Equation (3.23) with the partition function in the form of Equation (3.19). We write

$$\langle U_p \rangle = \frac{1}{6V} \frac{1}{Z} \frac{\partial}{\partial \left(\frac{\beta}{2}\right)} \sum_{\{p\}} W_\beta[p] W_H[p] (-1)^{\sum_{x,\mu} \mathcal{J}_{x,\mu}^{10}} \prod_{x,\mu} \delta(\mathcal{J}_{x,\mu}^{00} - \mathcal{J}_{x,\mu}^{11}) \delta(\mathcal{J}_{x,\mu}^{01} - \mathcal{J}_{x,\mu}^{10}) . \quad (3.28)$$

One can easily gather from this that the derivative with respect to $\beta/2$ will only act on the weight factor $W_\beta[p]$ and ignore all others. For the case of the plaquette expectation value we will briefly demonstrate the computation steps in the following. First we write

$$\begin{aligned} \mathcal{X} &= \prod_j \frac{\left(\frac{\beta}{2}\right)^{p_j}}{p_j!} = \left(\prod_j \frac{1}{p_j!}\right) \left(\frac{\beta}{2}\right)^{\sum_j p_j} \\ &\Rightarrow \frac{\partial \mathcal{X}}{\partial \left(\frac{\beta}{2}\right)} = \left(\prod_j \frac{1}{p_j!}\right) \left(\frac{\beta}{2}\right)^{(\sum_j p_j)-1} \cdot \sum_j p_j . \end{aligned}$$

We have written the weight factor $W_\beta[p]$ as \mathcal{X} and for illustrative purposes reduced the number of products to one. One can now split up the term and since the term $\frac{\beta}{2}$ does not depend on j convert the product over j into a sum in the exponent. Taking the derivative here is similar to taking the derivative of $\left(\frac{\beta}{2}\right)^n$, where n here is $\sum_j p_j$. This yields a factor of $(\sum_j p_j) - 1$ in the exponent. To restore this factor we multiply the equation by $1 = \frac{\beta}{\frac{\beta}{2}}$. Inserting the full expression for $W_\beta[p]$ we find the following expression:

$$\frac{\partial}{\partial \left(\frac{\beta}{2}\right)} \left[\prod_{x,\mu < \nu} \prod_{a,b,c,d} \frac{\left(\frac{\beta}{2}\right)^{p_{x,\mu\nu}^{abcd}}}{p_{x,\mu\nu}^{abcd}!} \right] = \frac{2}{\beta} \prod_{x',\mu' < \nu'} \prod_{a',b',c',d'} \frac{\left(\frac{\beta}{2}\right)^{p_{x',\mu'\nu'}^{a'b'c'd'}}}{p_{x',\mu'\nu'}^{a'b'c'd'}!} \times \sum_{x,\mu < \nu} \sum_{a,b,c,d} p_{x,\mu\nu}^{abcd} ,$$

where the product indices need to fulfill the following conditions: $x' \neq x$, $\mu' \neq \mu$, $\nu' \neq \nu$, $a' \neq a$, $b' \neq b$, $c' \neq c$, $d' \neq d$. Inserting this back into Equation (3.27) yields the plaquette expectation value:

$$\langle U_p \rangle = \frac{1}{6V} \frac{2}{\beta} \left\langle \sum_{x,\mu < \nu} \sum_{a,b,c,d} p_{x,\mu\nu}^{abcd} \right\rangle . \quad (3.29)$$

The derivation of the plaquette susceptibility in the dual representation requires to take another derivative of Eq. (3.28) with respect to the inverse gauge coupling and can be obtained by a straightforward calculation. The result of this calculation is the

following

$$\chi = \frac{1}{6V} \frac{4}{\beta^2} \left(\left\langle \left(\sum_{x,\mu<\nu} \sum_{a,b,c,d} p_{x,\mu\nu}^{abcd} \right)^2 \right\rangle - \left\langle \sum_{x,\mu<\nu} \sum_{a,b,c,d} p_{x,\mu\nu}^{abcd} \right\rangle^2 - \left\langle \sum_{x,\mu<\nu} \sum_{a,b,c,d} p_{x,\mu\nu}^{abcd} \right\rangle \right), \quad (3.30)$$

which looks similar to the term in Equation (3.26) with the exception of the last term which originates from the derivative of the prefactor $\frac{2}{\beta}$.

This concludes our discussion of the dualisation of $SU(2)$ lattice gauge theory. In the next chapter we will introduce the different methods we developed to deal with the sign problem and discuss the advantages as well as the disadvantages of each.

Chapter 4

Possible approaches for a simulation

As stated in the previous chapter, we have tried three different approaches to overcome the sign problems of the dualisation of $SU(2)$ lattice gauge theory in Monte Carlo simulations. The first one was to factor out the center group of $SU(2)$, dualise the theory and check whether we could achieve some new constraints for the dual variables in this way. We discuss this in Section 4.1.

The second idea was to find a new representation such that we may be able to resum the negative contributions and obtain positive overall weights. For this we rewrite the exponentiated term given in Equation (3.5) as a product with index $j_{x,\mu\nu}$ running from 1 to $p_{x,\mu\nu}^{abcd}$. The new index j is site-and direction dependent. We later on change variables and identify certain combinations of the colour indices as a colour flux living on the links of the lattice. The insights we got from that approach will be discussed in Section 4.2.

For the third and last approach of this thesis we constructed new dual variables out of the cycle occupation numbers. We then truncate the theory such that the cycle occupation numbers can only take specific values. Doing this we were able to obtain the well known spin algebra and relate it to the qubit regularisation method. This will be elaborated in more detail in Section 4.3.

4.1 Factoring out the center group of $SU(2)$

The first idea to overcome the sign problem was to change the representation of our gauge links. This is done by explicitly taking out the center of the group $SU(2)$, i.e., \mathbb{Z}_2 . In other words we replace the link variables

$$U_{x,\mu} \rightarrow \sigma_{x,\mu} U_{x,\mu} \quad , \quad (4.1)$$

with $\sigma_{x,\mu} \in \mathbb{Z}_2$. The hope of this was that it may produce additional constraints for the dual variables $p_{x,\mu\nu}^{abcd}$, which could not be seen in the original setting.

Inserting this representation in the partition function (3.5) gives

$$Z = \int D[U] \sum_{\{\sigma\}} \prod_{x,\mu < \nu} \prod_{a,b,c,d=0}^1 e^{\frac{\beta}{2}(\sigma_{x,\mu} U_{x,\mu}^{ab} \sigma_{x+\hat{\mu},\nu} U_{x+\hat{\mu},\nu}^{bc} \sigma_{x+\hat{\nu},\mu} U_{x+\hat{\nu},\mu}^{dc} * \sigma_{x,\nu} U_{x,\nu}^{ad} *)} , \quad (4.2)$$

where we have introduced $\sum_{\{\sigma\}}$ as the sum over all \mathbb{Z}_2 configurations σ . One immediately sees that the σ 's do not have colour indices, thus are not traced over and can be pulled out. Again, using a power series expansion we arrive at

$$Z = \int D[U] \sum_{\{\sigma\}} \prod_{\substack{x,\mu < \nu \\ a,b,c,d}} \sum_{p_{x,\mu\nu}^{abcd}=0}^{\infty} \frac{\left(\frac{\beta}{2}\right)^{p_{x,\mu\nu}^{abcd}}}{p_{x,\mu\nu}^{abcd}!} \left(\sigma_{x,\mu} \sigma_{x+\hat{\mu},\nu} \sigma_{x+\hat{\nu},\mu} \sigma_{x,\nu} U_{x,\mu}^{ab} U_{x+\hat{\mu},\nu}^{bc} U_{x+\hat{\nu},\mu}^{dc} * U_{x,\nu}^{ad} *\right)^{p_{x,\mu\nu}^{abcd}} .$$

The expansion indices $p_{x,\mu\nu}^{abcd}$ will later again be identified to be our dual variables. We introduce the weight factor $W_\beta[p]$ as given in Equation (3.10) and write the sum over all configurations of the cycle occupation numbers as $\sum_{\{p\}} = \prod_{x,\mu < \nu} \prod_{a,b,c,d} \sum_{p_{x,\mu\nu}^{abcd}=0}^{\infty}$. The partition function thus becomes

$$Z = \sum_{\{p\}} W_\beta[p] \int D[U] \sum_{\{\sigma\}} \prod_{\substack{x,\mu < \nu \\ a,b,c,d}} (\sigma_{x,\mu} \sigma_{x+\hat{\mu},\nu} \sigma_{x+\hat{\nu},\mu} \sigma_{x,\nu})^{p_{x,\mu\nu}^{abcd}} \left(U_{x,\mu}^{ab} U_{x+\hat{\mu},\nu}^{bc} U_{x+\hat{\nu},\mu}^{dc} * U_{x,\nu}^{ad} *\right)^{p_{x,\mu\nu}^{abcd}} . \quad (4.3)$$

We now only consider the term containing the sigmas, which reads

$$\sum_{\{\sigma\}} \prod_{x,\mu < \nu} (\sigma_{x,\mu} \sigma_{x+\hat{\mu},\nu} \sigma_{x+\hat{\nu},\mu} \sigma_{x,\nu})^{\sum_{a,b,c,d} p_{x,\mu\nu}^{abcd}} . \quad (4.4)$$

Here we have already converted the product over the colour indices into a sum in the exponent, since the sigmas do not depend on them. As the sigmas are elements of \mathbb{Z}_2 we can also express them in the following way: $\sigma_{x,\mu} = (-1)^{r_{x,\mu}}$. We have introduced a new variable $r_{x,\mu} \in \{0, 1\}$, therefore the sum over the configurations of σ now becomes a sum over the configurations of the variable r . With this and repeating for the variable $r_{x,\mu}$ the reorganising steps given in Appendix B, we can express the term in Equation (4.3) in the following way

$$\sum_{\{\sigma\}} \prod_{x,\mu < \nu} \left((-1)^{r_{x,\mu} + r_{x+\hat{\mu},\nu} - r_{x+\hat{\nu},\mu} - r_{x,\nu}}\right)^{Q_{x,\mu\nu}} ,$$

where we have introduced a shorthand notation for the exponent $\sum_{a,b,c,d} p_{x,\mu\nu}^{abcd} = Q_{x,\mu\nu}$. The signs for the individual r terms in the exponent were chosen in this particular way such that we can later express our result in terms of *differential forms on the lattice*,

which will be explained in more detail in Appendix C. Changing some of the signs of the terms in the exponentials is justified due to the identity $(-1)^n = (-1)^{-n}$.

Next we want to reorder the terms in the exponent in the following way: $(r_{x+\hat{\mu},\nu} - r_{x,\mu}) - (r_{x+\hat{\nu},\mu} - r_{x,\mu})$. In doing so, we are able to identify the term in the exponential as the *exterior derivative* differential form, which in its general form is given in the following way (cf. Equation (C.4)):

$$(dr)_{x,\mu_1\cdots\mu_l} = \sum_{k=1}^l (-1)^{k+1} [r_{x+\hat{k},\mu_1\cdots\hat{\mu}_k\cdots\mu_l} - r_{x,\mu_1\cdots\hat{\mu}_k\cdots\mu_l}] . \quad (4.5)$$

Here the circle above the index denotes that this index is left out in the sum. If we now take $l = 2$ and rename the directional indices $\mu_1 = \mu$ and $\mu_2 = \nu$ this identification is complete. Thus the term we are considering becomes

$$\sum_{\{r\}} \prod_{x,\mu<\nu} (-1)^{(dr)_{x,\mu\nu}} Q_{x,\mu\nu} = \sum_{\{r\}} (-1)^{\sum_{x,\mu<\nu} (dr)_{x,\mu\nu}} Q_{x,\mu\nu} .$$

We can now shift the differential operator from the r to the Q term by a partial integration where we end up with the term

$$\sum_{\{r\}} (-1)^{\pm \sum_{x,\mu} r_{x,\mu}} (\delta Q)_{x,\mu} ,$$

where the δ denotes the *boundary operator*. The partial integration here essentially transforms the 2-forms of the exponent $(dr)_{x,\mu\nu}$ and $Q_{x,\mu\nu}$ into 1-forms $r_{x,\mu}$ and $(\delta Q)_{x,\mu}$, living on the links. Pulling down the sums from the exponent and rewriting the sum over all configurations of r as $\sum_{\{r\}} = \prod_{x,\mu} \frac{1}{2} \sum_{r_{x,\mu}=0}^1$ we get

$$\prod_{x,\mu} \frac{1}{2} \sum_{r_{x,\mu}=0}^1 (-1)^{r_{x,\mu}} (\delta Q)_{x,\mu} = \begin{cases} +1 & \text{if } (\delta Q)_{x,\mu} \text{ even} \\ 0 & \text{if } (\delta Q)_{x,\mu} \text{ odd} \end{cases} ,$$

which implies an evenness constraint upon the term $(\delta Q)_{x,\mu}$. Using the definition of the boundary operator and introducing the evenness function $E(n)$ as

$$E(n) = \begin{cases} 1 & \text{if } n \text{ is even} \\ 0 & \text{if } n \text{ is odd} \end{cases} , \quad (4.6)$$

we can write the final result of the term in Equation (4.4) as

$$\prod_{x,\mu} E((\delta Q)_{x,\mu}) = \prod_{x,\mu} E \left(\sum_{\nu} \sum_{a,b,c,d} [p_{x,\mu\nu}^{abcd} - p_{p-\hat{\nu},\mu\nu}^{abcd}] \right) .$$

Inserting this back into the partition function (4.3) we get:

$$Z = \sum_{\{p\}} W_\beta[p] \int D[U] \prod_{x,\mu < \nu} \prod_{a,b,c,d} \left(U_{x,\mu}^{ab} U_{x+\hat{\mu},\nu}^{bc} U_{x+\hat{\nu},\mu}^{dc} U_{x,\nu}^{ad} \right)^{p_{x,\mu\nu}} \prod_{x,\mu} E((\delta Q)_{x,\mu}) . \quad (4.7)$$

One can now repeat the dualisation steps given in Chapter 3 to arrive at the final dualised result of this approach:

$$Z = \sum_{\{p\}} W_\beta[p] W_H[p] (-1)^{\sum_{x,\mu} \mathcal{J}_{x,\mu}^{10}} \prod_{x,\mu} \delta(\mathcal{J}_{x,\mu}^{00} - \mathcal{J}_{x,\mu}^{11}) \delta(\mathcal{J}_{x,\mu}^{01} - \mathcal{J}_{x,\mu}^{10}) \prod_{x,\mu} E((\delta Q)_{x,\mu}) . \quad (4.8)$$

This result looks very similar to the one obtained in Chapter 3, with the additional constraint of the evenness function. Unfortunately this constraint on the Q variable is not new but can be shown to correspond to the constraints for the \mathcal{J} -flux.

To summarise this approach, we were able to factorise out the center of the group and solve this part in closed form. After having done this, we could dualise the theory in the way given in Chapter 3. However this did not produce any new constraints of interest, which was the goal we would have hoped for.

4.2 Dualisation with index parametrisation

Our next approach to the sign problem was a method we called "index parametrisation". The idea here is to take the partition sum in Equation (3.2) with the original gauge action given in Equation (3.1), expand this in a power series which yields

$$Z = \sum_{\{p\}} W_\beta[p] \int D[U] \underbrace{\prod_{x,\mu < \nu} \left(\text{Tr} \left[U_{x,\mu} U_{x+\hat{\mu},\nu} U_{x+\hat{\nu},\mu}^\dagger U_{x,\nu}^\dagger \right] \right)^{p_{x,\mu\nu}}}_{(*)} , \quad (4.9)$$

and only afterwards write the trace operation as explicit sums over the colour indices. The key difference to the original approach is, that instead of taking the trace term to the power of the cycle occupation number, we now introduce another product with index $j_{x,\mu\nu}$, which is site dependent and runs from 1 to the cycle occupation number $p_{x,\mu\nu}$. Note that here the variables $p_{x,\mu\nu}$ do not get a colour index. For notational simplicity we sometimes neglect the indices of $j_{x,\mu\nu}$. When we apply this to the term (*) from Equation (4.5) we get

$$(*) = \left[\prod_{x,\mu < \nu} \prod_{j=1}^{p_{x,\mu\nu}} \sum_{a_{x,\mu\nu}^j} \sum_{b_{x,\mu\nu}^j} \sum_{c_{x,\mu\nu}^j} \sum_{d_{x,\mu\nu}^j} \right] \prod_{x,\mu < \nu} \prod_{j=1}^{p_{x,\mu\nu}} U_{x,\mu}^{a_{x,\mu\nu}^j} b_{x,\mu\nu}^j U_{x+\hat{\mu},\nu}^{b_{x,\mu\nu}^j} c_{x,\mu\nu}^j U_{x+\hat{\nu},\mu}^{c_{x,\mu\nu}^j} d_{x,\mu\nu}^j U_{x,\nu}^{d_{x,\mu\nu}^j} a_{x,\mu\nu}^j ,$$

where we see, that also our colour indices became local and pick up the product index j . One now may introduce the sum over all the colour configurations as follows

$$\sum_{\{a,b,c,d\}} = \prod_{x,\mu < \nu} \prod_{j_{x,\mu\nu}=1}^{p_{x,\mu\nu}} \sum_{a_{x,\mu\nu}^{j_{x,\mu\nu}}} \sum_{b_{x,\mu\nu}^{j_{x,\mu\nu}}} \sum_{c_{x,\mu\nu}^{j_{x,\mu\nu}}} \sum_{d_{x,\mu\nu}^{j_{x,\mu\nu}}} , \quad (4.10)$$

which leads us to the following expression for (*):

$$(*) = \sum_{\{a,b,c,d\}} \prod_{x,\mu < \nu} \prod_{j_{x,\mu\nu}=1}^{p_{x,\mu\nu}} U_{x,\mu}^{a_{x,\mu\nu}^{j_{x,\mu\nu}}} b_{x,\mu\nu}^{j_{x,\mu\nu}} U_{x+\hat{\mu},\nu}^{b_{x,\mu\nu}^{j_{x,\mu\nu}}} c_{x,\mu\nu}^{j_{x,\mu\nu}} U_{x+\hat{\nu},\mu}^* d_{x,\mu\nu}^{j_{x,\mu\nu}} c_{x,\mu\nu}^{j_{x,\mu\nu}} U_{x,\nu}^* a_{x,\mu\nu}^{j_{x,\mu\nu}} d_{x,\mu\nu}^{j_{x,\mu\nu}} . \quad (4.11)$$

We use the steps described in Appendix B to bring this term in a form similar to the integrand in Equation (3.8):

$$(*) = \sum_{\{a,b,c,d\}} \prod_{x,\mu} \left((U_{x,\mu})^{\sum_{\nu:\mu < \nu} \sum_{j_{x,\mu\nu}=1}^{p_{x,\mu\nu}} a_{x,\mu\nu}^{j_{x,\mu\nu}} b_{x,\mu\nu}^{j_{x,\mu\nu}}} \right) \left((U_{x,\mu})^{\sum_{\rho:\rho < \mu} \sum_{j_{x-\hat{\rho},\rho\mu}=1}^{p_{x-\hat{\rho},\rho\mu}} b_{x-\hat{\rho},\rho\mu}^{j_{x-\hat{\rho},\rho\mu}} c_{x-\hat{\rho},\rho\mu}^{j_{x-\hat{\rho},\rho\mu}}} \right) \\ \left((U_{x,\mu}^*)^{\sum_{\nu:\mu < \nu} \sum_{j_{x-\hat{\nu},\mu\nu}=1}^{p_{x-\hat{\nu},\mu\nu}} d_{x-\hat{\nu},\mu\nu}^{j_{x-\hat{\nu},\mu\nu}} c_{x-\hat{\nu},\mu\nu}^{j_{x-\hat{\nu},\mu\nu}}} \right) \left((U_{x,\mu}^*)^{\sum_{\rho:\rho < \mu} \sum_{j_{x,\rho\mu}=1}^{p_{x,\rho\mu}} a_{x,\rho\mu}^{j_{x,\rho\mu}} d_{x,\rho\mu}^{j_{x,\rho\mu}}} \right) , \quad (4.12)$$

where we had to shift the indices of the colour indices as well as of the summation index j , because they are both site dependent.

To proceed with the dualisation we need to choose a representation of the gauge links. We again chose the one given in (3.11). However, having the colour indices now explicitly as exponents, we came up with a clever way to represent the matrix elements $U_{x,\mu}^{ab}$. After a straightforward calculation we found that the matrix elements can be written as

$$U_{x,\mu}^{ab} = \left[(\cos(\theta_{x,\mu}) e^{i\alpha_{x,\mu}})^{1-b} \left(\sin(\theta_{x,\mu}) e^{i\beta_{x,\mu}} \right)^b \right]^{1-a} \times \\ \left[\left(-\sin(\theta_{x,\mu}) e^{-i\beta_{x,\mu}} \right)^{1-b} \left(\cos(\theta_{x,\mu}) e^{-i\alpha_{x,\mu}} \right)^b \right]^a , \quad (4.13)$$

where we use the colour index as a tool to switch on the different components of the matrix. This of course can be multiplied out and the term in (4.9) reduces to

$$U_{x,\mu}^{ab} = (-1)^{a-ab} (\cos(\theta_{x,\mu}))^{(1-a-b+2ab)} (\sin(\theta_{x,\mu}))^{(a+b-2ab)} e^{i\alpha_{x,\mu}(1-b-a)} e^{i\beta_{x,\mu}(b-a)} . \quad (4.14)$$

Inserting this into Equation (4.8) we arrive at the following, rather lengthy expression for (*):

$$\begin{aligned}
(*) = \prod_{x,\mu} & \left[(-1)^{\sum_{\nu:\mu<\nu} \left[\sum_{j_{x,\mu\nu}=1}^{p_{x,\mu\nu}} \left(a_{x,\mu\nu}^{j_{x,\mu\nu}} - a_{x,\mu\nu}^{j_{x,\mu\nu}} b_{x,\mu\nu}^{j_{x,\mu\nu}} \right) + \sum_{j_{x-\hat{\nu},\mu\nu}=1}^{p_{x-\hat{\nu},\mu\nu}} \left(d_{x-\hat{\nu},\mu\nu}^{j_{x-\hat{\nu},\mu\nu}} - d_{x-\hat{\nu},\mu\nu}^{j_{x-\hat{\nu},\mu\nu}} c_{x-\hat{\nu},\mu\nu}^{j_{x-\hat{\nu},\mu\nu}} \right) \right]} \right. \\
& (-1)^{\sum_{\rho:\rho<\mu} \left[\sum_{j_{x,\rho\mu}=1}^{p_{x,\rho\mu}} \left(a_{x,\rho\mu}^{j_{x,\rho\mu}} - a_{x,\rho\mu}^{j_{x,\rho\mu}} a_{x,\rho\mu}^{j_{x,\rho\mu}} \right) + \sum_{j_{x-\hat{\rho},\rho\mu}=1}^{p_{x-\hat{\rho},\rho\mu}} \left(b_{x-\hat{\rho},\rho\mu}^{j_{x-\hat{\rho},\rho\mu}} - c_{x-\hat{\rho},\rho\mu}^{j_{x-\hat{\rho},\rho\mu}} b_{x-\hat{\rho},\rho\mu}^{j_{x-\hat{\rho},\rho\mu}} \right) \right]} \\
& (\cos(\theta_{x,\mu}))^{\sum_{\nu:\mu<\nu} \left[\sum_{j_{x,\mu\nu}=1}^{p_{x,\mu\nu}} \left(1_{(x,\mu\nu)}^{j_{x,\mu\nu}} - b_{x,\mu\nu}^{j_{x,\mu\nu}} - a_{x,\mu\nu}^{j_{x,\mu\nu}} + 2 a_{x,\mu\nu}^{j_{x,\mu\nu}} b_{x,\mu\nu}^{j_{x,\mu\nu}} \right) \right]} \\
& (\cos(\theta_{x,\mu}))^{\sum_{\nu:\mu<\nu} \left[\sum_{j_{x-\hat{\nu},\mu\nu}=1}^{p_{x-\hat{\nu},\mu\nu}} \left(1_{(x-\hat{\nu},\mu\nu)}^{j_{x-\hat{\nu},\mu\nu}} - c_{x-\hat{\nu},\mu\nu}^{j_{x-\hat{\nu},\mu\nu}} - d_{x-\hat{\nu},\mu\nu}^{j_{x-\hat{\nu},\mu\nu}} + 2 d_{x-\hat{\nu},\mu\nu}^{j_{x-\hat{\nu},\mu\nu}} c_{x-\hat{\nu},\mu\nu}^{j_{x-\hat{\nu},\mu\nu}} \right) \right]} \\
& (\cos(\theta_{x,\mu}))^{\sum_{\rho:\rho<\mu} \left[\sum_{j_{x,\rho\mu}=1}^{p_{x,\rho\mu}} \left(1_{(x,\rho\mu)}^{j_{x,\rho\mu}} - a_{x,\rho\mu}^{j_{x,\rho\mu}} - d_{x,\rho\mu}^{j_{x,\rho\mu}} + 2 a_{x,\rho\mu}^{j_{x,\rho\mu}} d_{x,\rho\mu}^{j_{x,\rho\mu}} \right) \right]} \\
& (\cos(\theta_{x,\mu}))^{\sum_{\rho:\rho<\mu} \left[\sum_{j_{x-\hat{\rho},\rho\mu}=1}^{p_{x-\hat{\rho},\rho\mu}} \left(1_{(x-\hat{\rho},\rho\mu)}^{j_{x-\hat{\rho},\rho\mu}} - b_{x-\hat{\rho},\rho\mu}^{j_{x-\hat{\rho},\rho\mu}} - c_{x-\hat{\rho},\rho\mu}^{j_{x-\hat{\rho},\rho\mu}} + 2 b_{x-\hat{\rho},\rho\mu}^{j_{x-\hat{\rho},\rho\mu}} c_{x-\hat{\rho},\rho\mu}^{j_{x-\hat{\rho},\rho\mu}} \right) \right]} \\
& (\sin(\theta_{x,\mu}))^{\sum_{\nu:\mu<\nu} \left[\sum_{j_{x,\mu\nu}=1}^{p_{x,\mu\nu}} \left(b_{x,\mu\nu}^{j_{x,\mu\nu}} + a_{x,\mu\nu}^{j_{x,\mu\nu}} - 2 a_{x,\mu\nu}^{j_{x,\mu\nu}} b_{x,\mu\nu}^{j_{x,\mu\nu}} \right) \right]} \\
& (\sin(\theta_{x,\mu}))^{\sum_{\nu:\mu<\nu} \left[\sum_{j_{x-\hat{\nu},\mu\nu}=1}^{p_{x-\hat{\nu},\mu\nu}} \left(c_{x-\hat{\nu},\mu\nu}^{j_{x-\hat{\nu},\mu\nu}} + d_{x-\hat{\nu},\mu\nu}^{j_{x-\hat{\nu},\mu\nu}} - 2 d_{x-\hat{\nu},\mu\nu}^{j_{x-\hat{\nu},\mu\nu}} c_{x-\hat{\nu},\mu\nu}^{j_{x-\hat{\nu},\mu\nu}} \right) \right]} \\
& (\sin(\theta_{x,\mu}))^{\sum_{\rho:\rho<\mu} \left[\sum_{j_{x,\rho\mu}=1}^{p_{x,\rho\mu}} \left(a_{x,\rho\mu}^{j_{x,\rho\mu}} + d_{x,\rho\mu}^{j_{x,\rho\mu}} - 2 a_{x,\rho\mu}^{j_{x,\rho\mu}} d_{x,\rho\mu}^{j_{x,\rho\mu}} \right) \right]} \\
& (\sin(\theta_{x,\mu}))^{\sum_{\rho:\rho<\mu} \left[\sum_{j_{x-\hat{\rho},\rho\mu}=1}^{p_{x-\hat{\rho},\rho\mu}} \left(b_{x-\hat{\rho},\rho\mu}^{j_{x-\hat{\rho},\rho\mu}} + c_{x-\hat{\rho},\rho\mu}^{j_{x-\hat{\rho},\rho\mu}} - 2 b_{x-\hat{\rho},\rho\mu}^{j_{x-\hat{\rho},\rho\mu}} c_{x-\hat{\rho},\rho\mu}^{j_{x-\hat{\rho},\rho\mu}} \right) \right]} \\
& e^{i\alpha_{x,\mu} \sum_{\nu:\mu<\nu} \left[\sum_{j_{x,\mu\nu}=1}^{p_{x,\mu\nu}} \left(1_{(x,\mu\nu)}^{j_{x,\mu\nu}} - b_{x,\mu\nu}^{j_{x,\mu\nu}} - a_{x,\mu\nu}^{j_{x,\mu\nu}} \right) \right]} \\
& e^{i\alpha_{x,\mu} \sum_{\nu:\mu<\nu} \left[\sum_{j_{x-\hat{\nu},\mu\nu}=1}^{p_{x-\hat{\nu},\mu\nu}} \left(-1_{(x-\hat{\nu},\mu\nu)}^{j_{x-\hat{\nu},\mu\nu}} + c_{x-\hat{\nu},\mu\nu}^{j_{x-\hat{\nu},\mu\nu}} + d_{x-\hat{\nu},\mu\nu}^{j_{x-\hat{\nu},\mu\nu}} \right) \right]} \\
& e^{-i\alpha_{x,\mu} \sum_{\rho:\rho<\mu} \left[\sum_{j_{x,\rho\mu}=1}^{p_{x,\rho\mu}} \left(1_{(x,\rho\mu)}^{j_{x,\rho\mu}} - a_{x,\rho\mu}^{j_{x,\rho\mu}} - d_{x,\rho\mu}^{j_{x,\rho\mu}} \right) \right]} \\
& e^{-i\alpha_{x,\mu} \sum_{\rho:\rho<\mu} \left[\text{sum}_{j_{x-\hat{\rho},\rho\mu}}^{p_{x-\hat{\rho},\rho\mu}} \left(-1_{(x-\hat{\rho},\rho\mu)}^{j_{x-\hat{\rho},\rho\mu}} + b_{x-\hat{\rho},\rho\mu}^{j_{x-\hat{\rho},\rho\mu}} + c_{x-\hat{\rho},\rho\mu}^{j_{x-\hat{\rho},\rho\mu}} \right) \right]} \\
& e^{i\beta_{x,\mu} \left(\sum_{\nu:\mu<\nu} \left[\sum_{j_{x,\mu\nu}=1}^{p_{x,\mu\nu}} \left(b_{x,\mu\nu}^{j_{x,\mu\nu}} - a_{x,\mu\nu}^{j_{x,\mu\nu}} \right) + \sum_{j_{x-\hat{\nu},\mu\nu}=1}^{p_{x-\hat{\nu},\mu\nu}} \left(-c_{x-\hat{\nu},\mu\nu}^{j_{x-\hat{\nu},\mu\nu}} + d_{x-\hat{\nu},\mu\nu}^{j_{x-\hat{\nu},\mu\nu}} \right) \right] \right)} \\
& e^{-i\beta_{x,\mu} \left(\sum_{\rho:\rho<\mu} \left[\sum_{j_{x,\rho\mu}=1}^{p_{x,\rho\mu}} \left(d_{x,\rho\mu}^{j_{x,\rho\mu}} - a_{x,\rho\mu}^{j_{x,\rho\mu}} \right) + \sum_{j_{x-\hat{\rho},\rho\mu}=1}^{p_{x-\hat{\rho},\rho\mu}} \left(b_{x-\hat{\rho},\rho\mu}^{j_{x-\hat{\rho},\rho\mu}} - c_{x-\hat{\rho},\rho\mu}^{j_{x-\hat{\rho},\rho\mu}} \right) \right] \right) \right]} .
\end{aligned}$$

Note that the each of the terms in the equation above has a term-specific combination of colour indices in the exponent. Next we identify the colour index combinations in the exponents of the α and β terms as a quantity we refer to as *colour fluxes*. These quantities live on the links between the lattice sites. The flux variables are given as follows:

$$\begin{aligned}
I = 1 - b - a & \quad i = b - a & \quad K = 1 - d - a & \quad k = c - d \\
L = 1 - d - a & \quad l = d - a & \quad R = 1 - b - c & \quad r = c - b .
\end{aligned} \tag{4.15}$$

The flux denoted by the big letters match the combinations of the α exponent terms and

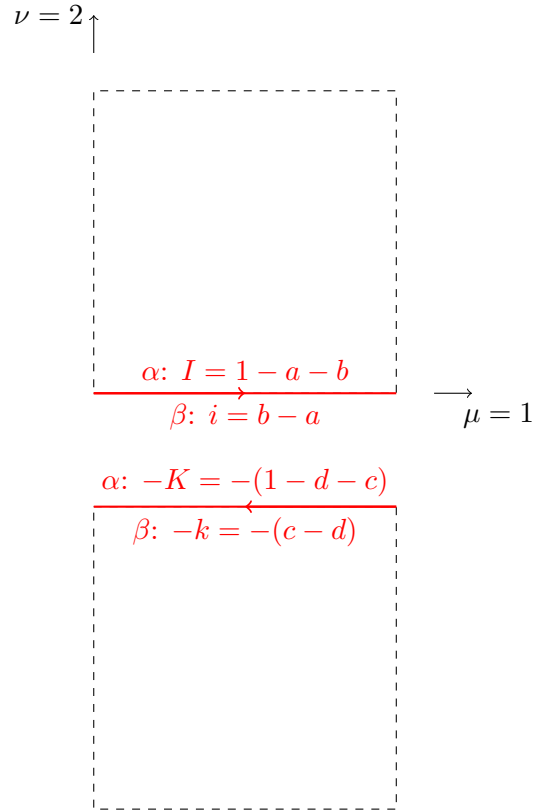


FIGURE 4.1: Illustration of the colour fluxes that arise from the combination of colour indices in (*). The origin of the colour fluxes is denoted by the α or β in front of the definition. Here we illustrate the plane $\mu < \nu$.

the small letter fluxes the ones in the exponent with the β term. These colour fluxes can be illustrated as shown in Figure 4.1 and 4.2. As illustrated in Figures 4.1 and 4.2 we have that the orientation of the fluxes is defined as the colour at site $x + \hat{i}$ minus the colour at site x , where \hat{i} denotes the unit vector in direction $\{\hat{1}, \hat{2}, \hat{3}, \hat{4}\}$. Thus they are positive if they run in mathematical positive direction and negative otherwise. This matches the orientation of the gauge links (cf. Section 2).

Using the definitions in (4.16) we can also consider the composite terms $a \cdot b$ that appear in (*). First we need to express a and b in terms of our new variables:

$$a = \frac{1 - I - i}{2} \quad b = \frac{1 - I + i}{2} . \quad (4.16)$$

A straightforward calculation then yields

$$a \cdot b = \frac{1}{4}(1 - 2I + I^2 - i^2) \quad (4.17)$$

$$a - a \cdot b = \left(\frac{1}{2} - \frac{i}{2}\right)^2 - \frac{I^4}{4} . \quad (4.18)$$

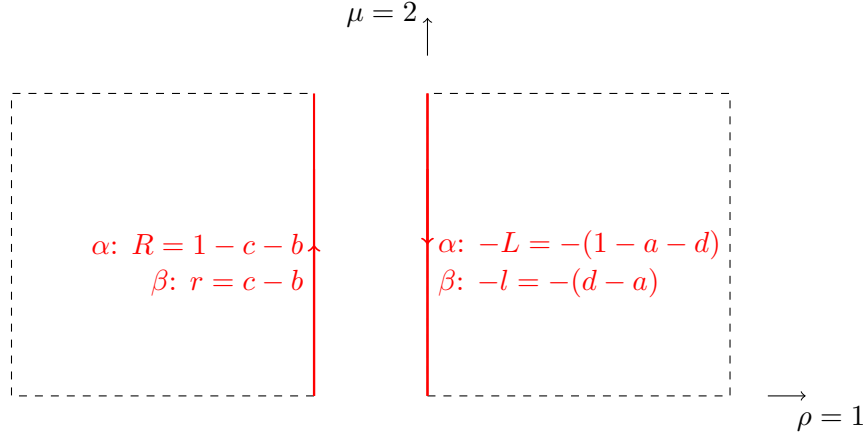


FIGURE 4.2: Illustration of the colour fluxes that arise from the combination of colour indices in (*). The origin of the colour fluxes is denoted by the α or β in front of the definition. Here we illustrate the plane $\rho < \mu$.

Substituting the colour index combinations with the terms given in (4.16), (4.17) and (4.18) the term (*) becomes

$$\begin{aligned}
(*) &= \prod_{x,\mu} \left[(-1)^{\sum_{\{\nu,jx,\mu\nu\}} \left(\frac{1-l_{x,\mu\nu}^{jx,\mu\nu}}{2} \right)^2 - \left(\frac{l_{x,\mu\nu}^{jx,\mu\nu}}{2} \right)^2 + \sum_{\{\nu,jx-\hat{\nu},\mu\nu\}} \left(\frac{1-k_{x-\hat{\nu},\mu\nu}^{jx-\hat{\nu},\mu\nu}}{2} \right)^2 - \left(\frac{l_{x-\hat{\nu},\mu\nu}^{jx-\hat{\nu},\mu\nu}}{2} \right)^2} \right. \\
& \quad (-1)^{\sum_{\{\rho,jx,\rho\mu\}} \left(\frac{1-l_{x,\rho\mu}^{jx,\rho\mu}}{2} \right)^2 - \left(\frac{l_{x,\rho\mu}^{jx,\rho\mu}}{2} \right)^2 + \sum_{\{\rho,jx-\hat{\rho},\rho\mu\}} \left(\frac{1-r_{x-\hat{\rho},\rho\mu}^{jx-\hat{\rho},\rho\mu}}{2} \right)^2 - \left(\frac{l_{x-\hat{\rho},\rho\mu}^{jx-\hat{\rho},\rho\mu}}{2} \right)^2} \\
& \quad (\cos(\theta_{x,\mu})) \sum_{\{\nu,jx,\mu\nu\}} \left(\frac{1 + \left(\frac{l_{x,\mu\nu}^{jx,\mu\nu}}{2} \right)^2 - \left(\frac{i_{x,\mu\nu}^{jx,\mu\nu}}{2} \right)^2}{2} \right) + \sum_{\{\nu,jx-\hat{\nu},\mu\nu\}} \left(\frac{1 + \left(\frac{K_{x-\hat{\nu},\mu\nu}^{jx-\hat{\nu},\mu\nu}}{2} \right)^2 - \left(\frac{k_{x-\hat{\nu},\mu\nu}^{jx-\hat{\nu},\mu\nu}}{2} \right)^2}{2} \right) \\
& \quad (\cos(\theta_{x,\mu})) \sum_{\{\rho,jx,\rho\mu\}} \left(\frac{1 + \left(\frac{l_{x,\rho\mu}^{jx,\rho\mu}}{2} \right)^2 - \left(\frac{i_{x,\rho\mu}^{jx,\rho\mu}}{2} \right)^2}{2} \right) + \sum_{\{\rho,jx-\hat{\rho},\rho\mu\}} \left(\frac{1 + \left(\frac{R_{x-\hat{\rho},\rho\mu}^{jx-\hat{\rho},\rho\mu}}{2} \right)^2 - \left(\frac{r_{x-\hat{\rho},\rho\mu}^{jx-\hat{\rho},\rho\mu}}{2} \right)^2}{2} \right) \\
& \quad (\sin(\theta_{x,\mu})) \sum_{\{\nu,jx,\mu\nu\}} \left(\frac{1 - \left(\frac{l_{x,\mu\nu}^{jx,\mu\nu}}{2} \right)^2 + \left(\frac{i_{x,\mu\nu}^{jx,\mu\nu}}{2} \right)^2}{2} \right) + \sum_{\{\nu,jx-\hat{\nu},\mu\nu\}} \left(\frac{1 - \left(\frac{K_{x-\hat{\nu},\mu\nu}^{jx-\hat{\nu},\mu\nu}}{2} \right)^2 + \left(\frac{k_{x-\hat{\nu},\mu\nu}^{jx-\hat{\nu},\mu\nu}}{2} \right)^2}{2} \right) \\
& \quad (\sin(\theta_{x,\mu})) \sum_{\{\rho,jx,\rho\mu\}} \left(\frac{1 + \left(\frac{l_{x,\rho\mu}^{jx,\rho\mu}}{2} \right)^2 - \left(\frac{i_{x,\rho\mu}^{jx,\rho\mu}}{2} \right)^2}{2} \right) + \sum_{\{\rho,jx-\hat{\rho},\rho\mu\}} \left(\frac{1 + \left(\frac{R_{x-\hat{\rho},\rho\mu}^{jx-\hat{\rho},\rho\mu}}{2} \right)^2 - \left(\frac{r_{x-\hat{\rho},\rho\mu}^{jx-\hat{\rho},\rho\mu}}{2} \right)^2}{2} \right) \\
& \quad e^{i\alpha_{x,\mu} \left[\left(\sum_{\{\nu,jx,\mu\nu\}} l_{x,\mu\nu}^{jx,\mu\nu} + \sum_{jx-\hat{\nu},\mu\nu=1}^{p_{x-\hat{\nu},\mu\nu}} - K_{x-\hat{\nu},\mu\nu}^{jx-\hat{\nu},\mu\nu} \right) - \left(\sum_{\{\rho,jx,\rho\mu\}} l_{x,\rho\mu}^{jx,\rho\mu} + \sum_{jx-\hat{\rho},\rho\mu} - R_{x-\hat{\rho},\rho\mu}^{jx-\hat{\rho},\rho\mu} \right) \right]} \\
& \quad e^{i\beta_{x,\mu} \left[\left(\sum_{\{\nu,jx,\mu\nu\}} i_{x,\mu\nu}^{jx,\mu\nu} + \sum_{jx-\hat{\nu},\mu\nu=1}^{p_{x-\hat{\nu},\mu\nu}} - k_{x-\hat{\nu},\mu\nu}^{jx-\hat{\nu},\mu\nu} \right) - \left(\sum_{\{\rho,jx,\rho\mu\}} l_{x,\rho\mu}^{jx,\rho\mu} + \sum_{jx-\hat{\rho},\rho\mu} - r_{x-\hat{\rho},\rho\mu}^{jx-\hat{\rho},\rho\mu} \right) \right]} \Bigg] ,
\end{aligned}$$

where we have introduced an abbreviation for the double sums, e.g., $\sum_{\{\nu,jx,m\mu\nu\}} = \sum_{\nu:\mu<\nu} \sum_{jx,\mu\nu=1}^{p_{x,\mu\nu}}$.

We recall that the colour indices (a, b, c, d) can only take the values 0 and 1. When

we insert this into the definition of the colour fluxes (4.16), we find that the colour fluxes can take values $-1, 0, 1$, depending on the current configuration of colour indices. However, as the fluxes denoted by the capital letters and their corresponding small letter fluxes $I \leftrightarrow i, L \leftrightarrow l, R \leftrightarrow r, K \leftrightarrow k$, individually contain the same colour indices, they are not independent of one another. Thus, if we have a configuration, e.g., $a = 0, b = 0$, according to (4.16) we have that $I = 1$ and $i = 0$ respectively. Inserting the different combinations leads to the following relation:

$$\begin{aligned} i_{x,\mu\nu}^{jx,\mu\nu} = 1 &\Rightarrow I_{x,\mu\nu}^{jx,\mu\nu} = 0 \\ i_{x,\mu\nu}^{jx,\mu\nu} = 0 &\Rightarrow I_{x,\mu\nu}^{jx,\mu\nu} = \pm 1 \\ i_{x,\mu\nu}^{jx,\mu\nu} = -1 &\Rightarrow I_{x,\mu\nu}^{jx,\mu\nu} = 0 \quad . \end{aligned}$$

This in turn allows us to express the exponents in (*) in terms of either the capital or the small fluxes, for which we chose the latter. This further reduces the (*) term, which now reads

$$\begin{aligned} (*) &= \prod_{x,\mu} \left[(-1)^{\sum_{\{\nu,jx,\mu\nu\}} \left(\frac{1-i_{x,\mu\nu}^{jx,\mu\nu}}{2} i_{x,\mu\nu}^{jx,\mu\nu} \right)^2 + \sum_{\{\nu,jx-\hat{\nu},\mu\nu\}} \left(\frac{1-k_{x-\hat{\nu},\mu\nu}^{jx-\hat{\nu},\mu\nu}}{2} k_{x-\hat{\nu},\mu\nu}^{jx-\hat{\nu},\mu\nu} \right)^2} \right. \\ & \quad (-1)^{\sum_{\{\rho,jx,\rho\mu\}} \left(\frac{1-l_{x,\rho\mu}^{jx,\rho\mu}}{2} l_{x,\rho\mu}^{jx,\rho\mu} \right)^2 + \sum_{\{\rho,jx-\hat{\rho},\rho\mu\}} \left(\frac{1-r_{x-\hat{\rho},\rho\mu}^{jx-\hat{\rho},\rho\mu}}{2} r_{x-\hat{\rho},\rho\mu}^{jx-\hat{\rho},\rho\mu} \right)^2} \\ & \quad (\cos(\theta_{x,\mu}))^{\sum_{\{\nu,jx,\mu\nu\}} \left(1 - (i_{x,\mu\nu}^{jx,\mu\nu})^2 \right) + \sum_{\{\nu,jx-\hat{\nu},\mu\nu\}} \left(1 - (k_{x-\hat{\nu},\mu\nu}^{jx-\hat{\nu},\mu\nu})^2 \right)} \\ & \quad (\cos(\theta_{x,\mu}))^{\sum_{\{\rho,jx,\rho\mu\}} \left(1 - (l_{x,\rho\mu}^{jx,\rho\mu})^2 \right) + \sum_{\{\rho,jx-\hat{\rho},\rho\mu\}} \left(1 - (r_{x-\hat{\rho},\rho\mu}^{jx-\hat{\rho},\rho\mu})^2 \right)} \\ & \quad (\sin(\theta_{x,\mu}))^{\sum_{\{\nu,jx,\mu\nu\}} (i_{x,\mu\nu}^{jx,\mu\nu})^2 + \sum_{\{\nu,jx-\hat{\nu},\mu\nu\}} (k_{x-\hat{\nu},\mu\nu}^{jx-\hat{\nu},\mu\nu})^2} \\ & \quad (\sin(\theta_{x,\mu}))^{\sum_{\{\rho,jx,\rho\mu\}} (l_{x,\rho\mu}^{jx,\rho\mu})^2 + \sum_{\{\rho,jx-\hat{\rho},\rho\mu\}} (r_{x-\hat{\rho},\rho\mu}^{jx-\hat{\rho},\rho\mu})^2} \\ & \quad e^{i\alpha_{x,\mu} \left(\sum_{\{\nu,jx,\mu\nu\}} l_{x,\mu\nu}^{jx,\mu\nu} + \sum_{jx-\hat{\nu},\mu\nu=1} p_{x-\hat{\nu},\mu\nu} - K_{x-\hat{\nu},\mu\nu}^{jx-\hat{\nu},\mu\nu} \right) - \left(\sum_{\{\rho,jx,\rho\mu\}} l_{x,\rho\mu}^{jx,\rho\mu} + \sum_{jx-\hat{\rho},\rho\mu} -R_{x-\hat{\rho},\rho\mu}^{jx-\hat{\rho},\rho\mu} \right)} \\ & \quad \left. e^{i\beta_{x,\mu} \left[\left(\sum_{\{\nu,jx,\mu\nu\}} i_{x,\mu\nu}^{jx,\mu\nu} + \sum_{jx-\hat{\nu},\mu\nu=1} p_{x-\hat{\nu},\mu\nu} - k_{x-\hat{\nu},\mu\nu}^{jx-\hat{\nu},\mu\nu} \right) - \left(\sum_{\{\rho,jx,\rho\mu\}} l_{x,\rho\mu}^{jx,\rho\mu} + \sum_{jx-\hat{\rho},\rho\mu} -r_{x-\hat{\rho},\rho\mu}^{jx-\hat{\rho},\rho\mu} \right) \right]} \right] . \end{aligned}$$

Inserting this back into Equation (4.9) we can evaluate the integral as shown in Chapter 3 by using the $SU(2)$ Haar measure. This then yields the following result for the

dual partition function

$$\begin{aligned}
Z = & \sum_{\{p\}} W_\beta[p] \sum_{\{i,k,l,r\}} \prod_{x,\mu} \\
& (-1)^{\sum_{\{\nu,j_{x,\mu\nu}\}} \left(\frac{1-i_{x,\mu\nu}^{j_{x,\mu\nu}}}{2} i_{x,\mu\nu}^{j_{x,\mu\nu}} \right)^2 + \sum_{\{\nu,j_{x-\hat{\nu},\mu\nu}\}} \left(\frac{1-k_{x-\hat{\nu},\mu\nu}^{j_{x-\hat{\nu},\mu\nu}}}{2} k_{x-\hat{\nu},\mu\nu}^{j_{x-\hat{\nu},\mu\nu}} \right)^2} \\
& (-1)^{\sum_{\{\rho,j_{x,\rho\mu}\}} \left(\frac{1-l_{x,\rho\mu}^{j_{x,\rho\mu}}}{2} l_{x,\rho\mu}^{j_{x,\rho\mu}} \right)^2 + \sum_{\{\rho,j_{x-\hat{\rho},\rho\mu}\}} \left(\frac{1-r_{x-\hat{\rho},\rho\mu}^{j_{x-\hat{\rho},\rho\mu}}}{2} r_{x-\hat{\rho},\rho\mu}^{j_{x-\hat{\rho},\rho\mu}} \right)^2} \\
& \frac{\left(\frac{G_{x,\mu\nu}^{iklr}}{2} \right)! \left(\frac{\bar{G}_{x,\mu\nu}^{iklr}}{2} \right)!}{\left(\left(\sum_{\nu:\mu<\nu} (\tilde{p}_{x,\mu\nu} + \tilde{p}_{x-\hat{\nu},\mu\nu}) + \sum_{\rho:\rho<\mu} (\tilde{p}_{x,\rho\mu} + \tilde{p}_{x-\hat{\rho},\rho\mu}) \right) / 2 + 1 \right)!} \times \\
& \delta \left(\sum_{\nu:\mu<\nu} \left(\tilde{I}_{x,\mu\nu} - \tilde{K}_{x-\hat{\nu},\mu\nu} \right) - \sum_{\rho:\rho<\mu} \left(\tilde{L}_{x,\rho\mu} - \tilde{R}_{x-\hat{\rho},\rho\mu} \right) \right) \\
& \delta \left(\sum_{\nu:\mu<\nu} \left(\tilde{i}_{x,\mu\nu} - \tilde{k}_{x-\hat{\nu},\mu\nu} \right) - \sum_{\rho:\rho<\mu} \left(\tilde{l}_{x,\rho\mu} - \tilde{r}_{x-\hat{\rho},\rho\mu} \right) \right) . \tag{4.19}
\end{aligned}$$

Here the letters with the tilde denote the colour flux variables, where the sum over the index j has been carried out. The $G_{x,\mu\nu}^{iklr}$ and $\bar{G}_{x,\mu\nu}^{iklr}$ are abbreviations for the following terms:

$$\begin{aligned}
G_{x,\mu\nu}^{iklr} = & \sum_{\nu:\mu<\nu} \left(\sum_{j_{x,\mu\nu}} \left(1 - \left(i_{x,\mu\nu}^{j_{x,\mu\nu}} \right)^2 \right) + \sum_{j_{x-\hat{\nu},\mu\nu}} \left(1 - \left(k_{x-\hat{\nu},\mu\nu}^{j_{x-\hat{\nu},\mu\nu}} \right)^2 \right) \right) + \\
& \sum_{\rho:\rho<\mu} \left(\sum_{j_{x,\rho\mu}} \left(1 - \left(l_{x,\rho\mu}^{j_{x,\rho\mu}} \right)^2 \right) + \sum_{j_{x-\hat{\rho},\rho\mu}} \left(1 - \left(r_{x-\hat{\rho},\rho\mu}^{j_{x-\hat{\rho},\rho\mu}} \right)^2 \right) \right) , \\
\bar{G}_{x,\mu\nu}^{iklr} = & \sum_{\nu:\mu<\nu} \left(\sum_{j_{x,\mu\nu}} \left(i_{x,\mu\nu}^{j_{x,\mu\nu}} \right)^2 + \sum_{j_{x-\hat{\nu},\mu\nu}} \left(k_{x-\hat{\nu},\mu\nu}^{j_{x-\hat{\nu},\mu\nu}} \right)^2 \right) + \\
& \sum_{\rho:\rho<\mu} \left(\sum_{j_{x,\rho\mu}} \left(l_{x,\rho\mu}^{j_{x,\rho\mu}} \right)^2 + \sum_{j_{x-\hat{\rho},\rho\mu}} \left(r_{x-\hat{\rho},\rho\mu}^{j_{x-\hat{\rho},\rho\mu}} \right)^2 \right) .
\end{aligned}$$

With this we have successfully reformulated the dual theory in terms of the colour micro fluxes and Equation (4.19) is the final version of the dual partition function in the index parametrisation. Although the approach seems very interesting, we decided to abandon it in favour of the approach explained in the next section.

4.3 Truncation and connection to qubit regularisation

The final approach we used was to truncate the already dualised theory such that it matches the terms expected for a method called *qubit regularisation*. This method is described in greater detail in [1] using the $O(3)$ -spin model as an example, but we nonetheless briefly want to summarise the main concepts and discuss why this is applicable to the dual $SU(2)$ lattice gauge theory. We want to stress that all of the stated equations in this chapter hold for all lattice sites x , all directional indices μ, ν and all colour indices.

The main goal of qubit regularisation is to develop a method which can be used to simulate a quantum (lattice) field theory on a quantum computer. This, as stated in [1], may prove particularly useful when simulating, e.g., non-equilibrium processes or strongly coupled theories. The reason for this is that in these cases the currently available classical computational resources are very limited. Quantum computation may help overcome this problem. In order to simulate a quantum field theory on a quantum computer one has to first apply lattice regularisation and furthermore use a method referred to in the paper as *qubit regularisation*. Basically this means formulating the theory using a local finite-dimensional Hilbert space which can then be represented with qubits. Thus when considering a theory in d dimensions, this formulation effectively makes the theory $d + 1$ dimensional. The paper gives an example of a qubit regularisation scheme called "D-theory approach", which claims that a $(d + 1)$ -dimensional quantum lattice Hamiltonian can be taken as a qubit regularisation of a traditional lattice quantum field theory in $d + 1$ spacetime dimensions. Next they construct the qubit regularisation of the $O(3)$ -sigma model using a singlet-triplet representation as states on each site of the lattice, after which they formulate the theory using worldlines.

There are a few reasons why we chose to try formulating the $SU(2)$ lattice gauge theory using qubit regularisation. In [1] each site gets added an additional finite dimensional Hilbert space in which a qubit lives. Since a qubit is a two-level system this additional dimension can be thought of as adding a layer at each site. The dual formulation of our $SU(2)$ lattice gauge theory can graphically be represented as consisting of 2, in this case, colour layers. Thus we can draw a straightforward analogy between these two formulations. Another reason is that $SU(2)$ and $SO(3)$ are related via the isomorphism $SU(2)/\mathbb{Z}_2 \cong SO(3)$ and furthermore $SU(2)$ is the universal cover group of $SO(3)$.

For the above stated analogy to work we constructed two new dual variables from the cycle occupation numbers. These new variables $V_{x,\mu\nu}^{abcd}$ and $D_{x,\mu\nu}^{abcd}$ are defined in the

following way:

$$V_{x,\mu\nu}^{abcd} = p_{x,\mu\nu}^{abcd} - p_{x,\mu\nu}^{\bar{a}\bar{b}\bar{c}\bar{d}} \quad , \quad (4.20)$$

$$D_{x,\mu\nu} = p_{x,\mu\nu}^{abcd} \cdot p_{x,\mu\nu}^{\bar{a}\bar{b}\bar{c}\bar{d}} \quad . \quad (4.21)$$

Here the bar above the colour index denotes the anti-colour or inverse colour index, i.e., $\bar{a} = 1 - a$. It is straightforward to see that the following relation holds for the variable V with the anti-colours:

$$V_{x,\mu\nu}^{\bar{a}\bar{b}\bar{c}\bar{d}} = -V_{x,\mu\nu}^{abcd} \quad . \quad (4.22)$$

Inverting the colour indices does not affect the variable $D_{x,\mu\nu}^{abcd}$. Using the definitions in (4.15) and (4.16) and exploiting the relation given in Equation (4.17) one can also easily change back to the cycle occupation number representation:

$$p_{x,\mu\nu}^{abcd} = \frac{|V_{x,\mu\nu}^{abcd}| + V_{x,\mu\nu}^{abcd}}{2} + D_{x,\mu\nu}^{abcd} \quad , \quad (4.23)$$

$$p_{x,\mu\nu}^{\bar{a}\bar{b}\bar{c}\bar{d}} = \frac{|V_{x,\mu\nu}^{abcd}| - V_{x,\mu\nu}^{abcd}}{2} + D_{x,\mu\nu}^{abcd} \quad . \quad (4.24)$$

Furthermore, to complete the analogy to the qubit model we needed to truncate the theory in such a way that the dual variables $p_{x,\mu\nu}^{abcd}$ can only take the values 0 and 1. This is a crude truncation since now for each plaquette (x, μ, ν) there can be either no loop or one loop winding around the plaquette for a specific configuration of colours. Inserting these truncated values into the definition of our new dual variables $V_{x,\mu\nu}^{abcd}$ and $D_{x,\mu\nu}^{abcd}$ we find that they can only take the following values:

$$V_{x,\mu\nu}^{abcd} \in \{0, \pm 1\} \quad ,$$

$$D_{x,\mu\nu}^{abcd} \in \{0, 1\} \quad .$$

As the V and D cannot be changed independently of each other we find that they come in 4 different combinations, which are displayed in Table 4.1. The table also helps to better illustrate the connection between the values of the truncated cycle occupation numbers and the new dual variables.

There are a few interesting features one can extract from Table 4.1. First we get a constraint for the new dual variables which reads

$$D_{x,\mu\nu}^{abcd} \leq 1 - |V_{x,\mu\nu}^{abcd}| \quad , \quad (4.25)$$

which is an important statement in the numerical simulation of the theory. Furthermore the numbers in Table 4.1 already hint at the singlet-triplet structure with the spin algebra. In analogy to spin states in quantum mechanics we now introduce a quantity

TABLE 4.1: Conversion table for connecting the two dual representations of our dual $SU(2)$ lattice gauge theory.

$p_{x,\mu\nu}^{\bar{a}\bar{b}\bar{c}\bar{d}} \backslash p_{x,\mu\nu}^{abcd}$	0	1
0	$V_{x,\mu\nu}^{abcd} = 0$ $D_{x,\mu\nu}^{abcd} = 0$	$V_{x,\mu\nu}^{abcd} = +1$ $D_{x,\mu\nu}^{abcd} = 0$
1	$V_{x,\mu\nu}^{abcd} = -1$ $D_{x,\mu\nu}^{abcd} = 0$	$V_{x,\mu\nu}^{abcd} = 0$ $D_{x,\mu\nu}^{abcd} = 1$

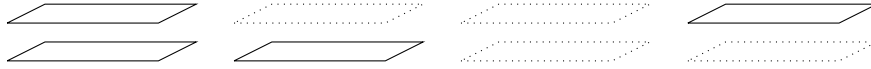


FIGURE 4.3: Illustration of example plaquette states where all the colours are in the same layer: on the far left is the singlet state $|1,0\rangle$, and then from left to right the triplet states in the order $|0,+1\rangle, |0,0\rangle, |0,-1\rangle$.

which we named *plaquette state* as

$$|D_{x,\mu\nu}^{abcd}, V_{x,\mu\nu}^{abcd}\rangle . \quad (4.26)$$

With this we are now able to complete the analogy of our dual variables with the qubit states from [1] and obtain the singlet-triplet representation like follows:

$$\begin{aligned} \text{plaquette singlet:} & \quad |1,0\rangle \\ \text{plaquette triplet:} & \quad \begin{cases} |0,+1\rangle \\ |0,0\rangle \\ |0,-1\rangle \end{cases} \end{aligned} \quad (4.27)$$

Note however that the notation differs from the conventional spin algebra, where the labels 0 and 1 are exchanged in the first entry of the state.

We can illustrate the plaquette states using the graphical representation of the ACCs introduced in Chapter 3. This representation is shown in Figure 4.1.

Figure 4.1 shows that the singlet state corresponds to the ACC and the anti-ACC winding around the same plaquette, where for the triplet state either the ACC or the anti-ACC is occupied. The loop in the bottom layer can be identified as the ACC $p_{x,\mu\nu}^{0000}$ and the one at the top to its anti-ACC $p_{x,\mu\nu}^{1111}$. The third option of the triplet is that all the occupation numbers in a given colour configuration vanish.

Having introduced the variable transformation and truncation we insert (4.18) and (4.19) into our dual partition function (3.20) and rewrite all the variables and fluxes in terms of our new dual variables $V_{x,\mu\nu}^{abcd}$ and $D_{x,\mu\nu}^{abcd}$. First we consider the weight factor $W_H[p]$ given in Equation (3.21), i.e., the sum of \mathcal{S} -fluxes. If we write this sum more

generally with colours a, b and anti-colours \bar{a}, \bar{b} we get:

$$\begin{aligned}
\mathcal{S}_{x,\mu}^{ab} + \mathcal{S}_{x,\mu}^{\bar{a}\bar{b}} = & \sum_{\nu:\mu<\nu} \left[\frac{|V_{x,\mu\nu}^{abss}| + V_{x,\mu\nu}^{abss}}{2} + D_{x,\mu\nu}^{abss} + \frac{|V_{x-\hat{\nu},\mu\nu}^{ssba}| + V_{x-\hat{\nu},\mu\nu}^{ssba}}{2} + D_{x-\hat{\nu},\mu\nu}^{ssba} \right] + \\
& + \sum_{\rho:\rho<\mu} \left[\frac{|V_{x,\rho\mu}^{assb}| + V_{x,\rho\mu}^{assb}}{2} + D_{x,\rho\mu}^{assb} + \frac{|V_{x-\hat{\rho},\rho\mu}^{sabs}| + V_{x-\hat{\rho},\rho\mu}^{sabs}}{2} + D_{x-\hat{\rho},\rho\mu}^{sabs} \right] + \\
& + \sum_{\nu:\mu<\nu} \left[\frac{|V_{x,\mu\nu}^{\bar{a}\bar{b}ss}| + V_{x,\mu\nu}^{\bar{a}\bar{b}ss}}{2} + D_{x,\mu\nu}^{\bar{a}\bar{b}ss} + \frac{|V_{x-\hat{\nu},\mu\nu}^{ss\bar{b}\bar{a}}| + V_{x-\hat{\nu},\mu\nu}^{ss\bar{b}\bar{a}}}{2} + D_{x-\hat{\nu},\mu\nu}^{ss\bar{b}\bar{a}} \right] + \\
& + \sum_{\rho:\rho<\mu} \left[\frac{|V_{x,\rho\mu}^{\bar{a}\bar{b}ss\bar{b}}| + V_{x,\rho\mu}^{\bar{a}\bar{b}ss\bar{b}}}{2} + D_{x,\rho\mu}^{\bar{a}\bar{b}ss\bar{b}} + \frac{|V_{x-\hat{\rho},\rho\mu}^{s\bar{a}\bar{b}s}| + V_{x-\hat{\rho},\rho\mu}^{s\bar{a}\bar{b}s}}{2} + D_{x-\hat{\rho},\rho\mu}^{s\bar{a}\bar{b}s} \right] .
\end{aligned}$$

If we use the relation given in Equation (4.17) the V terms without the modulus cancel and the term reduces to

$$\begin{aligned}
\mathcal{S}_{x,\mu}^{ab} + \mathcal{S}_{x,\mu}^{\bar{a}\bar{b}} = & \sum_{\nu:\mu<\nu} \left[|V_{x,\mu\nu}^{abss}| + 2 D_{x,\mu\nu}^{abss} + |V_{x-\hat{\nu},\mu\nu}^{ssba}| + 2 D_{x-\hat{\nu},\mu\nu}^{ssba} \right] + \\
& + \sum_{\rho:\rho<\mu} \left[|V_{x,\rho\mu}^{assb}| + 2 D_{x,\rho\mu}^{assb} + |V_{x-\hat{\rho},\rho\mu}^{sabs}| + 2 D_{x-\hat{\rho},\rho\mu}^{sabs} \right] . \quad (4.28)
\end{aligned}$$

Next we consider the \mathcal{J} -fluxes and the terms in the Kronecker delta of (3.20). Inserting (4.18) into the definition of the \mathcal{J} -fluxes yields

$$\begin{aligned}
\mathcal{J}_{x,\mu}^{ab} = & \sum_{\nu:\mu<\nu} \left[\frac{|V_{x,\mu\nu}^{abss}| + V_{x,\mu\nu}^{abss}}{2} + D_{x,\mu\nu}^{abss} - \left(\frac{|V_{x-\hat{\nu},\mu\nu}^{ssba}| + V_{x-\hat{\nu},\mu\nu}^{ssba}}{2} + D_{x-\hat{\nu},\mu\nu}^{ssba} \right) \right] - \\
& - \sum_{\rho:\rho<\mu} \left[\frac{|V_{x,\rho\mu}^{assb}| + V_{x,\rho\mu}^{assb}}{2} + D_{x,\rho\mu}^{assb} - \left(\frac{|V_{x-\hat{\rho},\rho\mu}^{sabs}| + V_{x-\hat{\rho},\rho\mu}^{sabs}}{2} + D_{x-\hat{\rho},\rho\mu}^{sabs} \right) \right] ,
\end{aligned}$$

which as a single term will be of interest when we discuss the sign. Last but not least we consider the arguments of the Kronecker deltas which now read:

$$\begin{aligned}
\mathcal{J}_{x,\mu}^{ab} - \mathcal{J}_{x,\mu}^{\bar{a}\bar{b}} = & \sum_{\nu:\mu<\nu} \left[\frac{|V_{x,\mu\nu}^{abss}| + V_{x,\mu\nu}^{abss}}{2} + D_{x,\mu\nu}^{abss} - \left(\frac{|V_{x-\hat{\nu},\mu\nu}^{ssba}| + V_{x-\hat{\nu},\mu\nu}^{ssba}}{2} + D_{x-\hat{\nu},\mu\nu}^{ssba} \right) \right] - \\
& - \sum_{\rho:\rho<\mu} \left[\frac{|V_{x,\rho\mu}^{\bar{a}\bar{b}ss\bar{b}}| + V_{x,\rho\mu}^{\bar{a}\bar{b}ss\bar{b}}}{2} + D_{x,\rho\mu}^{\bar{a}\bar{b}ss\bar{b}} - \left(\frac{|V_{x-\hat{\rho},\rho\mu}^{s\bar{a}\bar{b}s}| + V_{x-\hat{\rho},\rho\mu}^{s\bar{a}\bar{b}s}}{2} + D_{x-\hat{\rho},\rho\mu}^{s\bar{a}\bar{b}s} \right) \right] - \\
& - \left(\sum_{\nu:\mu<\nu} \left[\frac{|V_{x,\mu\nu}^{\bar{a}\bar{b}ss}| + V_{x,\mu\nu}^{\bar{a}\bar{b}ss}}{2} + D_{x,\mu\nu}^{\bar{a}\bar{b}ss} - \left(\frac{|V_{x-\hat{\nu},\mu\nu}^{ss\bar{b}\bar{a}}| + V_{x-\hat{\nu},\mu\nu}^{ss\bar{b}\bar{a}}}{2} + D_{x-\hat{\nu},\mu\nu}^{ss\bar{b}\bar{a}} \right) \right] - \right. \\
& \left. - \sum_{\rho:\rho<\mu} \left[\frac{|V_{x,\rho\mu}^{\bar{a}\bar{b}ss\bar{b}}| + V_{x,\rho\mu}^{\bar{a}\bar{b}ss\bar{b}}}{2} + D_{x,\rho\mu}^{\bar{a}\bar{b}ss\bar{b}} - \left(\frac{|V_{x-\hat{\rho},\rho\mu}^{s\bar{a}\bar{b}s}| + V_{x-\hat{\rho},\rho\mu}^{s\bar{a}\bar{b}s}}{2} + D_{x-\hat{\rho},\rho\mu}^{s\bar{a}\bar{b}s} \right) \right] \right) .
\end{aligned}$$

Again using (4.17) we see that the modulus of the V and the D terms cancel and this term straightforwardly reduces to

$$\mathcal{J}_{x,\mu}^{ab} - \mathcal{J}_{x,\mu}^{\bar{a}\bar{b}} = \sum_{\nu:\mu<\nu} \left[V_{x,\mu\nu}^{abss} - V_{x-\hat{\nu},\mu\nu}^{ssba} \right] - \sum_{\rho:\rho<\mu} \left[V_{x,\rho\mu}^{assb} - V_{x-\hat{\rho},\rho\mu}^{sabs} \right]. \quad (4.29)$$

Finally if we insert (4.18) into the definition of the weight factor $W_\beta[p]$, it becomes

$$W_\beta[p] = \left[\prod_{x,\mu<\nu} \prod_{a,b,c,d} \frac{\left(\frac{\beta}{2}\right)^{\left(\frac{|V_{x,\mu\nu}^{abcd}|+V_{x,\mu\nu}^{abcd}}{2} + D_{x,\mu\nu}^{abcd}\right)}}{\left(\frac{|V_{x,\mu\nu}^{abcd}|+V_{x,\mu\nu}^{abcd}}{2} + D_{x,\mu\nu}^{abcd}\right)!} \right]. \quad (4.30)$$

With all the terms from the dual partition sum (3.20) now given in terms of the new, truncated dual variables we are ready to carry out the simulations. In the next section we will explain the algorithms and update schemes we used to perform the simulation. We will also display and discuss the results obtained by the simulations.

Chapter 5

Numerical Simulation

The previous chapters compiled the theoretical description of the theory, its problems and how we want to solve them. This chapter now is devoted to the more practical part of the thesis, namely the numerical simulation of the theory and the calculation of the observables given in Section 3.2.

We have split this chapter into three subchapters, which feature the two different simulation ideas we used to simulate the theory. In the first part we explain how we simulated $SU(2)$ lattice gauge theory using the action given in Equation (3.1), which uses $SU(2)$ matrix valued gauge links. Since this is the original formulation of the theory, the results obtained from its simulation serve as a reference for the results obtained from the simulation of the dual representation. As it would take too much space to put the whole code in the thesis, we will instead show the algorithm in the form of a pseudo-code. The second part is mainly a conceptual part where we explain how to simulate the theory using the dual cycle occupation numbers $p_{x,\mu\nu}^{abcd}$ as our main degrees of freedom for the simulation. Last but not least, in the third subsection we describe how we simulated the theory using the new dual variables obtained by the truncation approach in Section 4.3.

5.1 Simulation of conventional $SU(2)$ lattice gauge theory

5.1.1 Description of the algorithm

For the simulation of the conventional formulation we start by considering the action given in Equation (3.1). Our fundamental degrees of freedom for the simulation here are the $SU(2)$ valued gauge links $U_{x,\mu}$. To simulate the theory and to calculate the observables, we use the Metropolis algorithm described in more detail in Section 2.3.

In the following we present the structure of our main program in the form of pseudo-code.

```

set nmeas = 106
set nequi = 105
set nskip = 20
β0 = 0.0
Δβ = 0.05
initialise neighbour field
set all gauge links to 2-dim. unit matrix
for i:0 → 80
    β = β0 + i · Δβ
    sweeps(nequi)
    for j:0 → nmeas-1
        sweeps(nskip)
        calculate-plaquette( j )
    end for
    plaquette-expectation-value = calculate-mean()
    chi = calculate-chi()
end for

```

In the beginning we set some parameters that determine the statistics of our simulation, as well as the equilibration and decorrelation. The number of the "measurements" we perform¹ per observable is set to 10^6 . The number of equilibrating updates *nequi*, we chose to be 10^5 . This is to make sure the algorithms equilibrated and provides a good basis for the computation of the observables. The next pre-set parameter is *nskip*, which is the number of gauge link updates performed in between the measurements. This process is necessary to reduce the autocorrelation between two consecutive measurements. The last two steps that need to be done before we start the simulation procedure are the initialisation of the neighbour field and then setting the gauge links to their starting value. The neighbour field is a multidimensional array, that contains the addresses of nearest neighbour lattice sites in each direction, i.e., $\mu \in \{\pm 1, \pm 2, \pm 3, \pm 4\}$, for every lattice site x . Regarding the starting value for our gauge fields, a suitable choice here is the 2-dimensional unit matrix: $\mathbb{I} = \begin{bmatrix} 1 & 0 \\ 0 & 1 \end{bmatrix}$.

¹Note that the parameter values suggested here are only typical numbers and the actually chosen values may depend on the specific goal of the simulation.

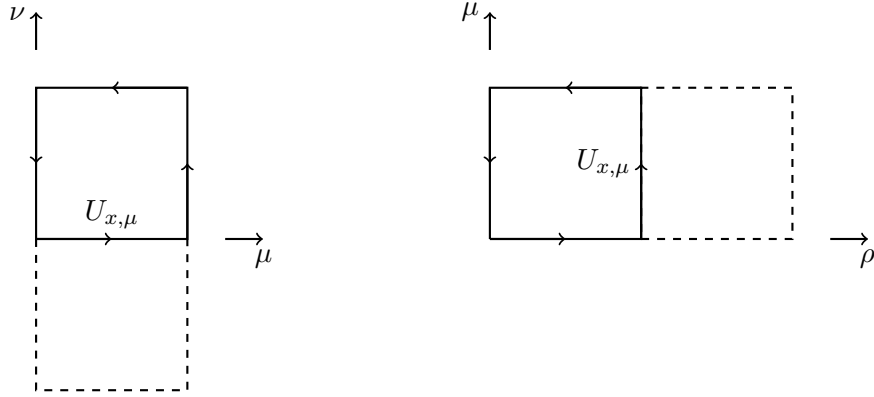


FIGURE 5.1: Illustration of the different cases of two neighbouring plaquettes which contain the gauge link $U_{x,\mu}$ we want to update.

When performing the simulation we are interested in how the theory behaves at different values of the inverse gauge coupling β . Thus we start with $\beta_0 = 0.0$ and increase it stepwise in a loop which in the example shown here runs over 80 steps of $\Delta\beta = 0.05$. We stress that the choice of the number 80 and $\Delta\beta = 0.05$ here is only for illustration and will be different depending on the task. Before we start calculating the observables for each of these iterations we perform *nequi* equilibrating updates of the gauge link configurations using the **sweeps** function which implements the Monte Carlo updates. The program then loops over the number of measurements, where it first performs *nskip* updates, using the **sweeps** function, to decorrelate the measurements. Then it calculates observables such as the value of the plaquette for the current measurement. The output of this measurement-loop is a set of *nmeas* values of the observables. We later use this set, which is a so-called *sample*, to calculate the observables we are interested in according to the formulas in Equations (3.26) and (3.27).

The updates of the gauge links are contained in the **sweeps** function, and we will shortly outline in the following how the gauge links are updated. For a more detailed description of how to generate new link candidates for the Metropolis update, see [7].

Consider the gauge link $U_{x,\mu}$. In d dimensions this link is contained in $2(d-1)$ plaquettes, which are illustrated in Figure 5.1. As described in Section 2.3, the Metropolis algorithm needs to offer a new link candidate $\tilde{U}_{x,\mu}$ in the vicinity of the old value $U_{x,\mu}$. To obtain this new candidate we perform a matrix multiplication of the following form:

$$\tilde{U}_{x,\mu} = XU_{x,\mu} \quad , \quad (5.1)$$

where X is a random element of $SU(2)$ close to the unit element. Here we make use of the fact, that we can write an $SU(2)$ matrix element X in the form

$$X = x_0 \mathbb{I} + i \vec{x} \cdot \vec{\sigma} \quad , \quad \vec{x} = \begin{bmatrix} x_1 \\ x_2 \\ x_3 \end{bmatrix} \quad , \quad (5.2)$$

with x_0, x_1, x_2, x_3 denoting 4 real coefficients and $\vec{\sigma}$ is the vector of the three Pauli matrices. We generate the coefficients by

$$\vec{x} = \varepsilon \frac{\vec{r}}{|\vec{r}|} \quad x_0 = \text{sign}(r_0) \sqrt{1 - \varepsilon^2} \quad . \quad (5.3)$$

The r_i , with $i = 0, 1, 2, 3$, denote random numbers which are uniformly distributed in $(-\frac{1}{2}, \frac{1}{2})$ and ε is a parameter that controls the spread of X around \mathbb{I} . We stress that the parameter ε can be tuned to optimize the acceptance rate.

Once we have generated the new candidate link variable, the program has to determine the Metropolis ratio ρ . This is obtained by dividing the weights of the new configuration by the weights of the old configuration, as is stated in Section 2.3. For our theory, the weight factors are Boltzmann factors of the form:

$$W_B[U] = e^{\frac{\beta}{2} \sum_p \text{Tr}[U_p]} \quad . \quad (5.4)$$

The quantity $U_p = U_{x,\mu} U_{x+\hat{\mu},\nu} U_{x+\hat{\nu},\mu}^\dagger U_{x,\nu}^\dagger$ denotes the product over the 4 link variables that make up a plaquette and the sum index p indicates that all the plaquettes are summed over. Using these weights the Metropolis ratio $\rho = \frac{W_B[\tilde{U}]}{W_B[U]}$ becomes

$$\rho = e^{\frac{\beta}{2} \sum_p [\text{Tr}[\tilde{U}_p] - \text{Tr}[U_p]]} \quad . \quad (5.5)$$

As an example we show how to calculate the Metropolis ratio for the update of the link $U_{x,\mu}$. For the computation we need to take into account only the plaquettes shown in Figure 5.1. If we now insert the definition for U_p in (5.5), the Metropolis ratio reads:

$$\rho = e^{\frac{\beta}{2} \sum_{x,\mu < \nu} \left[\text{Tr}[(\tilde{U}_{x,\mu} - U_{x,\mu}) U_{x+\hat{\mu},\nu} U_{x+\hat{\nu},\mu}^\dagger U_{x,\nu}^\dagger] + \text{Tr}[U_{x-\hat{\nu},\mu} U_{x-\hat{\nu}+\hat{\mu},\nu} (\tilde{U}_{x,\mu}^\dagger - U_{x,\mu}^\dagger) U_{x-\hat{\nu},\nu}^\dagger] \right]} \times \\ e^{\frac{\beta}{2} \sum_{x,\rho < \mu} \left[\text{Tr}[\tilde{U}_{x,\rho} U_{x+\hat{\rho},\mu} U_{x+\hat{\mu},\rho}^\dagger (\tilde{U}_{x,\mu}^\dagger - U_{x,\mu}^\dagger)] + \text{Tr}[U_{x-\hat{\rho},\rho} (\tilde{U}_{x,\mu} - U_{x,\mu}) U_{x-\hat{\rho}+\hat{\mu},\rho}^\dagger U_{x-\hat{\rho},\mu}^\dagger] \right]} \quad .$$

For convenience we introduce the notation $\Delta_{x,\mu} = \tilde{U}_{x,\mu} - U_{x,\mu}$ and write

$$\rho = e^{\frac{\beta}{2} \sum_{x,\mu < \nu} [\text{Tr}[\Delta_{x,\mu} U_{x+\hat{\mu},\nu} U_{x+\hat{\nu},\mu}^\dagger U_{x,\nu}^\dagger] + \text{Tr}[U_{x-\hat{\nu},\mu} U_{x-\hat{\mu},\nu} \Delta_{x,\mu}^\dagger U_{x-\hat{\nu},\nu}^\dagger]]} \times e^{\frac{\beta}{2} \sum_{x,\rho < \mu} [\text{Tr}[U_{x,\rho} U_{x+\hat{\rho},\mu} U_{x+\hat{\mu},\rho}^\dagger \Delta_{x,\mu}^\dagger] + \text{Tr}[U_{x-\hat{\rho},\rho} \Delta_{x,\mu} U_{x-\hat{\rho}+\hat{m}u,\rho}^\dagger U_{x-\hat{\rho},\mu}^\dagger]]} .$$

We now can use the cyclic permutation property of the trace and after performing some rearrangements of the gauge links we get the following

$$\rho = e^{\frac{\beta}{2} \sum_{x,\mu < \nu} [\text{Tr}[\Delta_{x,\mu} (U_{x+\hat{\mu},\nu} U_{x+\hat{\nu},\mu}^\dagger U_{x,\nu}^\dagger + U_{x-\hat{\nu},\mu}^\dagger U_{x-\hat{\mu},\nu} U_{x-\hat{\nu},\mu})]]} \times e^{\frac{\beta}{2} \sum_{x,\rho < \mu} [\text{Tr}[\Delta_{x,\mu} (U_{x+\hat{\mu},\rho} U_{x+\hat{\rho},\mu}^\dagger U_{x,\rho}^\dagger + U_{x-\hat{\rho}+\hat{m}u,\rho} U_{x-\hat{\rho},\mu}^\dagger U_{x-\hat{\rho},\rho})]]} . \quad (5.6)$$

This is then how we implemented the calculation of the Metropolis ratio in our program.

Finally, after the Metropolis ratio is calculated, the algorithm then generates a uniformly distributed random number in the interval $[0, 1]$ and checks whether ρ is larger or smaller than that number. If ρ is larger, the new configuration gets accepted, if it is smaller the old configuration is kept.

In the function **sweeps** this whole process is then carried out for all lattice sites and for all directions in a loop that allows one to update all degrees of freedom *nsweep* times. This then is again included in a loop over how many updates we want to carry out. In the following we show a pseudo-code version of the function **sweeps**.

sweeps(*nsweep*)

for *i*: 0 → *nsweep*-1

for site: 0 → (number of sites)-1

for *d*: 0 → dimensions - 1

generate update matrix *X* + compute new link configuration \tilde{U}

calculate Metropolis ratio ρ

generate uniformly distributed random number $r \in [0, 1]$

if: $r < \rho$ → accept new configuration

end for

end for

end for

end sweeps

5.1.2 Results

Here we are going to show the results obtained by the simulation of the theory using the conventional formulation on different lattice sizes. This will serve as reference data for the results obtained by the simulation with the truncated dual variables. We chose the following values for the pre-set parameters in the simulation:

- $nmeas = 10^5$,
- $nequi = 10^4$,
- $\Delta\beta = 0.1$,
- we perform 40 steps of $\Delta\beta$.

In using the conventional matrix formulation of the theory we expect the simulation to represent the theory correctly in the strong and the weak coupling regime. The correctness of our simulation data can be easily checked, by comparing it to the strong and the weak coupling expansion expression for the plaquette expectation value $\langle U_p \rangle$ and the susceptibility χ .

To shortly state how these expansions come about, the strong coupling expansion is a Taylor expansion of the plaquette expectation value and the partition function in powers of $\frac{\beta}{2}$. In contrast to this, the weak coupling approximation comes about when we expand the same quantities in powers of $\left(\frac{\beta}{2}\right)^{-1}$. The following formulae for the average plaquette value are taken from [12] and slightly adjusted to match the overall normalisation factor chosen in this work. The strong coupling expansion for the plaquette expectation value reads:

$$\langle U_p \rangle_s = \frac{\beta + \frac{\beta^3}{12} + 7\frac{\beta^5}{1536}}{2 + \frac{\beta^2}{4} + \frac{\beta^4}{96}} , \quad (5.7)$$

and for the weak coupling regime, the expansion reads:

$$\langle U_p \rangle_w = 2 - \frac{3}{2\beta} - \frac{0.26}{\beta^2} - \frac{0.58}{\beta^3} . \quad (5.8)$$

Applying Equation (3.25) to Eq. (5.7) and (5.8), we obtain the analytical results for the susceptibility in the strong as well as in the weak coupling regime. Performing this computation is straightforward and gives

$$\chi_s = \frac{7\beta^8 + 472\beta^6 + 6336\beta^4 + 9216\beta^2 + 73728}{2(\beta^4 + 24\beta^2 + 192)^2} , \quad (5.9)$$

for the strong coupling susceptibility and for the approximation in the weak coupling regime we get

$$\chi_w = \frac{3}{\beta^2} + \frac{1.04}{\beta^3} + \frac{3.48}{\beta^4} . \quad (5.10)$$

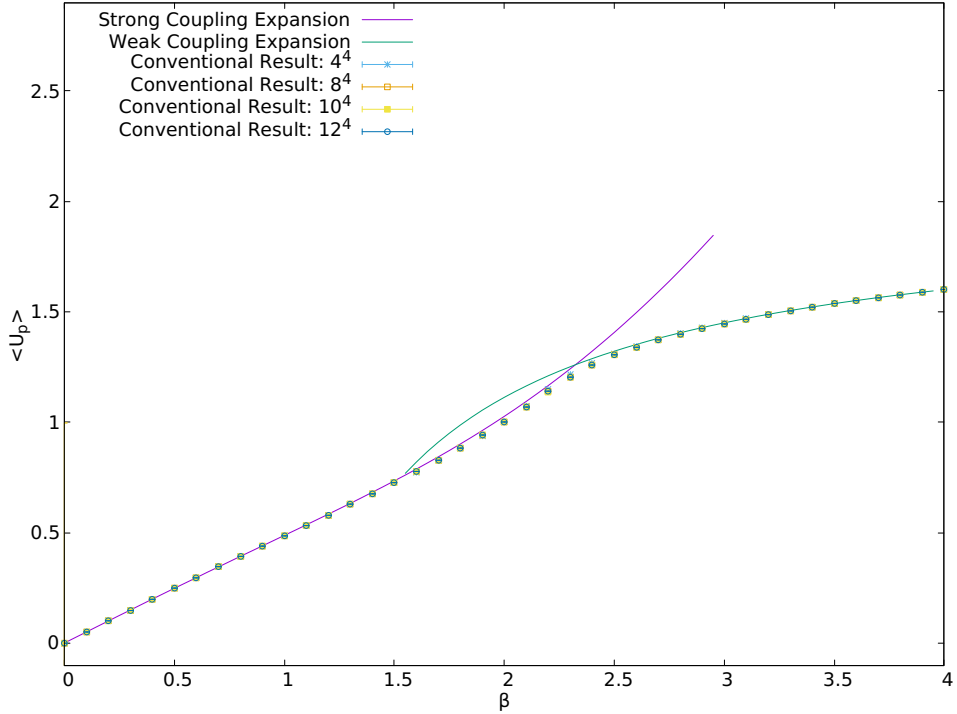


FIGURE 5.2: Results for the plaquette expectation value $\langle U_p \rangle$ of the conventional simulation as a function of the inverse gauge coupling β , calculated for lattice sizes 4^4 , 8^4 , 10^4 and 12^4 . As a comparison for our obtained data we have plotted the strong coupling expansion (purple) and the weak coupling expansion (green) of $SU(2)$ lattice gauge theory. Notice that the simulation data forms a smooth bridge between these two expansion curves and approaches the graphs asymptotically in the very strong and the very weak coupling regime. The errorbars here are too small to be seen, but in the middle region they are slightly bigger than in the strong and in the weak coupling region.

The subscript s and w in the above equations indicate the results for the strong and the weak coupling expansion respectively.

We are now ready to present and discuss our results. In Figure 5.2 we show the results for the plaquette expectation value obtained by the simulation using the conventional formulation of $SU(2)$ lattice gauge theory for lattice sizes 4^4 , 8^4 , 10^4 and 12^4 . As a comparison and to prove the validity of our simulations we have also plotted the respective analytic curve obtained from Equation (5.7). One immediately observes, regardless of the lattice size, that the simulation results are in very good agreement with the analytic curves and form a kind of bridge between the strong and the weak coupling expansion results. In the *transition region*, i.e., $2 < \beta < 2.5$ we observe a maximum of slope around $\beta = 2.2$ in our simulated data. This could in principle be taken as a hint for a phase transition. During our analysis of the data we also found, that for the bigger lattice size, the slope becomes less steep. But this deviation of the datapoints is extremely tiny and is known to be a (valid) finite volume effect. We will discuss the meaning of the maximum slope in a little more detail below. In the strong and the weak

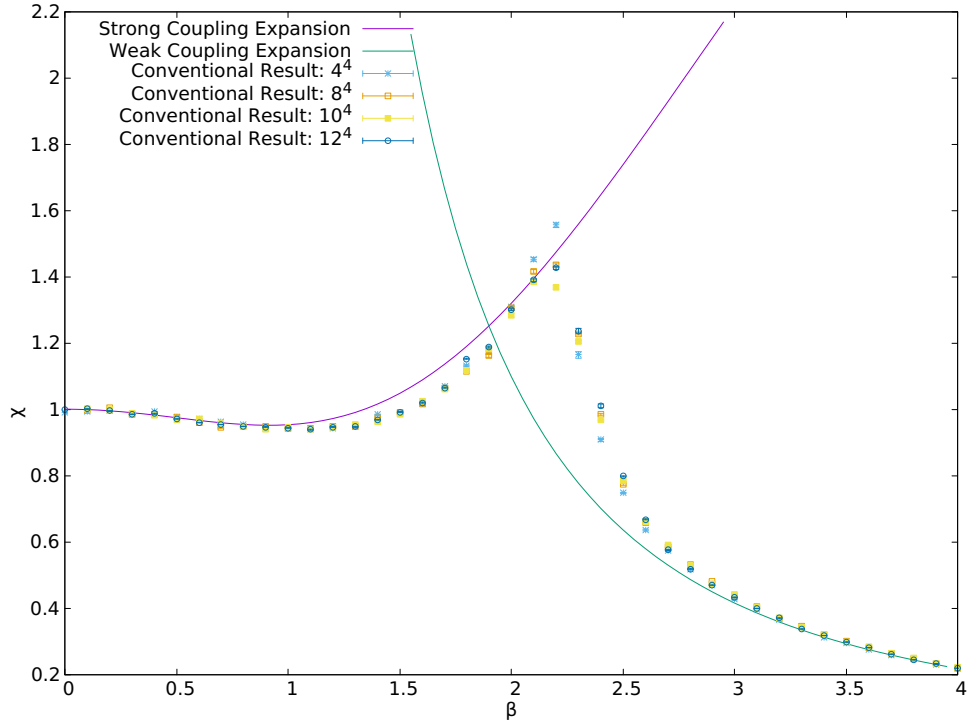


FIGURE 5.3: Results for the susceptibility χ obtained from the conventional simulation, plotted as a function of the inverse gauge coupling β . Shown here are the results for lattice sizes 4^4 , 8^4 , 10^4 and 12^4 . As a reference we have plotted the strong and weak coupling expansion results of the susceptibility for $SU(2)$ lattice gauge theory. The data approaches the expansion curves asymptotically in the ultrastrong and the ultraweak coupling regime, while in the intermediate region it again forms a bridge between the two curves. Note that the peak gets smoother with bigger lattice sizes. In the strong and weak coupling regime, the errorbars are again too small to be seen, whereas they can sometimes be spotted in the middle region.

region, the simulation data approaches the curve asymptotically. A slightly stronger deviation happens can be seen in the region $1.3 < \beta < 3.1$, which we will further refer to as *intermediate region*. When comparing the datapoints for the different lattice sizes one finds that they agree fairly well. We must stress here, that the errorbars are too small to be seen with the naked eye, but we assure that even zoomed in the data is in good agreement.

Figure 5.3 shows the results from our simulations for the susceptibility in comparison to the analytical strong and weak coupling expression from Equation (5.9) and (5.10). Also here one sees clearly that the data is in good agreement with the analytic results in the strong and the weak coupling regions, as it again approaches the expansion curves asymptotically. As stated before, also in this plot the simulation data is deviating from the analytic curve in the *intermediate region*. In this plot the deviation can be seen more clearly. Otherwise the data for the different lattice sizes shown in Figure 5.3 compare very well indicating that finite volume effects are small. Again we notice that also in this figure the datapoints for the bigger lattices are slightly lower in the intermediate

region than the data from the 4^4 lattice. The reason for this is the same as stated above.

A very interesting detail we observe is that there appears to be a peak of the susceptibility in the region where the plaquette expectation value graph showed the steepest slope. This peak together with the maximum slope could, because our lattice sizes are quite small, be taken as a hint for a phase transition in the continuum limit. However, as stated in [7] this is not a phase transition, but rather a singularity in the multi-dimensional coupling space of actions.

To elaborate a little further on this matter: $SU(2)$ lattice gauge theory has a finite temperature phase transition of first order. This phase transition can be obtained in two ways, either by varying the temporal extent of the lattice, e.g., $N_t = 8, 6, 4, 2$ or by keeping the temporal extent fixed and varying the gauge coupling β . In any case, the spatial directions of the lattice have to be much larger than the temporal extent. However, the study of this phase transition is not relevant for the work at hand and will not be discussed further. We also note, that this peak in the susceptibility gets slightly smoother with bigger lattice sizes. For the most part the errorbars are again too small to be seen.

5.2 Simulation using cycle occupation numbers (ACC's)

After dualising the theory (cf. Chapter 3) the cycle occupation numbers $p_{x,\mu\nu}^{abcd}$ (ACC) replace the gauge link variables as our degrees of freedom for the simulation. Therefore we have to use different update schemes, as we update completely different degrees of freedom that sit on plaquettes and obey constraints. Considering the constraints for the plaquette fluxes shown in Figure 3.3 we find that we can construct 3 valid update schemes for the dual theory that fulfill these constraints.

The first and simplest update is to change all plaquettes on the whole lattice in the form of a closed sheet winding around the periodic boundary conditions, making it a "global" update: We recall that the graphical representation of the ACC's winding in colour space is given in Figure 3.1. To generate these sheets the algorithm randomly chooses a colour value for each site of the lattice, thus constructing closed surfaces in each plane. This update trivially keeps the flux constraints in Equation (3.16) intact, with the requirement that all ACC's in a specific plane have the same orientation. These updates are performed for each plane individually. For the computation of the Metropolis ratio, each plaquette contributes a factor of $\frac{\beta}{2}$ plus combinatorial factors. Thus for small values of β these updates are not likely to get accepted, since the corresponding configurations here only contribute a small weight. A graphical representation of an example for this kind of updates is shown in Figure 5.2a.

The second update the algorithm performs is called "double plaquette update". Here the program offers to locally place an ACC and its anti-ACC at a specific site x . As

explained in Chapter 3, each corner of the ACC carries colour. To determine which ACC the algorithm offers to place, it randomly chooses the colour values for each corner of the plaquette it wants to update and then inverts the colour to build the anti-ACC. It can be easily shown that these configurations fulfill the constraints locally, such that we leave the plaquettes at the other sites unchanged and simply calculate the Metropolis ratio for this local contribution. Here each double plaquette contributes a factor of $\left(\frac{\beta}{2}\right)^2$ as well as the two combinatorial factors. The first of these factors reads

$$\frac{1}{(p_{x,\mu\nu}^{abcd} + 1) \cdot (p_{x,\mu\nu}^{\bar{a}\bar{b}\bar{c}\bar{d}} + 1)} \quad , \quad (5.11)$$

which comes from the $W_\beta[p]$ weight factor. The other combinatorial factor contributing to the computation of the Metropolis ratio stems from the weight factor $W_H[p]$ given in Equation (3.21) and reads

$$\frac{\left(\frac{\mathcal{S}_{x,\mu}^{ab} + \mathcal{S}_{x,\mu}^{\bar{a}\bar{b}}}{2} + 1\right) \cdot \left(\frac{\mathcal{S}_{x,\mu}^{\bar{a}\bar{b}} + \mathcal{S}_{x,\mu}^{ab}}{2}\right)}{\left(\frac{\mathcal{S}_{x,\mu}^{ab} + \mathcal{S}_{x,\mu}^{\bar{a}\bar{b}} + \mathcal{S}_{x,\mu}^{\bar{a}\bar{b}} + \mathcal{S}_{x,\mu}^{ab}}{2} + 2\right)} \quad . \quad (5.12)$$

The expressions shown in Equations (5.7) and (5.8) are for the case that we updated the 2 plaquettes $p_{x,\mu\nu}^{abcd}$ and $p_{x,\mu\nu}^{\bar{a}\bar{b}\bar{c}\bar{d}}$. All this makes these updates more likely to be accepted compared to the sheets in the small β region. This whole update procedure is then carried out in a loop over all sites of the lattice and in each direction. A graphical example of such an update is shown in the Figure 5.2b.

The two update schemes mentioned above are the only ones that exist in 2 dimensions. However if we go to 3 or 4 dimensions, one finds that there is another possible update for plaquette configurations, which we refer to as cube update. The idea here is to generate new configurations by locally placing a cube of closed colour flux at a site x . The cubes can in 4 dimensions be placed in 4 different ways when considering directions $\mu < \nu < \rho$, i.e., $(\hat{1} - \hat{2} - \hat{3})$, $(\hat{1} - \hat{2} - \hat{4})$, $(\hat{1} - \hat{3} - \hat{4})$ or $(\hat{2} - \hat{3} - \hat{4})$. Each face of the cube contains an ACC sitting in the corresponding plane $\mu < \nu$: $(\hat{1} - \hat{2})$, $(\hat{1} - \hat{3})$, $(\hat{2} - \hat{3})$, $(\hat{1} - \hat{4})$, $(\hat{2} - \hat{4})$, $(\hat{3} - \hat{4})$. The 6 ACC's on the cube, i.e., $p_{x,\mu\nu}^{abcd}$, $p_{x,\mu\rho}^{\bar{a}\bar{b}\bar{f}\bar{e}}$, $p_{x,\nu\rho}^{adhe}$, $p_{x+\hat{\rho},\mu\nu}^{\bar{e}\bar{f}\bar{g}\bar{h}}$, $p_{x+\hat{\nu},\mu\rho}^{dcgh}$, $p_{x+\hat{\mu},\nu\rho}^{\bar{b}\bar{c}\bar{g}\bar{f}}$, have to be arranged in such a way that they obey the constraints of the theory. Here the colours are denoted by the letters $a - h$ and letters with a bar $\bar{a} - \bar{h}$ represent the respective anti-colours. The reason why some of the cycle occupation number are labeled with anti-colours comes from the structure of the constraints of the dual colour space representation. But before we explain this property, we have to elaborate further on the features of the cube update.

As a simple example, consider the cubic updates without having 2 layers for each

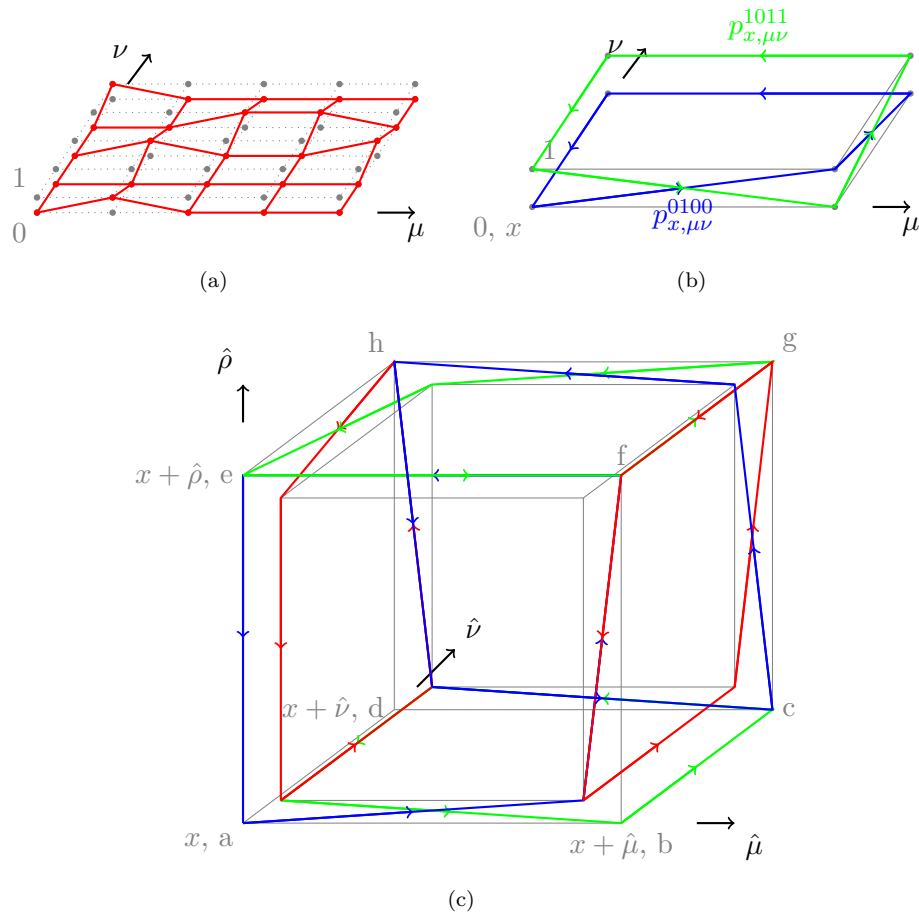


FIGURE 5.4: Graphical illustration of the update schemes for the dual simulation. In Subfigure (a) we show an example for the sheet updates winding around the periodic boundary conditions of a 5×5 lattice. Subfigure (b) shows the double plaquette update. Subfigure (c) illustrates the cube update with a specific example of ACC's on a cube. Here the inner cube is the 0 colour layer and the outer cube represents the colour layer 1. All of these update schemes keep the flux constraints intact. Note that (a) is a global update, whereas (b) and (c) are local updates.

plaquette available, e.g., $U(1)$ dual gauge theory in $d > 2$ dimensions. There the orientations of all plaquettes on the cube are uniquely determined after choosing the orientation of one of the plaquettes. If we choose the bottom plaquette to be positively oriented, the front plaquette needs to be negatively oriented to compensate the flux at the bottom-front edge. The left one then needs to be positively oriented, the top in negative direction, the back one is then again positively oriented and last but not least the right plaquette has to be oriented in negative direction. This choice of orientations is depicted in Figure 5.3. Then raising or lowering one of the plaquettes uniquely fixes how the other plaquettes around the cube need to be updated. This means for example, that if we choose the positively oriented ACC's to be raised by a value Δ then the negatively oriented plaquettes get lowered by Δ to compensate the flux.

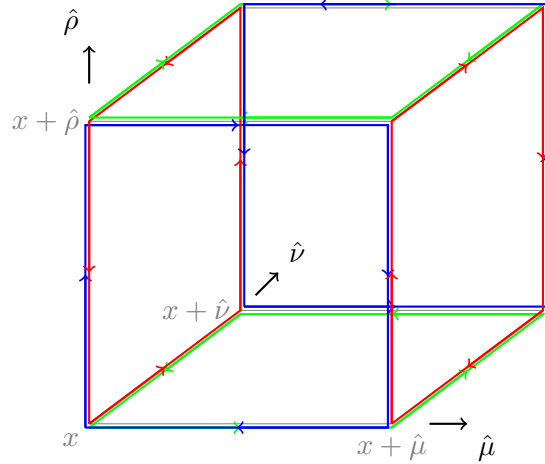


FIGURE 5.5: Illustration of a cube update in the $U(1)$ gauge theory. Note that here we need negatively oriented loops to cancel the flux at all edges. This is because here we do not have a second layer available at each site.

We are now ready to discuss the previously mentioned feature of the colour space dual representation of the $SU(2)$ theory. Here the ACC's that would be negatively oriented in the theory without 2 layers at each site can be replaced by their positively oriented anti-ACC. Repeating this for all the negatively oriented plaquettes of the cube shown in Figure 5.3 leaves us with a cube where the plaquettes are all positively oriented. It turns out that given a colour configuration for all sites of the cube, there exists only one way to arrange the ACC's such that their fluxes cancel out for each edge of the cube, such that we can construct a valid local update. An example configuration is shown in Figure 5.2c, where the ACC's contributing to the cube are: $p_{x,\mu\nu}^{0110}, p_{x,\mu\rho}^{1011}, p_{x,\nu\rho}^{0010}, p_{x+\hat{\rho},\mu\nu}^{1110}, p_{x+\hat{\nu},\mu\rho}^{0101}, p_{x+\hat{\mu},\nu\rho}^{0011}$. Notice that the ACC's are now all oriented in a mathematically positive sense. The way the algorithm generates a cube configuration is by randomly choosing 8 colour values for the 8 corners of the cube. It then constructs the ACC's and anti-ACC's for each site accordingly such that the flux at the edges of the cube is canceled out. Each cube contributes a factor of $\left(\frac{\beta}{2}\right)^6$ to the Metropolis ratio as well as combinatorial factors from the weights. We omit the full expressions of the combinatorial factors as they are rather long and do not provide any new insights. Note that in principle they look analogous to the ones given in Equations (5.7) and (5.8), but the construction here is more complicated due to the structure of the cube plaquettes. Considering all the contributions from the weight factors makes the cube updates very likely to get accepted at small β , which is also confirmed by our simulation.

Also the formulas how to compute the observables of interest have to be adapted to the new degrees of freedom for the simulation. The according formulas have been derived in Chapter 3.2.

5.3 Simulation using the truncated theory

5.3.1 The algorithm

In Chapter 3 we already explained the problem which arises from the dualised $SU(2)$ theory, i.e., the configurations depicted in Figure 3.5 which give rise to negative contributions. Thus to try simulating the theory we used the truncated version of the dual theory, described in Chapter 4.3.

The method and the updates to simulate this theory is identical to the one mentioned in the section above, but now we have again changed the degrees of freedom of our simulation. The algorithm now uses the dual variables which arise from the truncated cycle occupation numbers $p_{x,\mu\nu}^{abcd}$, i.e., $V_{x,\mu\nu}^{abcd}$ and $D_{x,\mu\nu}^{abcd}$.

Given below is a pseudo-code version of the program we wrote to simulate the truncated theory.

```

set nmeas = 106
set nequi = 105
set nskip = 20
 $\beta_0 = 0.0$ 
 $\Delta\beta = 0.05$ 
initialise neighbour field
for  $i: 0 \rightarrow 80$ 
     $\beta = \beta_0 + i \cdot \Delta\beta$ 
    sheet(nequi)
    double(nequi)
    cube(nequi)
    for  $j:0 \rightarrow \text{nmeas}-1$ 
        sheet(nskip)
        double(nskip)
        cube(nskip)
        calculate-plaquette( j )
    end for
    plaquette-expectation-value = calculate-mean()
    chi = calculate-chi()
end for

```

Again, as in the conventional simulation, we first initialise our number of measurements, the number of equilibrating updates and the number of skip updates between the measurements. The numbers were chosen to be the same as in the pseudo-code for the conventional simulation, but of course can be different, depending on the task of the actual run. Also the initialisation of the neighbour field is the same as in the original simulation.

As one can clearly see from the pseudo-code example, once we enter the loop over the β values, the code looks different compared to the pseudo-code example from the previous section. Here the algorithm needs to perform *nequi* equilibrating updates for the sheets, the double plaquettes and the cubes. Also in between the measurements the program performs *nskip* updates with the 3 mentioned functions. After performing the updates the program needs to compute the observables according to Equations (3.29) and (3.30), of course with $p_{x,\mu\nu}^{abcd}$ replaced by the definition given in (4.23).

In order to properly simulate the theory at small β , we need to apply reweighting. To shortly elaborate on how the reweighting technique works, we consider a Monte Carlo simulation at coupling β and the measurement of some observable $\mathcal{O}[\phi]$, where the ϕ 's are the configuration of the fields. The standard way to compute expectation values in Monte Carlo simulations is

$$\langle \mathcal{O} \rangle_\beta = \frac{1}{Z_\beta} \int D[\phi] W_\beta[\phi] \mathcal{O}(\phi) , \quad Z_\beta = \int D[\phi] W_\beta[\phi] , \quad (5.13)$$

where the subindex β of the expectation value denotes at which coupling the configurations are sampled for this computation or rather which coupling is taken into account by the weight factor $W_\beta[\phi]$. If we now consider the partition function of the theory at coupling β' , i.e., $Z_{\beta'} = \int D[\phi] W_{\beta'}[\phi]$, we can rewrite the expectation value from (5.7) in the following form

$$\langle \mathcal{O} \rangle_\beta = \frac{\frac{1}{Z_{\beta'}} \int D[\phi] W_{\beta'}[\phi] \mathcal{O}[\phi] \frac{W_\beta[\phi]}{W_{\beta'}[\phi]}}{\frac{1}{Z_{\beta'}} \int D[\phi] W_{\beta'}[\phi] \frac{W_\beta[\phi]}{W_{\beta'}[\phi]}} . \quad (5.14)$$

Notice how the terms in the numerator as well as in the denominator have the form of expectation values themselves, thus we can write:

$$\langle \mathcal{O} \rangle_\beta = \frac{\left\langle \mathcal{O}[\phi] \frac{W_\beta[\phi]}{W_{\beta'}[\phi]} \right\rangle_{\beta'}}{\left\langle \frac{W_\beta[\phi]}{W_{\beta'}[\phi]} \right\rangle_{\beta'}} . \quad (5.15)$$

We conclude that we can compute the observable at coupling β by calculating the expectation value of the observable multiplied with the ratio of the weights at the different

couplings β' divided by the expectation value of this ratio. To compute the expectation values on the right hand side, we sample the configurations at coupling β' during the simulation. Reweighting allows us to work at couplings $\beta' > \beta$ where the acceptance rate for updates is much better than at the target coupling β . We have implemented this technique in the computation of our observables. This made a comparison of the results obtained by the two simulation schemes possible.

We will now shortly explain how each of the update functions work. This again will mainly be done by discussing a pseudo-code formulation of the algorithm.

First we describe the function that updates the closed sheets of plaquettes. The following pseudo-code illustrates the general steps.

sheet(n sweep)

```

for  $j$ :  $0 \rightarrow \text{n sweep}-1$ 
  set Metropolis ratio  $\rho = 1.0$ 
  generate colour from set  $\{0, 1\}$  for each site
  for  $i$ :  $0 \rightarrow \text{planes}$ 
    choose  $\Delta$  either  $-1$  or  $+1$ 
    for  $x$ :  $0 \rightarrow \text{sites}$ 
      check whether  $V = 0$  at site  $x$ , given direction  $i$  and given colour combination
      if  $V = 0 \rightarrow V + \Delta$  and multiply  $\rho$  with corresponding weight factor
      if  $V \neq 0 \rightarrow \text{set } V = 0$  and multiply  $\rho$  with corresponding weight factor
    end for
  generate random number  $r \in [0, 1]$  and check  $r < \rho$ 
  if true  $\rightarrow$  accept the sheet
  check if the value of the anti-plaquette is 0 or 1
  if 1  $\rightarrow$  set variables  $V_{x,\mu\nu}^{abcd} = 0$  and  $V_{x,\mu\nu}^{\bar{a}\bar{b}\bar{c}\bar{d}} = 0$  and set variable  $D_{x,\mu\nu}^{abcd} = 1$ 
end for
end for
end sheet

```

Here we first set the Metropolis ratio to 1. This is justified as it is a multiplicative quantity in the individual weight contributions. Then the algorithm randomly chooses the colour indices for all the sites of the lattice. The algorithm then loops over all the planes, as the sheet updates can only be carried out in one plane at a time. The program then chooses a variable Δ to be -1 or $+1$, whereby it determines whether the dual

variables $V_{x,\mu\nu}^{abcd}$ are raised or lowered for all sites on this plane. Then the algorithm loops over all the sites, where it checks whether the plaquette on the current site is already occupied. Using this information, the program adjusts the V variable correspondingly and chooses the fitting weight factor for this case. This is then repeated for all the sites in the current plane. After completing this loop, it generates a random number between 0 and 1 and checks whether ρ is larger than the random number. If this is the case, the sheet gets accepted for the current plane and the algorithm moves on to the next plane.

Next we explain how the double plaquette update works. First we again show the pseudo-code version of the function.

```

double(nswEEP)
  for  $j$ : 0  $\rightarrow$  nswEEP-1
    for  $x$ : 0  $\rightarrow$  sites
      for  $d$ : 0  $\rightarrow$  planes
        set  $\rho = 1.0$ 
        randomly choose the 4 colour indices of the current plaquette
        check if ( $V$  and anti- $V$  variable) = 0
        check if  $D = 0$ 
          if  $D = 0 \rightarrow$  set  $D = 1$ 
          if  $D = 1 \rightarrow$  set  $D = 0$ 
          multiply  $\rho$  with corresponding weight factor
        check condition  $r \in [0, 1] < \rho$ , where  $r$  is random number
        if true, place double plaquette
      end for
    end for
  end for
end double

```

As the double plaquette update is a local update, we immediately update the degrees of freedom in all steps of the loop over all the lattice sites. The loop over the planes is included in the lattice site loop, simply for practical reasons. Inside these two loops we first set the Metropolis ratio to 1 for reasons explained before. Then the algorithm generates a plaquette update candidate by randomly choosing a colour index for the 4 corners of the plaquette. According to Table 4.1 the double plaquettes can only occur if the variable $V_{x,\mu\nu}^{abcd}$ and its counter part $V_{x,\mu\nu}^{\bar{a}\bar{b}\bar{c}\bar{d}}$ are zero. Thus the program has to check

if this condition is true. If it is true, the algorithm then needs to determine whether to put a double plaquette or to remove it. It does that by simply checking if the variable $D_{x,\mu\nu}^{abcd}$ is zero or not. If it is zero, the algorithm offers to put a double plaquette at the current site. Otherwise it offers to remove the double plaquette. The rest of the steps are then just the usual Metropolis steps. We stress here that in the case of the double plaquette update and the sheet updates, the weight factors from the \mathcal{S} -fluxes are updated immediately in each Metropolis acceptance step.

Finally, we need to explain the cube update. Again the pseudo-code helps to illustrate the general structure of this update.

cube(nsweep)

```

for  $j$ : 0  $\rightarrow$  nsweep-1
  for  $x$ : 0  $\rightarrow$  sites
    for  $d$ : 0  $\rightarrow$  set of planes
      set  $\rho = 1.0$ 
      choose  $\Delta$  from set  $\{-1, +1\}$ 
      randomly choose the 8 colour indices of the cube
      check if  $V$  and  $D$  variables are zero for all faces of the cube
        if true: increase and decrease the variables  $V$  by  $\pm\Delta$  accordingly
        compute weights and Metropolis ratio  $\rho$  for current configuration
        check if random number  $r \in [0, 1] < \rho$ 
          if true: accept new configuration of the  $V$ 's
          check whether the anti- $V$  variables are occupied
          if yes: set all  $V = 0$  and increase  $D$  variables for all faces
        if  $V$ 's and  $D$ 's  $\neq 0$ : remove the cube with generated configuration
      end for
    end for
  end for
end cube

```

Also the cube update is a local update, but it combines elements of both, the blanket and the double update scheme. In this update we propose a cube which has only a single ACC on each face, thus we need to choose a variable Δ . The value of Δ determines whether the plaquettes get increased or decreased. Then the algorithm needs to generate a colour configuration to offer, which is done by randomly choosing a colour index for the

8 sites contained in the cube. To determine whether the generated cube needs to be put on the lattice or taken away, the program checks if the links contained in the current offer cube configuration are already occupied or not. If they are all empty, it offers to put the cube onto the site in the given combination of planes. Next the algorithm computes the weight factors contributing to the cubes, which is here done according to Equations (4.28) and (4.30). Then it performs the usual Metropolis acceptance check, setting the corresponding V variables to their offered values if the configuration gets accepted. However it might be the case, that the anti-plaquettes are already occupied for all the plaquettes on the newly updated cube. This is a condition the algorithm needs to check. If this is the case, the program sets all the V and anti- V variables to zero and increases the D variables, making it effectively a double cube update in this particular case. If the initial check of whether all the plaquettes are empty fails, the program offers to remove the generated cube, computing again the weight factors and performing the usual Metropolis steps.

5.3.2 Results

In this section we will display the results obtained by simulating the theory using the truncated dual variables and compare to the results we achieved by using the conventional formulation of the theory. As a reference for both data sets, we have again plotted the analytic strong and weak coupling expansion curves, which are obtained from Equations (5.7) - (5.10). The results are obtained by setting the following starting parameters in the simulation:

- $nmeas = 10^5$,
- $nequi = 10^4$,
- $\Delta\beta = 0.1$,
- we perform 40 steps of $\Delta\beta$,
- reweighting factor 0.006.

We have performed a careful analysis of the reweighting factor and found, that using the value of 0.006 gives the best results. The value is chosen this small, because otherwise one runs into trouble when simulating using bigger lattices. There when calculating the reweighted results, some quantity exceeds the numerical boundary of the computer resulting in the output: "not a number" (nan).

In Figure 5.6 we compare the results for the plaquette expectation value obtained by the two different simulation schemes. The results shown here were computed for lattice sizes 4^4 , 8^4 , 10^4 and 12^4 .

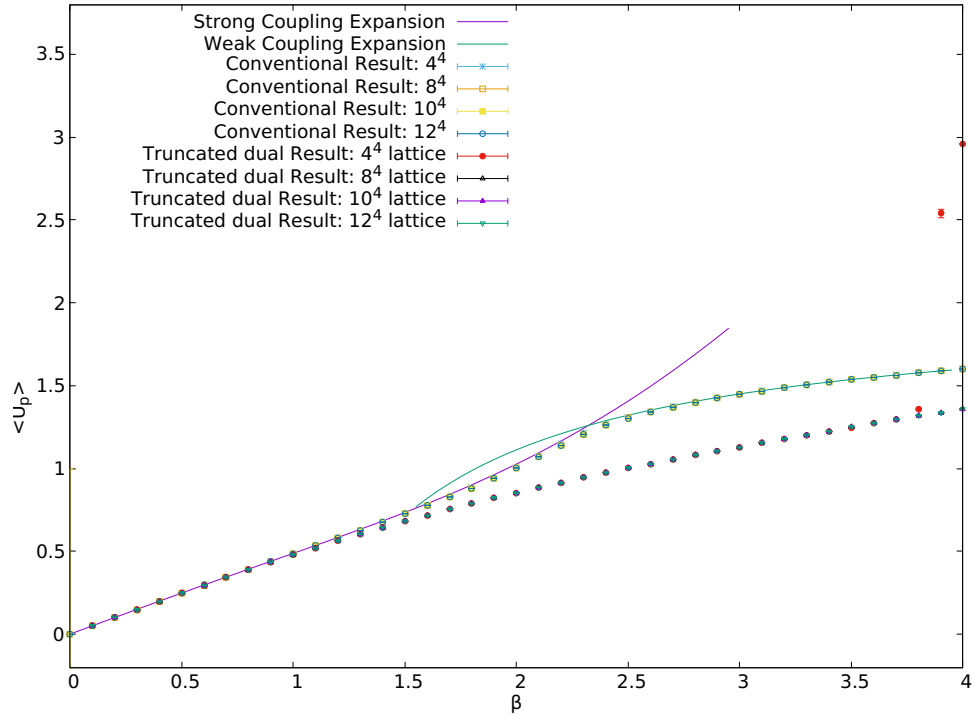


FIGURE 5.6: Comparison of the results for the plaquette expectation value $\langle U_p \rangle$ obtained by the conventional and the truncated simulation. We show the results for lattice sizes 4^4 , 8^4 , 10^4 and 12^4 and plot the analytic strong and weak coupling expansion curves as a reference. In the strong coupling regime the data from the two different simulations are almost identical as both approach the strong coupling curve asymptotically. The data only start to deviate more strongly above $\beta \approx 1.2$. Errorbars are too small to be seen for the most part.

The most important feature that one immediately notices is that the data from the truncated simulation fit the data of the conventional simulation very well in the strong coupling region. Both results approach the strong coupling expansion curve asymptotically. In this region the datapoints for the different simulation schemes agree well within error for all lattice sizes. As we have seen and discussed before, the data of the conventional simulation follows the expansion curves very closely and forms a connection between the two analytic curves. The results obtained by the truncated simulation start out linearly with the same slope as the conventional results up to $\beta = 1.2$. Beyond this value the data deviates from the conventional data and follows a slightly curved line going towards the weak coupling regime. This however can be explained as a direct effect of the truncation of the dual variables. Hence the truncated results do not form a smooth connection between the two expansion curves in the transition region. The data from the truncated simulation does not show any signs of a maximum slope, which obviously is in contrast to the results obtained by the conventional simulation.

Figure 5.7 compares the results we obtained for the susceptibility χ . As a reference we again plotted the expansion curves as well. One can clearly see, that the data from the truncated simulation matches the data obtained from the conventional simulation

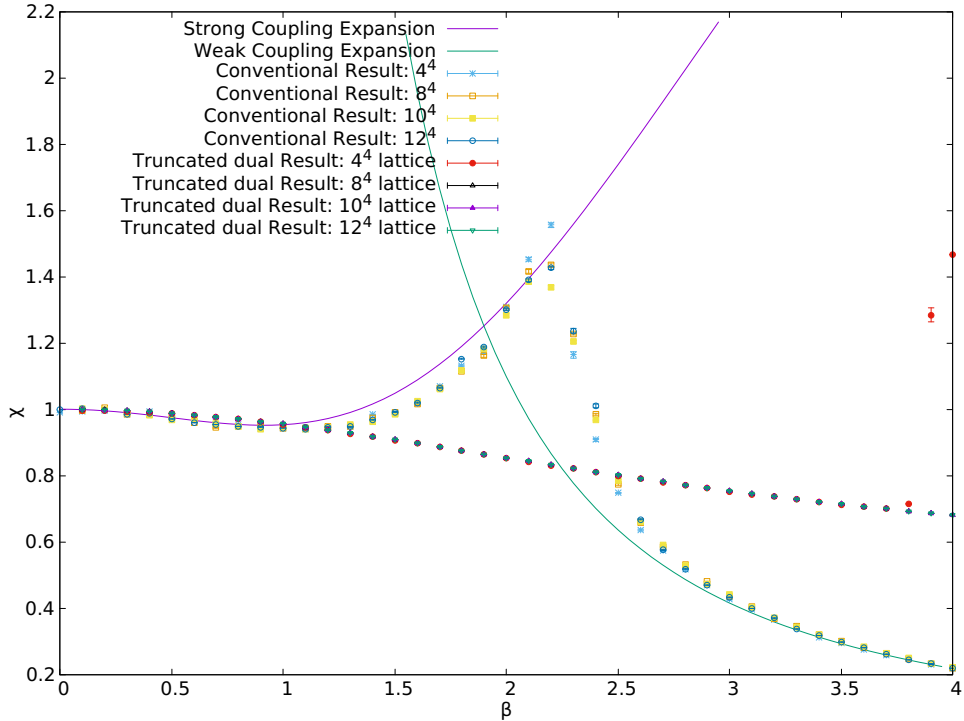


FIGURE 5.7: Comparison of the results for the susceptibility χ obtained by the truncated and the conventional simulation. Again as a reference we show the expansion curves. In the strong coupling region the data from the two simulations compares well, for any lattice size. The results start to deviate more strongly starting from $\beta = 1.2$ and beyond.

rather well in the strong coupling regime. The truncated results do not follow the strong coupling expansion curve beyond $\beta > 1.2$ after which the datapoints decrease almost linearly with increasing β . In contrast the data from the conventional simulation follows and connects the two expansion curves more closely.

We notice that in both graphs the data for the 4^4 lattice sizes starts to rise massively in the end. This deviation can be explained by the fact that in this region the sheet updates kick in. These sheet updates are suppressed in the bigger lattices and only play a role on the smaller lattices for rather large values of β . Finally we need to stress, that the errorbars are of the order $10^{-5} - 10^{-6}$ in both plots and thus are too small to be seen here. But the data for the different lattice sizes agree to a good degree.

Comparing the data of the two simulations we draw the conclusion, that our naive version of a qubit truncation is a valid formulation of $SU(2)$ lattice gauge theory in the strong coupling regime. Thus one can use the truncated version to accurately describe the physics in the strong coupling region. We also stress, that we performed a careful analysis of the relative sign from Equation (3.20) and find, that using our truncated version there appear no negative contributions in the simulation, at least in the region we looked at. Thus we have managed to circumvent the sign problem in a way, which

was the overall goal of this master thesis.

5.4 Error calculation

A short comment is in order regarding the error calculation in our simulations. This was done via the jackknife method, which we will shortly outline in the following. Consider a data set of N measurements. The first step is to divide this data set into N_B blocks of length $B = \frac{N}{N_B}$. This is just to make the blocks statistically independent. The next step is to go through the individual blocks and for each block b of size B we delete this block from the full set of data and compute the expectation value

$$\langle \mathcal{O} \rangle_{\beta}^b = \frac{\left\langle \mathcal{O}[\phi] \frac{W_{\beta}[\phi]}{W_{\beta_c}[\phi]} \right\rangle_{\beta'}}{\left\langle \frac{W_{\beta}[\phi]}{W_{\beta_c}[\phi]} \right\rangle_{\beta'}} . \quad (5.16)$$

Here the superindex $b \in \{1, 2, \dots, N_B\}$ denotes the block that is omitted from the data and the expectation values on the right hand side of the equation considers only the $N - B$ measurements which are not contained in block b . We display the expressions for the reweighting strategy, and β' here denotes the coupling we work with.

The last step is to compute the error according to the following formula:

$$\delta \langle \mathcal{O} \rangle_{\beta} = \frac{1}{N_B} \sqrt{\sum_{b=1}^{N_B} \left(\langle \mathcal{O} \rangle_{\beta}^b - \langle \mathcal{O} \rangle_{\beta} \right)^2} . \quad (5.17)$$

The sum runs over all the blocks and the average $\langle \mathcal{O} \rangle_{\beta}^b$ is used as a bias correction. The factor $\langle \mathcal{O} \rangle_{\beta}$ is the reweighted value of the full dataset. To further improve the determination of the statistical error one may study the error as a function of the blocksize. The error first grows with increasing blocksize until the blocksize becomes of the order of the autocorrelation, where the error values form a plateau. The values in the plateau then provide a good estimate of the true statistical error, taking into account autocorrelation effects.

The following plots provide some examples for more or less ideal versions of the error curve as a function of blocksize described in the previous paragraph. Here the forming of the plateau can be seen clearly in most figures and the value of the error can be readily determined from the plot. We must stress however, that these kind of plots do not always look like this, and more often than not, the plateau cannot be seen this clearly. Very often the reason for "blurry" plateaus are strong fluctuations in the error. Sometimes it can happen, that another plateau forms for bigger blocksizes. Here then one often chooses one of the plateaus consistently for all the datapoints. In these cases larger statistics would be needed for a reliable error estimation. One short comment is

in order regarding the blocksizes. These should ideally be chosen to be proper divisors of the number of measurements N , otherwise one can potentially find discontinuities in the error-blocksize-plots.

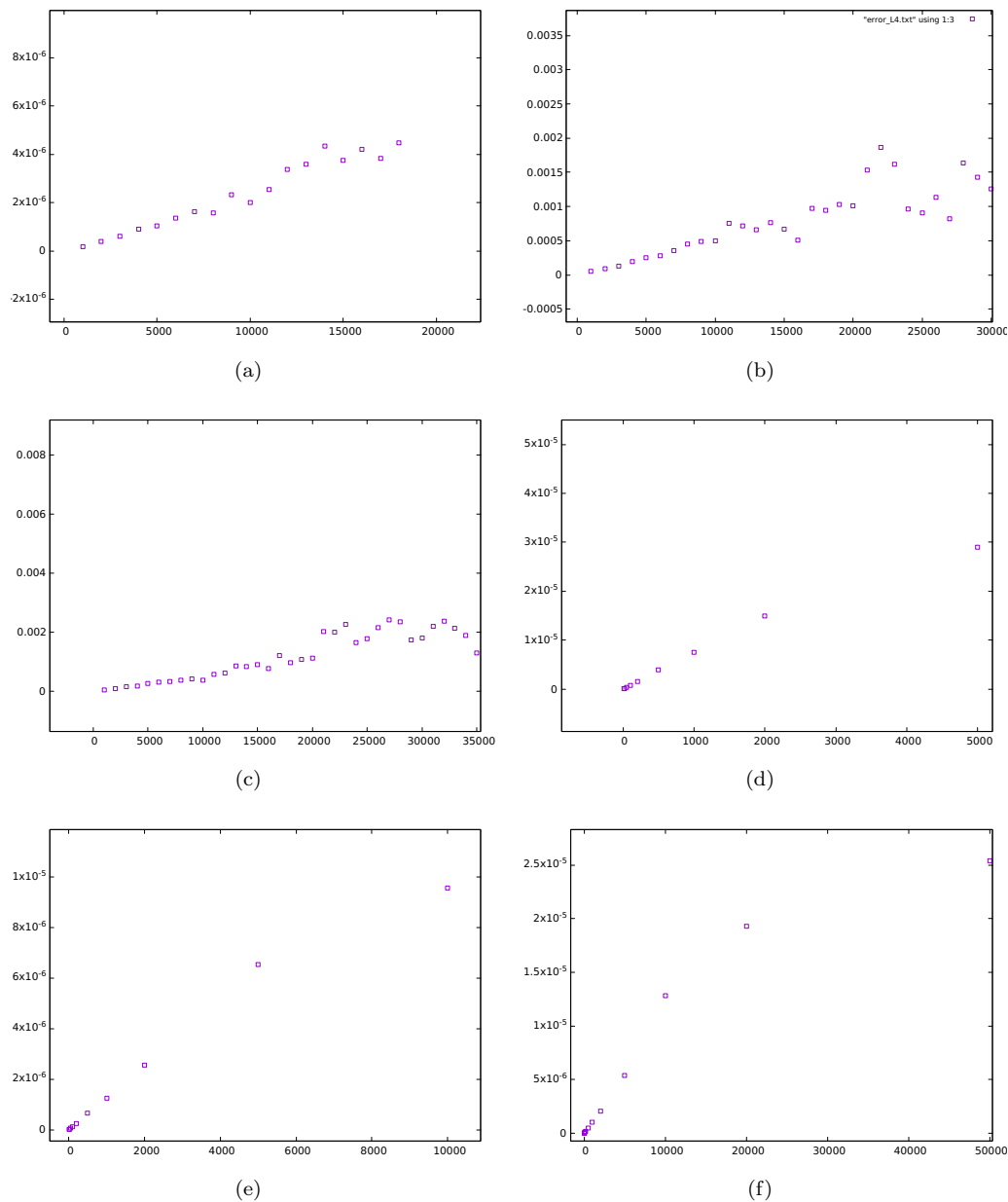


FIGURE 5.8: The value of the error (y-axis) plotted versus and the blocksizes (x-axis). Subfigure (a) shows an example of a rather ideal curve with almost no fluctuations in the error. Here the error increases with increasing blocksize until it saturates. In this example the error can be easily read of to be $\pm 5 \cdot 10^{-6}$. Subfigure (b) illustrates a less good example. It shows the formation of a kind of "blurry" plateau. One can nevertheless observe the saturation of the error. Note that the data starts to oscillate wildly after the plateau. Subfigure (c) shows the mentioned jumps in the plot, that can happen, when we use blocksizes that are not proper divisors. The plateau can still be made out. Subfigures (d)-(f) show ideal curves where only the proper divisor blocksizes were taken into account.

To shortly comment on the figures above. For Figures 5.8 (a)-(c) we have increased the blocksize by a factor 1000 in our analysis. Thus most of the blocksizes are not proper divisors. The effect these non-proper divisor blocksizes can have is clearly illustrated in Figure 5.8(c), where one can see the discontinuities in the datapoints. Figures 5.8 (d)-(f) used specific blocksizes which are indeed proper divisors.

In all of the figures the plateau can be more or less clearly seen. A lot of the plots we analysed for the error looked like Figure 5.8 (a). Despite the small fluctuations in the error plot, the plateau and thus the error can be very clearly determined.

Chapter 6

Summary

In this thesis we explored three main approaches to solving the sign problem of the dualised $SU(2)$ pure lattice gauge theory. As stated in Chapter 3, the sign arises because we need to choose an explicit representation of the $SU(2)$ matrices to carry out the dualisation procedure.

The first method we tried was to factor out the center of the group $SU(2)$, i.e., \mathbb{Z}_2 and see whether we manage to achieve some new constraints of the theory. The approach indeed produced constraints, however they could be identified with another set of constraints already contained in the dual theory. Thus we did not gain any new insights with this ansatz.

In the second approach we assigned a (site and direction-dependent) index to the colour degrees of freedom and performed the dualisation procedure. In doing so we managed to represent the partition sum in terms of colour micro fluxes sitting on the links of the lattice. This index formulation has a rather nice geometrical representation. The hope of this approach was to resum the negative contributions coming from the relative sign to obtain positive overall weights. Analysing the possible contributions in terms of the micro fluxes, we found that resummation might be possible. However, further analysis is needed to make a definite statement about this matter. We decided to abandon this approach in favour of the truncation approach.

The third and final ansatz in this thesis was the truncation approach. Here we truncated the dual variables of the original dual theory, such that they can only take values $-1, 0, +1$. We then introduced new dual variables such that our dual theory resembles the representation of a qubit regularised theory. Using the new variables we obtained a singlet-triplet representation of our theory, meaning that we get states which obey the spin algebra. Furthermore this approach has a nice geometrical representation. The hope of this ansatz was, that in truncating the theory the negative contributions would not be present anymore.

Once we developed the formalism of the approach we performed simulations for the

truncated theory and the conventional $SU(2)$ matrix theory. Comparing the results of these two simulations we found, that the data agrees very well in the strong coupling regime. This was one of the goals of the truncation approach. The second and of course the main goal of this thesis was to analyse whether the sign problem is solved by this approach. During the simulation we analysed the sign for the valid configurations and found, that the relative sign was always positive. Thus with this approach we have managed to find a dual formulation of the theory, which works well in the strong coupling regime and circumvents the sign problem successfully.

It will be interesting to see if in the future this truncation approach can also be applied to the dual formulation of $SU(3)$, as this is the next higher non-abelian Lie group.

Appendix A

Reordering of the $U(1)$ gauge links

Here we show the steps of the calculation done in Chapter 2.4.1.

$$\begin{aligned}
& \prod_{x,\nu<\rho} (U_{x,\nu\rho})^{m_{x,\nu\rho}} = \prod_{x,\nu<\rho} (U_{x,\nu} U_{x+\hat{\nu},\rho} U_{x+\hat{\rho},\nu}^* U_{x,\rho}^*)^{m_{x,\nu\rho}} = \\
& = \prod_{x,\nu<\rho} (U_{x,\nu})^{m_{x,\nu\rho}} \prod_{x,\nu<\rho} (U_{x+\hat{\nu},\rho})^{m_{x,\nu\rho}} \prod_{x,\nu<\rho} (U_{x+\hat{\rho},\nu}^*)^{m_{x,\nu\rho}} \prod_{x,\nu<\rho} (U_{x,\rho}^*)^{m_{x,\nu\rho}} = \\
& = \prod_{x,\nu} \prod_{\rho:\nu<\rho} (U_{x,\nu})^{m_{x,\nu\rho}} \prod_{x,\rho} \prod_{\nu:\nu<\rho} (U_{x+\hat{\nu},\rho})^{m_{x,\nu\rho}} \prod_{x,\nu} \prod_{\nu:\nu<\rho} (U_{x+\hat{\rho},\nu}^*)^{m_{x,\nu\rho}} \prod_{x,\rho} \prod_{\rho:\nu<\rho} (U_{x,\rho}^*)^{m_{x,\nu\rho}} .
\end{aligned}$$

In the first term one can simply convert the product over the index ρ into a sum in the exponent

$$\prod_{x,\nu} (U_{x,\nu})^{\sum_{\rho:\nu<\rho} m_{x,\nu\rho}} , \quad (\text{A.1})$$

and the term is in the form we want. To rewrite the second term to the form of only a product over $U_{x,\nu}$ instead of $U_{x+\hat{\nu},\rho}$, we first convert the product over ν into a sum in the exponent as before and find

$$\prod_{x,\rho} (U_{x+\hat{\nu},\rho})^{\sum_{\nu:\nu<\rho} m_{x,\nu\rho}} .$$

After that we shift the product index x to $x' = x + \hat{\nu}$ and obtain

$$\prod_{x',\rho} (U_{x',\rho})^{\sum_{\rho:\nu<\rho} m_{x'-\hat{\nu},\nu\rho}} ,$$

which gives rise to the same product over all sites since we use periodic boundary conditions. All that is left to do now is to relabel the directional indices $\rho \rightarrow \nu$ and $\nu \rightarrow \rho$ and we can relabel the product index x' back to x , with which the term then reads

$$\prod_{x',\nu} (U_{x',\nu})^{\sum_{\rho:\rho<\nu} m_{x'-\hat{\rho},\rho\nu}} . \quad (\text{A.2})$$

The third term works analogously: we convert the product into a sum in the exponent and shift the product index x to $x' = x + \hat{\rho}$ after which we can simply rename the product index back to x

$$\prod_{x,\nu} (U_{x',\nu}^*)^{\sum_{\nu:\nu<\rho} m_{x-\hat{\rho},\nu\rho}} . \quad (\text{A.3})$$

Now for the last term, we repeat the same steps as before, converting the product again into a sum in the exponent and then relabeling the indices as done for the second term.

We finally arrive at

$$\prod_{x,\nu} (U_{x,\nu}^*)^{\sum_{\rho:\rho<\nu} m_{x,\rho\nu}} . \quad (\text{A.4})$$

If we now insert the Equations (A.1) - (A.4) back into the starting equation, we get

$$\prod_{x,\nu} (U_{x,\nu})^{\sum_{\rho:\nu<\rho} [m_{x,\nu\rho} - m_{x'-\hat{\rho},\rho\nu}] + \sum_{\rho:\rho<\nu} [m_{x'-\hat{\rho},\rho\nu} - m_{x,\rho\nu}]} . \quad (\text{A.5})$$

Appendix B

Reordering for the gauge links of $SU(2)$ lattice gauge theory

Here we show the steps necessary to bring Equation (3.7) into the more convenient form of Equation (3.8). For the rewriting we start with recollecting the term in the integral of Equation (3.7)

$$\prod_{x,\mu < \nu} \prod_{a,b,c,d} (U_{x,\mu}^{ab} U_{x+\hat{\nu},\mu}^{bc} U_{x+\hat{\nu},\mu}^{dc} * U_{x,\nu}^{ad} *)^{p_{x,\mu\nu}^{abcd}} .$$

We now factorise the term into individual products

$$\prod_{x,\mu < \nu} \prod_{a,b,c,d} (U_{x,\mu}^{ab})^{p_{x,\mu\nu}^{abcd}} \prod_{x,\mu < \nu} \prod_{a,b,c,d} (U_{x+\hat{\mu},\nu}^{bc})^{p_{x,\mu\nu}^{abcd}} \prod_{x,\mu < \nu} \prod_{a,b,c,d} (U_{x+\hat{\nu},\mu}^{dc} *)^{p_{x,\mu\nu}^{abcd}} \prod_{x,\mu < \nu} \prod_{a,b,c,d} (U_{x,\nu}^{ad} *)^{p_{x,\mu\nu}^{abcd}} . \quad (\text{B.1})$$

We start with the first term of this expression and write the products more explicitly

$$\prod_{x,\mu < \nu} \prod_{a,b,c,d} (U_{x,\mu}^{ab})^{p_{x,\mu\nu}^{abcd}} = \prod_x \prod_{\mu} \prod_{\nu: \mu < \nu} \prod_{a,b,c,d} (U_{x,\mu}^{ab})^{p_{x,\mu\nu}^{abcd}} = \prod_{x,\mu} \prod_{a,b} (U_{x,\mu}^{ab})^{\sum_{\nu: \mu < \nu} \sum_{c,d} p_{x,\mu\nu}^{abcd}} , \quad (\text{B.2})$$

where the products over ν , c and d have been converted into sums in the exponent since the $U_{x,\mu}^{ab}$ term does not depend on them. With this we have brought the first term into the desired form.

In the second term of (B.1) we again first consider those products the gauge link does not depend on and convert them into sums in the exponent

$$\prod_x \prod_{\nu} \prod_{\mu: \mu < \nu} \prod_{a,b,c,d} (U_{x+\hat{\mu},\nu}^{bc})^{p_{x,\mu\nu}^{abcd}} = \prod_x \prod_{\nu} \prod_{\mu: \mu < \nu} \prod_{b,c} (U_{x+\hat{\mu},\nu}^{bc})^{\sum_{a,d} p_{x,\mu\nu}^{abcd}} .$$

Now we can start with the relabeling of indices, we first shift x to $x' = x + \hat{\mu}$, and find

$$\prod_{x'} \prod_{\nu} \prod_{\mu: \mu < \nu} \prod_{b,c} (U_{x',\nu}^{bc})^{\sum_{a,d} p_{x'-\hat{\mu},\mu\nu}^{abcd}} ,$$

by which we achieved that the gauge link U does not depend on μ any more such that we can convert the product into a sum in the exponent and write

$$\prod_{x'} \prod_{\nu} \prod_{b,c} (U_{x',\nu}^{bc})^{\sum_{\mu: \mu < \nu} \sum_{a,d} p_{x'-\hat{\mu},\mu\nu}^{abcd}} .$$

We can relabel the product indices in the following way: $\nu \rightarrow \mu$ and $\mu \rightarrow \rho$, where we have introduced a new index ρ . With this the term becomes

$$\prod_{x'} \prod_{\mu} \prod_{b,c} (U_{x',\mu}^{bc})^{\sum_{\rho: \rho < \mu} \sum_{a,d} p_{x'-\hat{\rho},\rho\mu}^{abcd}} .$$

The final step is to interchange the colour indices $b \leftrightarrow a$, $c \leftrightarrow b$, thereby changing the order in which they appear in the expansion variable $p_{x-\hat{\rho},\rho\mu}^{abcd}$ to $p_{x-\hat{\rho},\rho\mu}^{cabd}$. If we now change the index x' back to x the final form of the term reads

$$\prod_x \prod_{\mu} \prod_{a,b} (U_{x,\mu}^{ab})^{\sum_{\rho: \rho < \mu} \sum_{c,d} p_{x-\hat{\rho},\rho\mu}^{cabd}} . \quad (\text{B.3})$$

The rewriting of the last two terms work analogously and we arrive at

$$\prod_x \prod_{\mu} \prod_{a,b} (U_{x,\mu}^{ab *})^{\sum_{\nu: \mu < \nu} \sum_{c,d} p_{x-\hat{\nu},\mu\nu}^{dcba}} , \quad (\text{B.4})$$

for the third term of Equation (B.1), and at

$$\prod_x \prod_{\mu} \prod_{a,b} (U_{x,\mu}^{ab *})^{\sum_{\rho: \rho < \mu} \sum_{c,d} p_{x,\rho\mu}^{adcb}} , \quad (\text{B.5})$$

for the fourth term. Putting all of the terms together yields

$$\prod_{x,\mu} \prod_{a,b} (U_{x,\mu}^{ab})^{\sum_{\nu: \mu < \nu} \sum_{c,d} p_{x,\mu\nu}^{abcd} + \sum_{\rho: \rho < \mu} \sum_{c,d} p_{x-\hat{\rho},\rho\mu}^{cabd}} (U_{x,\mu}^{ab *})^{\sum_{\nu: \mu < \nu} \sum_{c,d} p_{x-\hat{\nu},\mu\nu}^{dcba} + \sum_{\rho: \rho < \mu} \sum_{c,d} p_{x,\rho\mu}^{adcb}} . \quad (\text{B.6})$$

One notices that in each term the colour indices c, d that are summed in the exponents, but note that they appear in different positions in the ordered list of colour indices of the plaquette occupation numbers. For notational convenience we can introduce a summation index s to indicate the summation over the two indices c, d . Equation (B.6)

then reduces to

$$\prod_{x,\mu} \prod_{a,b} (U_{x,\mu}^{ab})^{\sum_{\nu:\mu<\nu} p_{x,\mu\nu}^{abss} + \sum_{\rho:\rho<\mu} p_{x-\hat{\rho},\rho\mu}^{sabs}} (U_{x,\mu}^{ab*})^{\sum_{\nu:\mu<\nu} p_{x-\hat{\nu},\mu\nu}^{ssba} + \sum_{\rho:\rho<\mu} p_{x,\rho\mu}^{aass}} , \quad (\text{B.7})$$

which is now the form that is given in Equation (3.8).

Appendix C

Differential forms on the lattice

In this appendix we discuss differential forms on the lattice since they were used quite often in our work. This section is only a summary of the most important properties of differential forms and follows closely the discussion of this topic of [13].

Here we consider a d -dimensional lattice with periodic boundary conditions with sites denoted as $x = (x_1, x_2, \dots, x_d)$. We have imposed periodic boundary conditions therefore the elements of a site x_i can take the value $1, 2, \dots, N_i$ and $x_i = N_{i+1} \equiv x_i = 1$. The next step in is to introduce a general quantity called r -cells which is defined as the set of sites

$$c^{(r)}(x)_{\mu_1 \mu_2 \dots \mu_r} = \{x\} \cup \{x + \hat{\mu}_i | 1 < i < r\} \cup \dots \cup \{x + \hat{\mu}_1 + \dots + \hat{\mu}_r\} \quad , \quad (\text{C.1})$$

where $\hat{\mu}_i$ denotes the unit vector in direction μ . Note that we require canonically ordered directions $\mu_1 < \mu_2 < \dots < \mu_r$. More conventionally we can also introduce a general labeling of direction as $c^{(r)}(x)_{\mu_1 \mu_2 \dots \mu_i \dots \mu_j \dots \mu_r} = -c^{(r)}(x)_{\mu_1 \mu_2 \dots \mu_j \dots \mu_i \dots \mu_r}$, where the sign refers to the orientation of the cell. To give some examples, if we take $r = 0$ we have 0-cells which correspond to sites. The next higher differential structure is $r = 1$ namely 1-forms which can be interpreted as links. Continuing this, 2-forms are plaquettes and so on.

The paper [13] then introduces an operator which acts on the r -cells called *boundary operator* ∂ and gives the oriented sum of the $c^{(r-1)}$ -cells contained in the $c^{(r)}$ -cell

$$\partial c^{(r)}(x)_{\mu_1 \mu_2 \dots \mu_r} = \sum_{k=1}^r (-1)^{k+1} \left[c^{(r-1)}(x + \hat{\mu}_k)_{\mu_1 \mu_2 \dots \hat{\mu}_k \dots \mu_r} - c^{(r-1)}(x)_{\mu_1 \mu_2 \dots \hat{\mu}_k \dots \mu_r} \right] \quad . \quad (\text{C.2})$$

The $\hat{\mu}_k$ here indicates that the index μ_k is omitted. Also we define the co-boundary operator $\hat{\partial}$ which gives the oriented sum of the $r + 1$ cells that contain the cell $c^{(r)}$ in

their boundaries,

$$\hat{\partial}c^{(r)}(x)_{\mu_1\mu_2\cdots\mu_r} = \sum_{\nu \neq \mu_1\cdots\mu_r} c^{(r+1)}(x)_{\mu_1\mu_2\cdots\mu_r,\nu} - c^{(r+1)}(x - \hat{\nu})_{\mu_1\mu_2\cdots\mu_r,\nu} \quad , \quad (\text{C.3})$$

These two operators obey two conventions, namely $\partial c^{(0)} = 0$, which is the derivative of 0-forms, i.e., sites, and introduce the convention $\hat{\partial}c^{(d)} = 0$, which says that the co-boundary of the d -cell vanishes. Furthermore they are both nilpotent, i.e., $\partial^2 = 0$ and $\hat{\partial}^2 = 0$, which is straightforward to show.

Next [13] introduces the concept of the dual lattice $\tilde{\Lambda}$, where the sites are located at the centers of the d -cells of Λ , i.e., $\tilde{x} = x + \frac{1}{2}(\hat{1} + \hat{2} + \cdots + \hat{d})$. It is straightforward to relate the r -cells to their dual $d - r$ -cells, but as we do not explicitly use this we refrain from writing this out here.

To describe the fields r -forms $A_{c^{(r)}}$ are introduced, which are objects living on an r -cell. If a specific r -cell $c^{(r)}(x)_{\mu_1\cdots\mu_r}$ with $\mu_1 < \mu_2 < \cdots < \mu_r$ is considered, they use the notation $A(x)_{\mu_1\cdots\mu_r}$. Also for the r -forms the convention $A(x)_{\mu_1\mu_2\cdots\mu_i\cdots\mu_j\cdots\mu_r} = -A(x)_{\mu_1\mu_2\cdots\mu_j\cdots\mu_i\cdots\mu_r}$ is used as it inherits the orientation of the r -cells.

The final quantities which are important to us are the *exterior derivative operator* d and the *boundary operator* δ . The exterior derivative is defined as

$$(dA)(x)_{\mu_1\cdots\mu_r} = \sum_{k=1}^r (-1)^{k+1} [A(x + \hat{\mu}_k)_{\mu_1\cdots\hat{\mu}_k\cdots\mu_r} - A(x)_{\mu_1\cdots\hat{\mu}_k\cdots\mu_r}] \quad , \quad (\text{C.4})$$

which maps an $(r - 1)$ -form $A_{c^{(r-1)}}$ to an r -form $A_{c^{(r)}}$. Again we denote the index that is omitted from the sum with a circle above. Written in the more general formulation Equation (C.4) reads

$$(dA)(x)_{c^{(r)}} = \sum_{c^{(r-1)} \in \partial c^{(r)}} A_{c^{(r-1)}} \quad . \quad (\text{C.5})$$

It is straightforward to show that the operator d is nilpotent, i.e., $d^2 = 0$ and furthermore there is the convention that $dA_{c^{(d)}} = 0$.

The boundary operator δ in turn is defined to map an $(r + 1)$ -form $A_{c^{(r+1)}}$ to an r -form $A_{c^{(r)}}$ in the following way:

$$(\delta A)(x)_{\mu_1\cdots\mu_r} = \sum_{\nu} [A(x)_{\mu_1\cdots\mu_r,\nu} - A(x - \hat{\nu})_{\mu_1\cdots\mu_r,\nu}] \quad . \quad (\text{C.6})$$

Also here there exists a convention namely $\delta A_{c^{(0)}} = 0$ and the nilpotency of the operator is straightforward to show, i.e., $\delta^2 = 0$. Again using the more general formulation (C.6)

reads

$$(\delta A)(x)_{c^{(r)}} = \sum_{c^{(r+1)} \in \hat{\partial} c^{(r)}} A_{c^{(r+1)}} . \quad (\text{C.7})$$

Appendix D

Dualisation of \mathbb{Z}_2 gauge theory

In Chapter 4.1 we factorised out the center of group $SU(2)$, which is \mathbb{Z}_2 to try and achieve new constraints. As shown there, we were able to solve the \mathbb{Z}_2 part in closed form and get a new constraint. Unfortunately, this newly obtained constraint corresponded to a constraint that the dual theory had already implemented. However, it is still interesting to dualise the \mathbb{Z}_2 theory and use it as a model theory to explore new ideas. \mathbb{Z}_2 is particularly suited for this, since it features only two elements $\{-1, 1\}$.

We start out with the partition function

$$Z = \prod_{x,\mu} \frac{1}{2} \sum_{U_\mu(x)=\pm 1} \prod_{x,\mu<\nu} e^{\beta U_\mu(x) U_\nu(x+\hat{\mu}) U_\mu^*(x+\hat{\nu}) U_\nu^*(x)} , \quad (\text{D.1})$$

with $U_\mu(x) \in \mathbb{Z}_2$. We now expand the exponential in a Taylor-series which yields:

$$Z = \prod_{x,\mu} \frac{1}{2} \sum_{U_\mu(x)=\pm 1} \prod_{x,\mu<\nu} \sum_{n_{\mu\nu}(x)=0}^{\infty} \frac{\beta^{n_{\mu\nu}(x)}}{n_{\mu\nu}(x)!} (U_\mu(x) U_\nu(x+\hat{\mu}) U_\mu^*(x+\hat{\nu}) U_\nu^*(x))^{n_{\mu\nu}(x)} . \quad (\text{D.2})$$

The idea now is to split the expansion index in the following way

$$n_{\mu\nu}(x) = s_{\mu\nu}(x) + 2k_{\mu\nu}(x) , \quad (\text{D.3})$$

with $s_{\mu\nu}(x) \in \{0, 1\}$ and $k_{\mu\nu}(x) \in \mathbb{N}_0$. This can be done because of the property that all elements of \mathbb{N}_0 can be written as a combination of an even and an odd part. We stress that the product $U_\mu(x) U_\nu(x+\hat{\mu}) U_\mu^*(x+\hat{\nu}) U_\nu^*(x) \in \{-1, +1\}$. Raising this product to the power of an even number always yields 1, which is then just a multiplicative factor. Inserting the splitting into (D.2) we get

$$Z = \sum_{\{U\}} \prod_{x,\mu} \sum_{\{s\}} \sum_{\{k\}} \prod_{x,\mu<\nu} \frac{\beta^{s_{\mu\nu}(x)+2k_{\mu\nu}(x)}}{(s_{\mu\nu}(x) + 2k_{\mu\nu}(x))!} (U_\mu(x) U_\nu(x+\hat{\mu}) U_\mu^*(x+\hat{\nu}) U_\nu^*(x))^{s_{\mu\nu}(x)} ,$$

where we introduced the sum over all configurations of the gauge links

$\sum_{\{U\}} = \prod_{x,\mu} \frac{1}{2} \sum_{U_\mu(x)=\pm 1}$ and the sums over all configurations of the expansion indices $s_{\mu\nu}(x)$ and $k_{\mu\nu}(x)$ as $\sum_{\{s\}} = \prod_{x,\mu<\nu} \sum_{s_{\mu\nu}(x)=0}^1$ and $\sum_{\{k\}} = \prod_{x,\mu<\nu} \sum_{s_{\mu\nu}(x)\in\mathbb{N}_0}$. Note that we have already omitted the product to the power of the even number, since it is not relevant.

We then perform the reordering steps shown in Appendix A and Appendix B and arrive at the following expression for the partition function

$$Z = \sum_{\{s\}} \sum_{\{k\}} \prod_{x,\mu<\nu} \frac{\beta^{s_{\mu\nu}(x)+2k_{\mu\nu}(x)}}{(s_{\mu\nu}(x) + 2k_{\mu\nu}(x))!} \times \prod_{x,\mu} \frac{1}{2} \sum_{U_\mu(x)=\pm 1} (U_\mu(x))^{\sum_{\nu:\mu<\nu} [s_{\mu\nu}(x) - s_{\mu\nu}(x-\hat{\nu})] - \sum_{\rho:\rho<\mu} [s_{\rho\mu}(x) - s_{\rho\mu}(x-\hat{\rho})]} . \quad (\text{D.4})$$

The sum over the gauge link variables can be evaluated to be in $\{0, 2\}$. Using the normalisation factor in front of the sum over the link variables, we can then represent this term using the evenness function $E(x)$. With this the partition function reads

$$Z = \sum_{\{s\}} \sum_{\{k\}} \prod_{x,\mu<\nu} \frac{\beta^{s_{\mu\nu}(x)+2k_{\mu\nu}(x)}}{(s_{\mu\nu}(x) + 2k_{\mu\nu}(x))!} \prod_{x,\mu} E \left(\sum_{\nu:\mu<\nu} [s_{\mu\nu}(x) - s_{\mu\nu}(x-\hat{\nu})] - \sum_{\rho:\rho<\mu} [s_{\rho\mu}(x) - s_{\rho\mu}(x-\hat{\rho})] \right) . \quad (\text{D.5})$$

The argument of the evenness function is given in terms of differential forms (cf. Appendix C) and can be denoted as $(\delta S)_{x,\mu}$.

To obtain the fully dualised form, we finally need to consider the term

$$\sum_{k\in\mathbb{N}_0} \frac{\beta^{s_{\mu\nu}(x)+2k_{\mu\nu}(x)}}{(s_{\mu\nu}(x) + 2k_{\mu\nu}(x))!} .$$

We note that for $s_{\mu\nu}(x) = 0$ this is the series representation of $\cosh(\beta)$ and for $s_{\mu\nu}(x) = 1$ this corresponds to the series representation of $\sinh(\beta)$. We write

$$\sum_{k\in\mathbb{N}_0} \frac{\beta^{s_{\mu\nu}(x)+2k_{\mu\nu}(x)}}{(s_{\mu\nu}(x) + 2k_{\mu\nu}(x))!} = \cosh(\beta) (\tanh(\beta))^{s_{\mu\nu}(x)} ,$$

which gives the correct result, depending on the choice of $s_{\mu\nu}(x) \in \{0, 1\}$. Putting this expression back into (D.5) we find the full dual representation of the \mathbb{Z}_2 gauge theory:

$$Z = \sum_{\{s\}} \prod_{x, \mu < \nu} \cosh(\beta) (\tanh(\beta))^{s_{\mu\nu}(x)} \prod_{x, \mu} E((\delta S)_{x, \mu}) \quad . \quad (\text{D.6})$$

$$Z = (\cosh(\beta))^{V \frac{d(d-1)}{2}} \prod_{x, \mu < \nu} \sum_{s_{\mu\nu}(x)=0}^1 (\tanh(\beta))^{s_{\mu\nu}(x)} \prod_{x, \mu} E((\delta S)_{x, \mu}) \quad . \quad (\text{D.7})$$

Here V denotes the volume of the lattice and the factor $\frac{d(d-1)}{2}$ gives the adjacent surfaces in the respective dimension.

We notice that the partition sum now only features one dual variable: $s_{\mu\nu}(x)$. If we compare the splitting to the $SU(2)$ model, the variable $s_{\mu\nu}(x)$ would correspond to a single ACC winding around a specific configuration at plaquette $(x, \mu\nu)$. However, in the $SU(2)$ theory we also have configurations where an ACC and its anti-ACC winding around the same plaquette $(x, \mu\nu)$ simultaneously. We refer to this contributions as *double plaquettes*. We have shown, that in this simple model, the "double plaquettes", do not contribute. This finding lead us to consider the possibility that this might also be the case in the dual $SU(2)$ theory.

Acknowledgements

First and foremost, I would like to thank my advisor Christof Gattringer for the extraordinary supervision of my master thesis and for introducing me to this very interesting and challenging topic. He always had an open ear for any physical or technical question of any sort and he always took the time to discuss and explain everything in great detail. I did not take this kind of caring supervision for granted, but I am very glad that you guided me through my Bachelor and my Master Thesis successfully, even though in the beginning you were not really enthusiastic about taking on a bachelor student. Thank you for everything you have done for me, I thoroughly enjoyed working with you.

Furthermore I thank Oliver Orasch, who was always quick to provide valuable answers to all of my technical questions.

Thank you also to Michael M., Lucijan and Markus for many entertaining conversations about physics and various other nerd stuff.

A huge Thank You to my parents for their continuous support throughout my studies and also for not losing faith in me and pushing me up again, whenever I was feeling down. A big thank you also goes out to my sister, who has always played a massive part in my life and was always there for me, no matter the situation.

A massive Thank You goes to my girlfriend, for taking interest in my passion and enduring an absent minded boyfriend for hours without any major complaints.

Last but not least, I would like to thank my roommate Andreas. The last two years living together were, I think it is safe to say, the most fun period of my life so far. Also I would like to thank my good old buddy Steve, for his continuous reminder, that work isn't everything. Thank you for being such great friends. Thank you also to Michael S. for the very enjoyable discussions about god, the universe and everything and for joining me in the quest of the high speed bachelor.

The results in this thesis were mostly obtained by the High Performance Cluster "Sauron" in Graz. Thank you for immensely accelerating my work!

Bibliography

- [1] H. Singh, S. Chandrasekharan. *Qubit regularization of the $O(3)$ sigma model*. *Phys. Rev. D*, 100:054505, Sep 2019. doi: 10.1103/PhysRevD.100.054505.
- [2] T. Kloiber. *Dual approach to lattice field theories*. *PhD Thesis, University of Graz*, 2019.
- [3] C. Gattringer, C. Marchis. *Abelian color cycles: a new approach to strong coupling expansion and dual representations for non-abelian lattice gauge theory*. *Nuclear Physics B*, 916:627–646, March 2016.
- [4] M. E. Peskin, D. V. Schroeder. *An Introduction to Quantum Field Theory*. Westview Press, 1995. Reading, USA: Addison-Wesley (1995) 842 p.
- [5] M. D. Schwartz. *Quantum Field Theory and the Standard Model*. Cambridge UK: Cambridge University Press, 2013. ISBN 978-1-107-03473-0.
- [6] S. Weinberg. *The Quantum Theory of Fields*. Cambridge UK: Cambridge University Press, 1995. ISBN 0-521-55001-7.
- [7] C. Gattringer, C. B. Lang. *Quantum Chromodynamics on the Lattice: An Introductory Presentation*. Lecture Notes in Physics ISSN 0075-8450. Springer Heidelberg Dordrecht London New York, 2009. ISBN 978-3-642-01849-7.
- [8] R. P. Feynman. *Space-Time Approach to Non-Relativistic Quantum Mechanics*. *Rev. of Mod. Phys.*, 20:367, Dezember 1948.
- [9] Jean Zinn-Justin. Quantum field theory and critical phenomena. *Int. Ser. Monogr. Phys.*, 113:1–1054, 2002.
- [10] H. A. Kramers, G. H. Wannier. *Statistics of the Two-Dimensional Ferromagnet. Part II*. *Phys. Rev.*, 60:263–276, Dezember 1941. doi: 10.1103/PhysRev.60.263.
- [11] C. Marchis, C. Gattringer. Dual representation of lattice qcd with worldlines and worldsheets of abelian color fluxes. *Phys. Rev. D*, 97(3):034508, 2018. doi: 10.1103/PhysRevD.97.034508.

-
- [12] B. Lautrup, M. Nauenberg. *Correlations and Specific Heat of the $SU(2)$ Lattice Gauge Model*. *Physical Review Letters*, 45, December 1980.
- [13] C. Gattringer, T. Sulejmanpasic. *Abelian gauge theories on the lattice: θ -Terms and compact gauge theory with(out) monopoles*. *Nuclear Physics B*, 943, June 2019.
doi: 10.1016/j.nuclphysb.2019.114616.